Accurate Identification of Dynamic Coefficients of Fluid Film Journal Bearings

---

A

Dissertation

Presented to

the faculty of the School of Engineering and Applied Science

University of Virginia

---

in partial fulfillment

of the requirements for the degree

Doctor of Philosophy

by

Pedro Herrera

May 2024

APPROVAL SHEET

This

Dissertation

is submitted in partial fulfillment of the requirements
for the degree of

Doctor of Philosophy

Author: Pedro Herrera

This Dissertation has been read and approved by the examing committee:

Advisor: Christopher Goyne

Advisor:

Committee Member: Natasha Smith

Committee Member: Houston Wood

Committee Member: Robert Rockwell

Committee Member: David Green

Committee Member:

Committee Member:

Accepted for the School of Engineering and Applied Science:

Jennifer L. West, School of Engineering and Applied Science

May 2024

ABSTRACT

The linearized stiffness and damping coefficients of fluid film journal bearings play a key role in predicting vibration levels and stability margins in high-performance rotating machinery. The need for accurate values of these coefficients grows in importance as higher speeds, higher loads, and new operation conditions demand more exact rotordynamic predictions. The subject of this study aims to increase the accuracy and relevance of experimentally derived dynamic coefficients by covering the three following objectives: 1) propose a new method for improving uncertainty estimations for experimentally derived dynamic coefficients, 2) propose a new method for a more accurate identification of the dynamic coefficients, and 3) develop a set of design guidelines for a test rig capable of meeting the demanding dynamic test conditions relevant to modern industrial machinery.

This dissertation first presents an analysis of uncertainty estimations applicable to dynamic coefficients obtained by single-sample single-frequency dynamic tests. The effect of the non-linearity of the dynamic coefficients on the uncertainty estimated by the Taylor Series Method is analyzed, for the first time, and the Monte Carlo Method is presented as a more accurate approach to estimating these uncertainties. Results of analyses for these two methods are presented and compared to published values from previously reported studies. This dissertation also proposes a novel method for converting the random uncertainty in the output of a sensor from the time domain to the frequency domain. It is found that this conversion is quite beneficial for improving the accuracy of the identified coefficients. In one example, uncertainty estimations of ±84% are reduced to just ±6% by using the proposed method. These analyses reveal that

uncertainty estimations from the Taylor Series Method are not entirely reliable without additional checks of non-linearity; and that converting the random uncertainty from sensors to the frequency domain, by using the novel method here, is useful for achieving smaller uncertainty estimations than with traditional methodology.

Classical techniques to experimentally identify the dynamic coefficients of a fluid film journal bearing assume that the dynamic forces and displacements are measured exactly at the midplane of the bearing. However, the actual measurements are usually taken at some distance away from the bearing (miscollocation). In addition, the flexible behavior of the rotor may be important. As a result, a significant error could be included in the identified coefficients if these conditions are not considered. Therefore, this dissertation proposes a new method to accurately identify the eight dynamic coefficients of fluid film journal bearings by accounting for miscollocation of sensors and rotor flexibility. Numerical validation shows the error in the identified coefficients to be less than 0.001% when the proposed identification method is applied to three different rotor-bearing configurations. These configurations included a test bearing floating around a rotor, a rotor floating within the clearance of two identical journal bearings, and a rotor floating within two different journal bearings.

Finally, despite many years of measurement and testing, the dynamic characterization of fluid film bearings is still a field in progress; and the need for more experimental testing and validation under more demanding conditions has produced a demand for new test rigs, particularly those with a capacity to reach speeds on the order of 20,000 rpm and test bearings with diameters of 150 mm and larger. Therefore, this dissertation also develops and presents, for the first time, a guideline for researchers and engineers involved in the design of a test rig for the dynamic characterization of radial fluid film bearings. This guideline covers the design steps, starting with an analysis of the input information provided as industry needs, translating those needs into design requirements, next designing and/or selecting the critical components of the rig in order to meet the design requirements, and finally verifying the suitability of the design process. The

purpose of this guideline is to inform the test rig design process, such that the designer has a directed focus and can make accurate and fast decisions. Recommendations are provided along with specific background information for the designer to consider.

ACKNOWLEDGEMENT

This dissertation is the achievement of six long years of hard academic work and personal challenges. My first gratitude is to God, although I am still in the process of assimilating many of the opportunities (challenges) presented during these years. God has also acted through many people that have contributed in many different ways to this successful completion. It is difficult to mention on a single page the support of everyone during these six years; however, I thank everyone, from the bottom of my heart, for their contribution to this dissertation and to my life.

I am very grateful to Dr. Cristopher Goyne and Dr. Robert Rockwell for their guidance, contributions and suggestions, so I could define the concrete objectives of this dissertation, develop all the work to meet these objectives, and finally perform a successful completion of this document and its defense.

I would also like to give my sincerest appreciation to the committee members: Dr. Natasha Smith, Dr. David Green, and Dr. Houston Wood. Their time, interest and feedback has been important to shape and improve this dissertation. Additionally, my special gratitude to Dr. Wood, as he was my first contact and key for my acceptance into the ROMAC research group, and despite his well-deserved retirement he continued to support my research work by continuing to serve on my committee.

My colleagues at ROMAC and MAE have been also important to provide advice, support and the company and chat of a team member that was always necessary to energize my spirit. Many thanks to Neal, Nathaniel, Wisher and Faisal. Special thanks to Lori, who has been always

providing good advice, so I could improve aspects of my life and usually has stretched her time to listen to my stories as a graduate student at UVA.

Finally, I would like to thank my family for their love and support, which was the most valuable energy to keep developing this work, despite the difficulties and the hard times that made think how wise it was to pursue this PhD. My parents, Pedro and Alix, and my sisters, Lizeth and Alix, have always supported me anytime I needed their advice and assistance, during these years.

I also want to acknowledge the financial assistance provided by the ROMAC research group and the Mechanical and Aerospace Engineering Department, so I could develop my studies and this PhD dissertation.

TABLE OF CONTENTS

LIST OF FIGURES

LIST OF TABLES

Chapter 1

Introduction

Rotating machinery such as centrifugal and reciprocating pumps and compressors, fans, turbines, and electric motors and generators have played an important role in the development of industry and in general of our society. In most cases, inherent to rotating machinery is the transformation of the mechanical energy of a fluid into the rotation and torque of a rotor, or vice versa. The impact of this energy transformation is that fluids can be transported in pipelines over long distances, and the energy of water or fuels can be transformed to electrical power or the thrust of an airplane. The spinning of the rotor plays the role of being the input or output channel in this energy transformation. However, the housing of the machinery is static and therefore some important machine components are required to connect the rotor and the housing. The bearings are the components performing this connection, and they must mechanically support and transmit the loads of the rotor and allow its free rotation. Fluid film journal bearings are one type of bearing that is especially suited to perform this function in heavy industrial rotating machinery due to an ability to support high loads and work at high rotating speeds with lower friction than other types of bearings. An important feature of fluid film journal bearings is that their dynamic characteristics significantly influence the lateral rotordynamic behavior of the rotor. For any journal bearing, these dynamic characteristics can be represented by eight dynamic coefficients, and the accurate

determination of these coefficients is critical for performing an accurate rotodynamic analysis. This is particularly important given that these coefficients change as a function of the rotating speed. The overall goal of this dissertation is to present contributions to enable a more accurate experimental determination of the dynamic coefficients of a fluid film journal bearing.

1.1 FLUID FILM JOURNAL BEARINGS

Fluid film journal bearings are the bearings considered in this dissertation and a brief description is provided here to highlight the important underlying physics. In these bearings a thin layer of viscous lubricant separates the rotor and the pad of the bearing, with no contact between the surfaces. This thin layer of viscous lubricant (usually oil) is produced when there is a relative motion (ω rotation) and a converging geometry between the rotor and the pad of the bearing. This converging geometry is given by the difference between the radius of the bearing R_B and the radius of the journal R_J, and the result is a small radial clearance. Under these conditions, the lubricant is continuously dragged into the clearance volume by a hydrodynamic action that also produces a hydrodynamic pressure distribution (Figure 1.1).

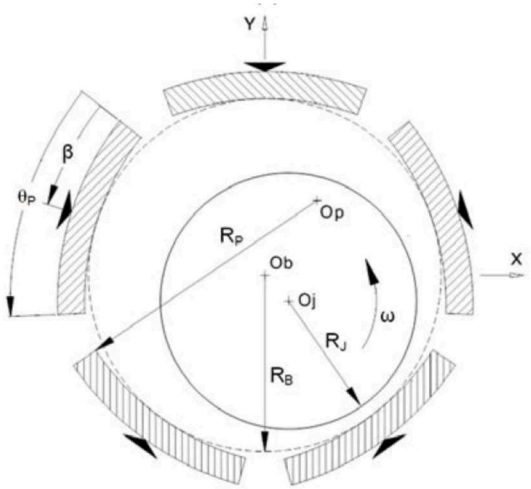

Figure 1.1: Bearing Geometry - reproduced from [1]

This distribution of hydrodynamic pressure provides the fluid film journal bearing with the capacity to support high-magnitude lateral loads (static and dynamic) received by the rotor, while avoiding contact between the journal (rotor) and the bearing surface. Additionally, this pressure distribution is specific for the dimensions and the geometry of the lubricant film at any instant. Therefore, the resultant hydrodynamic force of each pressure distribution is associated with a single radial location of the rotor with respect to the bearing, as given by the instantaneous geometry of the lubricant film.

In practical situations, the rotor always experiences some dynamic force, either from the process or from uneven mass distributions, and when this situation is combined with the non-linear nature of the hydrodynamic force from the bearings, then this creates a complex framework for including the hydrodynamic bearing forces in any rotordynamic analyses.

The standard approach for this situation [2] is to represent the hydrodynamic force of the bearing as a first-order Taylor approximation of the instantaneous position and velocity of the center of the rotor around the location given by only considering the static forces. Using this approach, the following two expressions are obtained for a 2D representation (*x* and *y* direction) of the bearing force:

$$F_x = F_{x0} + \frac{\partial F_x}{\partial X}\Delta X + \frac{\partial F_x}{\partial Y}\Delta Y + \frac{\partial F_x}{\partial \dot{X}}\Delta \dot{X} + \frac{\partial F_x}{\partial \dot{Y}}\Delta \dot{Y} \qquad (1.1)$$

$$F_Y = F_{Y0} + \frac{\partial F_Y}{\partial X}\Delta X + \frac{\partial F_Y}{\partial Y}\Delta Y + \frac{\partial F_Y}{\partial \dot{X}}\Delta \dot{X} + \frac{\partial F_Y}{\partial \dot{Y}}\Delta \dot{Y} \qquad (1.2)$$

Where F_x and F_y are the components of the bearing force in the *x* and *y* directions, F_{x0} and F_{y0} the static components of the bearing force acting in the *x* and *y* directions, and ΔX, ΔY, $\Delta \dot{X}$, $\Delta \dot{y}$ are the instantaneous location and velocity of the center of the rotor.

Now, the eight dynamic coefficients of a fluid film journal bearing can be introduced, such that equations (1) and (2) can be expressed as:

$$\begin{bmatrix} F_X \\ F_Y \end{bmatrix} = \begin{bmatrix} F_{X0} \\ F_{Y0} \end{bmatrix} - \begin{bmatrix} K_{XX} & K_{XY} \\ K_{YX} & K_{YY} \end{bmatrix} \begin{pmatrix} \Delta X \\ \Delta Y \end{pmatrix} - \begin{bmatrix} C_{XX} & C_{XY} \\ C_{YX} & C_{YY} \end{bmatrix} \begin{pmatrix} \Delta \dot{X} \\ \Delta \dot{Y} \end{pmatrix} \qquad (1.3)$$

where the dynamic bearing coefficients, are defined according to table 1:

Stiffness Coefficients	Damping Coefficients
$K_{XX} = -\frac{\partial F_X}{\partial X}$	$C_{XX} = -\frac{\partial F_X}{\partial \dot{X}}$
$K_{XY} = -\frac{\partial F_X}{\partial Y}$	$C_{XY} = -\frac{\partial F_X}{\partial \dot{Y}}$
$K_{YX} = -\frac{\partial F_Y}{\partial X}$	$C_{YX} = -\frac{\partial F_Y}{\partial \dot{X}}$
$K_{YY} = -\frac{\partial F_Y}{\partial Y}$	$C_{YY} = -\frac{\partial F_Y}{\partial \dot{Y}}$

Table 1.1: Definition of dynamic coefficients

Note that four of the dynamic coefficients are defined as the change of the component of the force in one direction over the change of the position or velocity in that same direction. They are called the direct or main coefficients and include K_{xx}, K_{yy}, C_{xx}, *and* C_{yy}. The four remaining dynamic coefficients are defined as the change of the force in one direction, over the change of the position or velocity in the orthogonal direction. They are called the cross-coupled coefficients and include K_{xy}, K_{yx}, C_{xy}, *and* C_{yx}. The implication of this is that a change in the position or velocity of the rotor does not only produce a fluid film bearing force in the same direction of the change but also in the orthogonal direction.

Equation 1.3 shows that identifying the dynamic coefficients of a fluid film journal bearing has a key role in the representation of the bearing forces, and the consequent rotordynamic predictions.

1.2 MOTIVATION

This section provides the motivations for this dissertation work and articulates new contributions on the following three specific topics.

1.2.1 Motivation for a better understanding of the uncertainty related to experimentally obtained dynamic coefficients of fluid film journal bearings

As with any experimental measurement, experimentally obtained dynamic coefficients do not reveal the exact, true values of the coefficients, but instead give ranges of results (uncertainty), within which the true values of the coefficients are located. Therefore, the user of a rotodynamic report should be aware of what uncertainty is associated with the dynamic coefficients, because that is affecting the predictions in the report.

Figure1.2 presents an example of how the uncertainty range of a coefficient could affect the predictions of a critical speed in rotating machinery. Figure 1.2 is an undamped critical speed map taken from [2], where the thick black lines show the evolution of the undamped critical speeds as functions of bearing stiffness. It will be assumed for this example that the true value of the stiffness, K_{xx} or K_{yy}, is 10^5 lbf/in, and that the uncertainty associated with the coefficients is 40% (red lines), similar to values reported in [3].

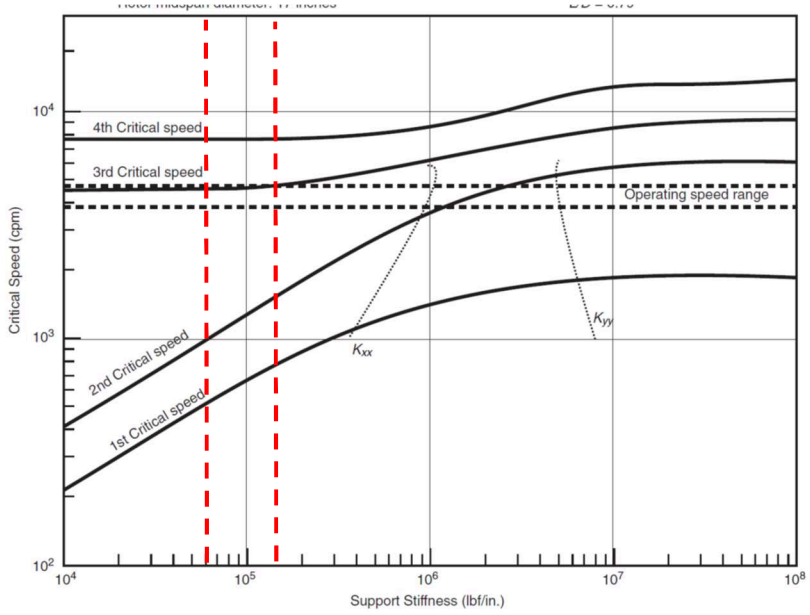

Figure 1.2: Effect of the uncertainty on predictions of undamped critical speeds

Then, the dashed red lines represent the range of possible true values for the stiffness, and the crossing of these red lines with the thick black lines determines the range of the possible undamped critical speeds for this rotor-bearing system. The effect of the uncertainty is most significant for the first two critical speeds. The first critical speed is predicted to be somewhere between 500 and 800 rpm, which is a substantial range. If the desired operating speed is within or near this range it would be difficult to know if or what modifications should be introduced to the components and in which direction. Therefore, dynamic coefficients with smaller uncertainty estimations have a tangible benefit in improving the quality of rotordynamic predictions expected by a user.

The previous paragraphs highlight the importance of the following points:

- The data should be processed such that the estimated uncertainty range truly represents the behavior of the dynamic coefficients (reliability). This dissertation will present an analysis of an existing method that could be providing uncertainty estimations of dynamic coefficients with significant inaccuracies. These inaccuracies are the result of a simplifying assumption of the method.
- As higher rotating speeds are demanded, the uncertainty estimations of the dynamic coefficients also increase due to increasing the synchronous frequency of the rotation. Therefore, it is also important to consider new possibilities in hardware and processing techniques to produce smaller uncertainty estimations. Otherwise, the uncertainty may grow to a value that the measured coefficients are useless for rotordynamics analyses. This dissertation proposes a new method to analyze data, with the benefit that uncertainty estimations will be significantly reduced, as compared to previous techniques.

1.2.2 Motivation for including the rotor flexibility and the real axial location of displacement sensors when identifying the dynamic coefficients of fluid film journal bearings

Techniques to experimentally obtain the eight dynamic coefficients of a fluid film journal bearing usually relate direct measurements of dynamic displacements (vibration) of the rotor and dynamic forces (excitation), acting ideally at the midplane of the bearing, which avoids considering the flexibility of the rotor.

In the past, most industry requirements were focused on low-speed applications, which was convenient for dynamic tests in research environments and produced rotating speeds far away from the critical speeds and with very little response from the flexibility of the test rotor. These speeds combined with short rotors and low loads led to a rigid or quasi-rigid behavior of the rotor and the reasonable assumption that the lateral vibration of the rotor was the same along its axial length. Therefore, these conditions made irrelevant the axial location of the displacement sensor with respect to the midplane of the bearing.

However, more recent industry requirements for increased rotor speed has inevitably involved some degree of flexible behavior of the rotor. Then, it should be important to include within the analysis the consideration that displacement sensors are located axially at some distance from the center of the bearing and are therefore measuring vibrations with different amplitude and phase than the vibrations that occur at the axial center of the bearing.

Despite the fact that the flexibility of the rotor could have a significant impact on the identification of accurate dynamic coefficients, the literature on this topic is very limited. A few approaches that consider the flexibility of the rotor have been presented [4,5]; however, their scope of applicability is limited and in almost all cases the methods rely on the assumption that the sensors are located as close as possible to the midplane of the bearing, such that the difference can be neglected.

This dissertation proposes a new approach to identify the dynamic coefficients of one or two identical or different fluid film journal bearings. This new approach includes the rotor flexibility, as

well as the non-collocation of the dynamic displacements sensors with respect to the bearing midplane.

1.2.3 Motivation for contributing guidelines for the design of a test rig to identify the dynamic coefficients of fluid film journal bearings

The dynamic characterization of fluid film journal bearings is a field in continuous progress, aligned with the new industry demands in terms of rotating speed, loads, and diameter of the fluid film journal bearings. Keeping pace with this progress requires the design and construction of new test rigs, updated to the demands of industry and research.

However, the design of such a test rig is a complex technical task involving: the design and selection of several main components, the harmonious integration of the technical and operational characteristics of the equipment, and the integration of several engineering disciplines including mechanical, electrical, and instrumentation. On top of these complexities, current demands point to rigs spinning faster than 15,000 rpm and journal diameters larger than 100 mm, which increases the investment to hundreds of thousands of dollars and makes more sensible the integration of the components and the dynamic behavior of the rig as a unit. These increased demands in speed, size, and power also bring rotodynamic and safety challenges that did not exist with smaller rigs; but the most important challenge is perhaps to maintain the ability to produce and reliably measure small radial vibrations of less than 12.5 μm to not exceed a safe displacement where the bearing force is still validly represented by equation (1.3).

Despite the technical complexities mentioned above and the increased cost of these rigs, the literature provides scant design guidelines and key aspects to consider, for the researcher involved in the task of this design. Some researchers have described the rigs they have designed or used and, although some descriptions are quite complete, there are many important design details that are omitted. Thus, there is room in the literature for a contribution of important

guidelines, so that the design work can move faster, more confidently, and with less possibility for expensive mistakes.

1.3 DISSERTATION OBJECTIVES

This section presents the following three main objectives of this dissertation, that align with each of the main motivations of this study:

1. The first objective of this dissertation is to analyze the methods to produce uncertainty estimations of dynamic coefficients obtained by single-sample, single-frequency dynamic tests. One section of the analysis studies why two different methods (the Taylor Series Method and the Monte Carlo Method) to estimate the uncertainty of experimentally estimated dynamic coefficients produce different uncertainty results, despite using the same data and conditions. Assumptions of the Taylor Series Method are analyzed in detail to explain the difference in results. Finally, a new method is proposed that, for the same data and conditions, produces smaller uncertainty estimations for the dynamic coefficients.
2. The second objective is to analyze the influence of the miscollocation of the displacement sensors with respect to the midplane of the bearing and the flexibility of the test rotor, during the identification of the dynamic coefficients of a fluid film journal bearing. As test conditions become more demanding, it is important to consider the impact of these conditions in the identification method, and to find approaches to include corrections to estimate dynamic coefficients closer to the true values. A new method is proposed to identify the eight dynamic coefficients of a fluid film journal bearing that accounts for rotor flexibility and non-collocation of the displacement sensors with respect to the midplane of the bearings.
3. The third objective is to present a detailed guideline on how to design a test rig, aimed to experimentally estimate the eight dynamic coefficients of a radial tilting-pad bearing.

Guidelines are intended to cover test rigs for different rotating speeds and bearing diameters, including updated requirements of up to 20,000 rpm and diameters of around 127 mm.

1.4 DISSERTATION STRUCTURE

The remainder of this dissertation is comprised of four chapters.

Chapter 2 presents a comparative analysis of uncertainty estimations of dynamic coefficients of fluid film journal bearings, applied to three different bearing cases, using the Taylor Series Method and the Monte Carlo Method. These analyses are applicable to dynamic coefficients obtained by techniques in the frequency domain and by single-sample single-frequency tests. The analysis includes reasoning to explain the different estimations generated by these two methods. This chapter also presents a new approach to estimate the uncertainty for dynamic coefficients which produces significantly smaller uncertainty estimations for three considered bearing cases.

Chapter 3 presents a new approach and method to identify the dynamic coefficients of fluid film journal bearings. This new approach includes the flexibility of the test rotor and the dynamic displacements measured by sensors located at any axial location with respect to the midplane of the bearing. The distinctive feature of this approach is that it eliminates the errors that come with assuming the dynamic displacement at the location of the sensors is the same as at the midplane of the bearings. Results are presented showing the application of this new approach to a typical test configuration of a floating bearing housing with one single test bearing, and to a configuration of a floating test rotor supported by two identical or two different fluid film journal bearings.

Chapter 4 presents a complete guideline on how to design a test rig with capacity to identify the eight dynamic coefficients of a fluid film journal bearing. This chapter is subdivided into four sections. The first subsection covers background information on the customer needs required to start a design process and the technical implications of those needs. The second subsection covers the technical process on how to translate the customer needs into technical requirements

that will guide the design. The third subsection presents the main components of a test rig and the detailed steps to design and select those components. Finally, the fourth subsection presents verifications to be performed on the assembled test rig, as the final objective of the design is to have a rig working as a single unit and not as isolated individual components.

Finally, Chapter 5 summarizes the contributions and conclusions of the research work presented in this dissertation.

1.5 CONTRIBUTIONS OF THIS DISSERTATION

Chapter 2 presents for the first time an analysis of two existing uncertainty methods applied to the experimental determination of dynamic coefficients and performs a comparison of their uncertainty estimations. In addition, Chapter 2 also presents for the first time, a new approach to analyze the dynamic data during a dynamic test that can lead to considerably smaller uncertainty estimations than with the traditional method. Chapter 3 introduces, for the first time, a new approach to identify the dynamic coefficients of one or two identical or different fluid film journal bearings, including the rotor flexibility and non-collocation of the dynamic displacement sensors with respect to the bearing midplane. Chapter 4 presents, for the first time in literature, a complete set of guidelines for the design of a test rig to determine the dynamic coefficients of a fluid film journal bearing. The design of such a rig is a complex task involving: the design and selection of several main components, the harmonious integration of the technical and operational characteristics of these components, and the integration of several engineering disciplines including mechanical, electrical, and instrumentation. Therefore, the purpose of this last chapter is to provide a designer with key background information to reduce complexities and accelerate the design process.

Chapter 2

Propagation of Uncertainty in Experimental Dynamic Coefficients of Fluid Film Journal Bearings

There is a constant demand for heavy rotating machinery such as gas turbines and centrifugal compressors to operate at higher rotating speeds and larger loads to achieve better levels of performance and efficiency. These new conditions of operation are simultaneously implemented with restrictions on the weight and size of some components, putting more pressure on the rotordynamic design. A rotordynamic design should include the characteristics of the bearing components, in addition to the characteristics of the rotor, and bearings usually play a key role in defining this rotordynamic behavior [1, 6].

Fluid film bearings are widely used in heavy rotating machinery due to special features, such as high load capacities, long life, and favorable influence on the rotordynamic behavior from significant amounts of damping [7]. These bearings are typically represented in rotordynamic analyses by eight linearized dynamic coefficients: four represent the stiffness properties, and four represent the damping properties [8, 9].

The dynamic coefficients are not directly measured. Instead, they are usually obtained by measurements of applied force excitations and the subsequent rotor response [10]. Unfortunately,

these measurements will never reveal real or true values, no matter how accurate the instruments are, due to sources of experimental uncertainty, such as: calibration variations, electromagnetic noise, and temperature variations, among others. The consequence of this is that the experimenter obtains dynamic coefficients within a range that contains the true values, but without being able to precisely determine the true values. This range is defined, in rigorous terms, as the uncertainty of a measurement or the uncertainty related to a result, and it could be determined by statistical sampling and/or by performing an uncertainty analysis. The purpose of this study is to analytically estimate the uncertainty applicable to experimental single-sample (sample size =1) single-frequency (only one excitation frequency) dynamic coefficients, obtained by techniques in the frequency domain. The uncertainty estimations to be presented will be obtained by propagating the random uncertainty of the displacement and force measurements.

Kostrzewsky and Flack [11] developed the first method to propagate the uncertainty in the measured dynamic displacements and forces, leading to an analytical estimation of the uncertainty in experimentally obtained dynamic coefficients. This method is applicable to single-sample dynamic coefficients, obtained by the application of single-frequency harmonic excitations. The core of this method is based on the general guidelines by Kline and McClintock [12], or referred by others as the Taylor Series Method (TSM), because this expansion is the core mathematical approach. Partial derivatives providing the amount of change in the dynamic coefficients by unitary changes in displacements are calculated numerically in [11], due to the lack of a standard analytical formula. This method was applied to the eight experimentally obtained dynamic coefficients for a three-lobe test bearing operating at 2,500 rpm. Estimated uncertainty for the stiffness coefficients was around 3%, and around 25% for the damping coefficients.

The dynamic coefficients of a 70 mm diameter tilting-pad bearing were experimentally obtained by Wygant et al [3], and the uncertainty was estimated using the method developed in [11]. Measurements were taken of the dynamic excitation force and the dynamic displacement of

the floating test bearing, while the velocity and acceleration of the test bearing were found analytically as the first and second derivative of the displacement. Random uncertainties were applied and propagated for the magnitude of the dynamic displacement of the test bearing and the magnitude of the excitation force. Reported uncertainties for the main stiffness coefficients were in the range from 5 to 82%, and for the main damping coefficients from 7 to 92%. Cross-coupled coefficients presented considerable larger uncertainties.

An alternate method for the computation of experimentally obtained dynamic coefficients was developed and presented by Rouvas et al [13]. This method relies on the averaging of signals, in the frequency domain by using Power Spectrum Density (PSD) formulations, to reduce noise and provide more accurate coefficients. Moreover, when this method is applied to multi-sample tests obtained by the application of multi-frequency harmonic forces, the uncertainty on the coefficients can be estimated using the analysis in [14].

More recently, an uncertainty quantification on the numerical modeling of a 40 mm diameter tilting-pad bearing spinning at 4,200 rpm was performed by Pereira and Nicoletti [15]. This study implemented the Monte Carlo method to propagate some expected uncertainty in the bearing clearance and find and envelope of results for the dynamic coefficients. This envelope of results is then statistically analyzed to find the probability of failure of the bearing with respect to certain reference situations.

Barsanti et al. [16] presented a novel uncertainty analysis for dynamic coefficients, that combines a statistical sampling (multi-sample test) with a statistical technique called Bootstrap to find the confidence intervals of the obtained dynamic coefficients. A particular feature of this proposed analysis is that the confidence interval is not dependent on the distribution of the population, contrary to the Monte Carlo method.

Based on the above studies, there has been over the last 30 years, an increased awareness of the importance of estimating and reporting the uncertainty when obtaining experimental dynamic coefficients. Two uncertainty methods (TSM and PSD) have practically dominated the

field, and basically no upgrades or reviews have been made of them, since these methods were proposed. In particular, the method in [11] was developed with the implicit assumption of a linear behavior of the dynamic coefficients with respect to the measured variables. However, to our knowledge no rigorous validation of this assumption has been performed, and its impact on uncertainty estimations is not clear. Conversely, alternate techniques, such as the Monte Carlo Method (MCM) can be easily applied now, due to modern computers, and no simplifying assumptions are required to perform the uncertainty estimations. Finally, the method in [11] has also propagated the random uncertainty of the transducers in the time domain, which could be producing larger uncertainty estimations, as compared to other methods. Therefore, this study also explores the use of an analytical conversion to the frequency domain as a means of reducing uncertainty estimations of the dynamic coefficients.

Reliable uncertainty estimations in experimental dynamic coefficients are required for the purpose of validating dynamic coefficients from bearing codes. Kocur et al. [17] conducted a survey, providing a rotor model and the geometry of a 5-pad tilting pad bearing, to industrial users, vendors of rotating equipment, consultants, and educators, in order to compare their analytical predictions of the dynamic coefficients. This survey showed variations in dynamic coefficient predictions of up to 1,000%, highlighting the need of a reliable validation.

The purpose of this study is to present an analysis of the available methods to determine the uncertainty of single-sample experimental dynamic coefficients, when excited by the application of single-frequency harmonic forces. More specifically, this study addresses the following three aspects:

1. Most often, the uncertainty of single-sample dynamic coefficients has been determined using the TSM [3, 11, 18, 19], based on linear assumptions; however, dynamic coefficients could exhibit a non-linear response. The analysis presented here is the first effort to quantify the error in the uncertainty estimations due to the linear assumption of the TSM. Additionally, the

non-linearities could be reflected as asymmetric rather than the symmetric uncertainty that the TSM produces.

2. The second part of this study presents the Monte Carlo Method (MCM) and its use as a validation tool to confirm the findings of the previous analysis and to quantify how the non-linearities might impact the uncertainty estimations by the TSM. The MCM is applied without any assumption or simplification in the identification of the coefficients, in order to obtain a more faithful representation of the uncertainty behavior during real tests.
3. Finally, the uncertainty of single-sample dynamic coefficients has traditionally been determined by propagating the random error of the measurements in the time domain. However, this study proposes a novel method that converts that random error from the time domain to the frequency domain. This method shows a reduced spread of measurements in the frequency domain, which, as will be discussed, significantly reduces the uncertainty estimations.

This chapter has the following structure: first a method section that includes some uncertainty concepts and the framework for the replicated hardware and identification model used in this study; second, an analysis section showing the non-linear behavior of coefficients and its impact on the TSM, simulations with the MCM, and details of an analytical method to convert random uncertainty from the time domain to the frequency domain; third a section with results comparing the different analyses; and finally a conclusion section discusses the significant findings.

To our knowledge, this study presents the first analysis that shows the effect of non-linear behavior of dynamic coefficients on the uncertainties estimated by the TSM. The quantification of these effects is obtained by propagating the uncertainties with a MCM in the identification model for the dynamic coefficients, without any simplifying assumption. Additionally, a novel analytical method is proposed to transform random uncertainty from the time domain to the frequency domain, leading to smaller uncertainties for dynamic coefficients in single-sample tests.

2.1 METHOD FOR THE ANALYSIS

This section has three primary objectives: to provide a brief description of useful concepts on measurement uncertainty, to describe the three bearing cases used for the uncertainty analyses in this study, and to describe the mathematical model to estimate the uncertainties in the dynamic coefficients when using the MCM.

2.1.1 Uncertainty

The objective of performing a measurement is to obtain the true value of a measurand. However, in real situations there is always a source of error that is out of the control of or unknown to the experimenter, such that the true value is not perfectly measured. Therefore, a well-conceived experiment must also estimate the limits within which the true value is located; for example, the range of results for a large population is an indication of this uncertainty. A quantitative indication of the uncertainty is important, because it allows the target audience to know the reliability of the measurement and to compare measurements from different sources or obtained under different conditions.

Traditionally, measurements errors have been classified in two categories: systematic and random [20, 21]. A systematic error is any error that remains constant if measurements are repeated during the same test. Thus, gathering additional test data will not help to identify them. Some examples of systematic errors are: imperfect calibrations, biased reduction models, and environmental conditions.

A random error is any error that varies randomly during a test and produces scatter in the measurements. Electrical noise is a typical cause of random error in sensors or transducers. This electrical noise is reflected as a random behavior in the sensor's output with the important consequence that the output of a sensor cannot be known more reliably than the amount of this noise. When this electrical noise is translated into the output units of the sensor it is called

resolution. The resolution of displacement and force sensors is typically one of the main causes of uncertainty propagating to the dynamic coefficients.

2.1.2 Bearing cases for the uncertainty analyses

Three different bearing cases, selected from a set of bearings tested in [3], are subject to uncertainty analyses and estimations presented in this chapter.

The bearings in [3] were preloaded 5-pad tilting pad bearings and were tested at 900, 1,650, and 2,250 rpm, with speed/load conditions producing Sommerfeld numbers from 0.1 to 2.0. Dynamic loads were not specifically detailed. However, it was reported that typical forced orbits were 25 µm peak to peak (pk-pk). Based on this information, the three bearing cases were selected with bearing parameters and operating and test conditions, as shown in table 2.1. Cases 1 and 2 have forced orbits of around 25 µm as reported in [3], while case 3 replicates case 1, but limits the dynamic load to 500 N. The force limit in case 3 was implemented due to test rig specifications reported in [22].

	Case 1	Case 2	Case 3
Journal Dia.	70 mm	70 mm	70 mm
L/D ratio	0.75	0.75	0.75
Offset	0.5	0.5	0.5
Cb	78 µm	78 µm	78 µm
Preload	0.3	0.3	0.3
Pad Thickness	12.7 mm	12.7 mm	12.7 mm
Speed	900 rpm	2,250 rpm	900 rpm
Static Load	1,000 N	550 N	1,000 N
Sommerfeld	0.2	0.9	0.2
Amplitude Oscillation	12.7 µm 0-Pk	12.7 µm 0-Pk	Given by 500 N
Lubricant	ISO VG 32		
Viscosity at 40° C	0.0256 N.s/m^2		
Viscosity at 55° C	0.0157 N.s/m^2		
Oil Inlet Temperature	51.1 ± 0.7° C		

Table 2.1: Parameters for bearing cases

The test rig configuration in [3] is shown in figure 2.1 and modeled for the uncertainty analyses as composed of a rotor with a nominal diameter of 70 mm, supported by two precision ball

bearings with a gap of 209 mm. The test bearing was mounted in a floating bearing housing and dynamically excited by two orthogonal external shakers. Two force transducers measured the applied dynamic excitation and eddy current probes measured the relative displacement between the housing and the rotor, in the x and y directions. More specific details of the test rig are found in [22].

Uncertainty analyses in this chapter apply only random uncertainties to amplitude and phase of dynamic displacements and forces, with values given in table 2.2 for a 97,5% confidence interval. Values of uncertainty in amplitude replicate the same values in [3], while the value of uncertainty in phase was taken from a study in [11] operating the same test rig. Therefore, uncertainty estimations in [3] are the comparison line for all the uncertainty estimations in this study.

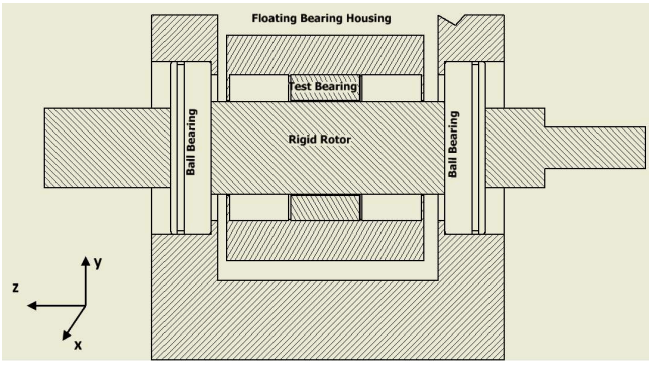

Figure 2.1: Test rig configuration

Variable	Measurement Uncertainty
Magnitude of Dynamic Force	± 0.45 [N]
Magnitude of Dynamic Displacement	± 2.5 [µm]
Phase Angle	± 1.0 [degrees]

Table 2.2: Measurement Uncertainty Levels

2.1.3 The model to estimate uncertainties in the dynamic coefficients

The uncertainty analyses presented in this chapter are performed by two different methods: the TSM and the MCM. However, both methods will require the use of a mathematical model that

relates the dynamic displacements and forces with the bearing dynamic coefficients. This section describes the 2-D mathematical model used in this chapter.

Considering the orbits to be analyzed are less than 20% of the diametral clearance, the dynamic bearing forces are modeled by the eight linearized dynamic coefficients corresponding to the particular bearing, static load and speed being analyzed. The following equation of motion (EOM) is obtained:

$$\begin{bmatrix} M_h & 0 \\ 0 & M_h \end{bmatrix} \begin{pmatrix} \ddot{x} \\ \ddot{y} \end{pmatrix} + \begin{bmatrix} C_{XX} & C_{XY} \\ C_{YX} & C_{YY} \end{bmatrix} \begin{pmatrix} \dot{x} \\ \dot{y} \end{pmatrix} + \begin{bmatrix} K_{XX} & K_{XY} \\ K_{YX} & K_{YY} \end{bmatrix} \begin{pmatrix} x \\ y \end{pmatrix} = \begin{bmatrix} f_X \\ f_Y \end{bmatrix}.. \qquad (2.1)$$

In this equation, f_X and f_Y are the forces applied by the orthogonal external shakers to the floating bearing housing, and M_h is the mass corresponding to this bearing housing. x and y are the small orthogonal dynamic relative displacements between the bearing housing and the rotor induced by f_X and f_Y; while $\dot{x}$ and $\dot{y}$ are the velocities corresponding to these relative displacements, and $\ddot{x}$ and $\ddot{y}$ are the related accelerations.

One additional consideration for the model is that f_X and f_Y are single-frequency harmonic excitations, which can be expressed in complex notation as,

$$f_x(t) = Re[F_x e^{i(\omega t - \emptyset_x)}] \qquad (2.2)$$

$$f_y(t) = Re[F_y e^{i(\omega t - \emptyset_y)}] \qquad (2.3)$$

where ω is the excitation frequency and is synchronous with the rotating speed of the rotor, as reported in [3]. Variables φ_X and φ_Y represent the phase lag angles of the excitations, with respect to a certain reference, for example a keyway. The response of the system to the excitations are the dynamic displacements x and y, hence, they can also be represented in complex notation as,

$$x(t) = Re[X e^{i(\omega t - \beta_x)}] \qquad (2.4)$$

$$y(t) = Re[Y e^{i(\omega t - \beta_y)}] \qquad (2.5)$$

where β_X and β_Y are the phase lag angles related to $x(t)$ and $y(t)$.

Velocity and acceleration can be expressed as time derivatives of (4) and (5), and substitution in (1) leads to:

$$\begin{bmatrix}(K_{xx} - M_h\omega^2) + i\omega C_{xx} & K_{xy} + i\omega C_{xy} \\ K_{yx} + i\omega C_{yx} & (K_{yy} - M_h\omega^2) + i\omega C_{yy}\end{bmatrix}\begin{pmatrix}Xe^{i(-\beta_x)} \\ Ye^{i(-\beta_y)}\end{pmatrix} = \begin{pmatrix}F_x e^{i(-\emptyset_x)} \\ F_y e^{i(-\emptyset_y)}\end{pmatrix} \quad (2.6)$$

During a test the magnitude and phase of dynamic forces and dynamic displacements are measured, and with this data the eight dynamic coefficients are calculated. However, two independent rounds of forces and displacements are required, and equation (2.6) is expanded and terms rearranged, to include both rounds of measurements, in the following form,

$$\begin{bmatrix}(K_{xx} - M_h\omega^2) + i\omega C_{xx} & K_{xy} + i\omega C_{xy} \\ K_{yx} + i\omega C_{yx} & (K_{yy} - M_h\omega^2) + i\omega C_{yy}\end{bmatrix} = \begin{bmatrix}F_{X1} & F_{X2} \\ F_{Y1} & F_{Y2}\end{bmatrix}\begin{bmatrix}X_1 & X_2 \\ Y_1 & Y_2\end{bmatrix}^{-1} \quad (2.7)$$

All forces and displacements on the righthand side of (2.7) are complex numbers, exactly as they were on equation (2.6). However, in (2.7) they are written in a simplified way, and the indices 1 and 2 refer to the first and second rounds of measurements.

The approach in this chapter for the uncertainty analyses followed the next steps:

1. For each bearing case in table 2.1 numerical dynamic coefficients are found by using MAXBRG [23], which is an industry-standard finite element computer code for performing steady state thermo-elasto-hydrodynamic (TEHD) analysis of tilting-pad bearings. These dynamic coefficients are cited as the “reference” coefficients throughout this chapter.
2. With the dynamic coefficients from step 1 and utilizing equation (2.6), dynamic excitations are entered to produce forced dynamic orbits with amplitudes of around 25 μm peak to peak, as reported in [3]. Two rounds of dynamic excitations and orbits are produced, and they will be cited as the “reference” dynamic forces and displacements for subsequent sections of this chapter.
3. By using equation (2.7) and the “reference” values of dynamic forces and displacements, then partial derivatives can be calculated for the TSM, or random or specific values of

uncertainty in force and/or displacement can be applied to the reference values to produce "errored" dynamic coefficients (MCM).

2.2 UNCERTAINTY ANALYSIS

This section covers the three main objectives of this chapter that were explained in the introduction section. This section first explains the TSM and performs an analysis of the non-linear behavior of uncertainty of dynamic coefficients. It also explains why this behavior could affect the uncertainty estimations generated by this method. In the second place, this section implements a MCM to find uncertainties for dynamic coefficients. Finally, an analysis is presented to analytically transform random uncertainty of instruments to the frequency domain. It is shown that random uncertainties are significantly smaller in the frequency domain than in the time domain, so this transformation is useful to produce refined uncertainty estimations for the dynamic coefficients. The calculations for the analyses were developed and implemented in Matlab.

2.2.1 The Taylor Series Method and analysis on linearity of uncertainty in dynamic coefficients.

The Taylor Series Method (TSM) is a method aimed at estimating the uncertainty in a result *r*, when r is a function of *J* experimentally measured variables, V_i, as expressed in equation (2.8). When the uncertainty of these variables is known and expressed as u_i, the uncertainty in the result *r*, expressed as u_r, is treated as a propagation of the uncertainty of the variables and the value can be estimated with equation (2.9), as instructed in [11, 12]. Detailed explanations and background for this method are covered in [20].

The TSM has been a preferred method to estimate uncertainties of dynamic coefficients. This section will present an analysis on the relevance of some important features of the method.

$$r = r(V_1, V_2, \ldots, V_J) \qquad (2.8)$$

$$u_r^2 = \left(\frac{\partial r}{\partial V_1}\right)^2 u_{V1}^2 + \left(\frac{\partial r}{\partial V_2}\right)^2 u_{V2}^2 + \ldots + \left(\frac{\partial r}{\partial V_J}\right)^2 u_{VJ}^2 \qquad (2.9)$$

The level of accuracy of the uncertainty estimation provided by equation (2.9) will depend on how strictly the following conditions are fulfilled:

1. The experimental result *r* should be a linear function of the variables V_i
2. The uncertainty in each one of the V_i variables should be completely independent from the others.

According to equation (2.7), any dynamic coefficient in this chapter, whether stiffness or damping, could be expressed as a general mathematical function of the following variables,

$$f = f(F_{x1}, F_{x2}, F_{y1}, F_{y2}, X_1, X_2, Y_1, Y_2, M_h) \qquad (2.10)$$

and it can be seen from equations (2.8), (2.9), and (2.10) that the uncertainty related to each dynamic coefficient is a result of the propagation of the uncertainty in the dynamic forces and displacements, and the mass of the housing. However, one assumption in this study is that the true mass of the housing is known, so it does not contribute to the uncertainty of the coefficients.

Equation (2.9), assuming the linearity of the coefficients, has been a common method used by researchers to determine the uncertainty in single-sample dynamic coefficients [3, 11, 18, 19, 24, 25]. However, no study has analyzed if this linearity assumption is having a relevant impact on the uncertainty estimations by equation (2.9), considering the non-linearity of dynamic coefficients [26]. This study performs, for the first time, an analysis of this specific topic on the particular bearing cases in table 2.1, with the aim of establishing how reliable the uncertainty estimations in dynamic coefficients are for these bearing cases, when estimated by the TSM, under the linear assumption.

The variation in the value of a dynamic coefficient around a set point, defined as δf, can be determined as a function of the variation in all the individual variables of equation (2.10), defined as δV_i, by using a Taylor Series Expansion, as expressed in equation (2.11). One important remark about the Taylor expansion written here is that it only includes first and second order partial derivative terms, for the sake of simplicity, but that does not mean that significant higher order terms do not exist.

$$\delta f = \sum_{i=1}^{n} \frac{\partial f}{\partial Vi} \delta V_i + \sum_{i=1}^{n} \sum_{j=1}^{n} \frac{\partial^2 f}{\partial V_i \partial V_j} . \frac{(\delta V_i)^2}{2!} + \ldots \qquad (2.11)$$

If the uncertainty for each dynamic coefficient (δf) is as a quasi-linear function of the random uncertainty of dynamic forces and displacements, when each δV_i is substituted by the values of uncertainty in table 2.2, then a predominant relative weight of first order related terms would be expected in the Taylor Series Expansion. The relative weight of second or higher order terms should be zero or very small when compared to individual first order terms. The relative weight of each component of the Taylor expansion is found by dividing equation (2.11) by the reference or initial value of each coefficient provided by MAXBRG. For example, for stiffness K_{yy}, it would lead to the following expression,

$$\frac{\delta K_{yy}}{K_{yy}} = \sum_{i=1}^{n} \frac{\partial K_{yy}}{\partial Vi} \frac{\delta V_i}{K_{yy}} + \sum_{i=1}^{n} \sum_{j=1}^{n} \frac{\partial^2 K_{yy}}{\partial V_i \partial V_j} . \frac{(\delta V_i)^2}{K_{yy} \ . \ 2!} + \ldots \qquad (2.12)$$

Derivatives for equation (2.12) are calculated around the ‘reference’ coefficients, forces, and displacements, by applying centered finite differences methods in equation (2.7).

Figure 2.2 shows the uncertainty of the main dynamic coefficients, for bearing cases in table 2.1, when random uncertainties of 2.5 μm are applied to dynamic displacements X_1 and Y_2. Figure 2.2 also shows the uncertainty as contributed by first order or second order direct terms of equation (2.12), in order to better evaluate if the uncertainty is behaving linearly. Contribution of other variables (F_{x1}, F_{x2}, F_{y1}, F_{y2}, X_2, Y_1) to the uncertainty of the coefficient was calculated to be less than 0.3%, and for this reason it is not shown in figure 2.2.

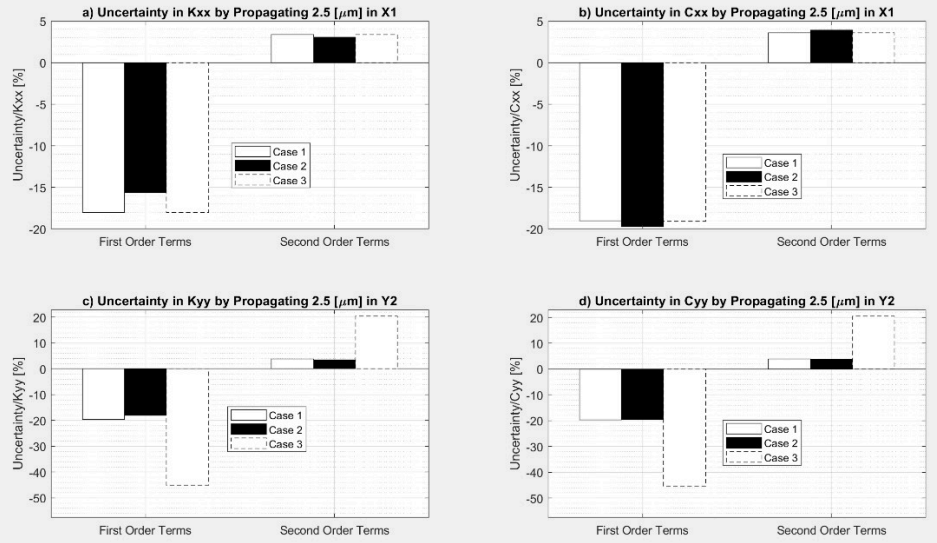

Figure 2.2: Uncertainty of dynamic coefficients evaluated as a Taylor Series Expansion

Figure 2.2 shows that second order terms have noticeable weight over the uncertainty of the coefficients. For example, figure 2.2b shows that for bearing case 2 the relative impact of the second order terms due to the uncertainty in X_1 is 3.89%, which is around 20% (3.89/19.73) of the relative impact of the first order terms. For three bearing cases, the impact of second order terms can be quantified from around 18% to 45% of the variation of the most significant first order term for each coefficient. These numbers indicate the non-linear behavior of uncertainty, for the analyzed cases, and therefore that the linear uncertainty estimations provided by the TSM will not have the best level of accuracy. As a rough approximation, the TSM is underpredicting or overpredicting the uncertainty by the relative percentage of variation associated with the second order term.

The non-linearity of the dynamic coefficients is affecting the accuracy of the uncertainty estimation provided by the TSM, and it may also have the additional consequence of violating the symmetric behavior assumed by the TSM. Equation (2.9) estimates the uncertainty u_r in a result r, but in reality, the TSM is predicting that the uncertainty is $\pm u_r$, due to the symmetric behavior of linear functions. Therefore, the second step in the analysis is to evaluate whether the non-linearity

of the coefficients produces an asymmetric behavior of the uncertainty, that is not captured by the TSM.

The symmetric or asymmetric behavior of the uncertainty is evaluated by applying individual positive and negative identical variations to each one of "reference" values of the variables in equation (2.10) and then finding the variation produced in each one of the dynamic coefficients. The mathematical model for this evaluation is equation (2.7). A symmetric behavior will produce approximately the same absolute variation in the coefficient for a positive or negative variation of the same size in the same variable.

Tables 2.3 and 2.4 show the variation in the main coefficients when ±2.5 μm variations are applied to the amplitudes of X_1 and Y_2. For example, the variation of K_{yy} (bearing case 1) is 16.4% ($\Delta K_{yy}/K_{yy}$), when a variation of +2.5 μm is applied to Y_2. Meanwhile, when the applied variation to Y_2 is -2.5 μm, the variation of K_{yy} is 24.5%. The different variation of the coefficients, depending on the sign of the variation applied to the variables, clearly suggests an asymmetric behavior of the uncertainty, which constitutes another source of inaccuracy for the uncertainty estimations provided by the TSM.

		Relative Variation of Coefficient [%]	
	Bearing Case	Variation to X_1:-2.5 μm	Variation to X_1:+2.5 μm
K_{xx}	1	22.28	-15.15
	2	19.47	-13.06
	3	22.28	-15.15
C_{xx}	1	23.53	-16.00
	2	24.57	-16.48
	3	23.53	-16.00

Table 2.3: Asymmetric response of uncertainty of Kxx and Cxx

The analysis performed in this section reveals the non-linearity and asymmetric behavior of the uncertainty for the specific conditions analyzed here, but more importantly it highlights the Taylor Series Method could fail to provide reliable uncertainty estimations for dynamic coefficients, due to its linear assumption. This finding cannot be generalized to all conditions,

nonetheless, it should be interpreted as a warning that additional verifications of linearity and symmetry should be considered when using the TSM to estimate uncertainty.

		Relative Variation of Coefficient [%]	
	Bearing Case	Variation to Y_2:-2.5 µm	Variation to Y_2:+2.5 µm
K_{yy}	1	24.48	-16.41
	2	22.40	-15.08
	3	82.73	-31.09
C_{yy}	1	24.57	-16.47
	2	24.25	-16.33
	3	83.04	-31.21

Table 2.4: Asymmetric response of uncertainty of Kyy and Cyy

2.2.2 The Monte Carlo Method.

The Monte Carlo Method (MCM) is a statistical technique predicting the possible outcomes in a situation, when the inputs to this situation are comprised of random processes with known or assumed probability density functions. The simulation of a random process was a powerful, but inefficient technique requiring significant computational time. One of the first applications of this method is traced to ENIAC (Electronic Numerical Integrator and Computer) and the prediction of nuclear processes at the end of the 1940's [27]. For some time, this method was restricted to exceptional situations and research groups with access to state-of-the-art computers. Now, with the widespread availability of affordable and high-performance computers, the MCM has become more popular and accessible due to its power [28].

The MCM can be applied to uncertainty analyses as the random errors in the measurements are treated as the inputs, and the MCM will provide a distribution of possibles outcomes for the dynamic coefficients, from which the uncertainty range is obtained. The numerical analysis with the MCM creates a population of *n* different situations when *n* different random errors are applied to the readings of the instruments. By applying this *n* combinations to the identification model in equation (2.7) a set of *n* dynamic coefficients is produced, despite the true dynamic coefficients

are constant. Therefore, by propagating the random uncertainty of the instruments, the random uncertainty of the coefficients is estimated.

Despite the simplicity of the MCM and that the steps can be implemented with the assistance of many widely available math simulation/programming software codes, it has been a method with little usage to estimate uncertainties for experimental dynamic coefficients. The main features of the MCM when applied to uncertainty estimations in experimental dynamic coefficients are the following:

1. There is no need of simplifying assumptions to estimate the uncertainties because the MCM is not relying on a single result. The MCM is generating possible results for the dynamic coefficients, based on using random possibilities, within the programmed limits.
2. The Monte Carlo simulation is especially well-suited to represent the random behavior of sensor output, and additionally the user may program any frequency distribution or shape for any input variable. Therefore, the simulation can provide a closer similarity to the expected behavior of the sensors during a test.
3. The Monte Carlo simulation runs as many random cases as the user considers necessary, providing the same number of results. Consequently, the user can analyze a histogram of uncertainty rather than a single value.

The uncertainty in the amplitude and phase of the dynamic displacements and forces will be represented as gaussian distributions because the analysis in [10] showed the results by the TSM are best suited to represent the propagation of uncertainties with these distributions. The mean of the distribution will be assigned to the “reference” values of displacements and forces, while the uncertainty values in table 2.2 will be assigned as 2.24 times the standard deviation, to replicate confidence intervals of 97.5% as reported in [3]. Figure 2.3 shows the applied steps by this analysis, in Matlab, to propagate the random error (simulated by the random generator

functions in Matlab) of the dynamic forces and displacements and find the uncertainty estimations for the dynamic coefficients. The selected number of simulations was 1,000,000 and the acceptance criteria was that for five simulation processes the upper and lower limits of the confidence interval (97.5%) had to be within ±1% of their average.

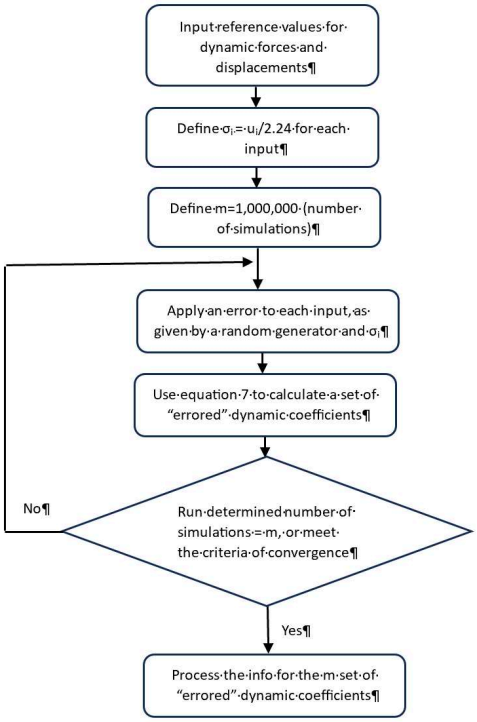

Figure 2.3: Flowchart for uncertainty estimations by the MCM

Figures 2.4, 2.5, and 2.6 presents the histogram of the main coefficients, for the three bearing cases in table 2.1, when uncertainty is estimated by the MCM. All histograms are asymmetric, confirming the finding in the previous analysis. For example, the asymmetric uncertainty estimated by the MCM for K_{yy} -bearings case 1 (figure 2.4b) is 16.5% to the left of the "reference" coefficient, and 24.6% to the right; while the symmetric uncertainty estimated by the TSM is 20%. The difference in the estimations is nearly identical to that previously attributed to the missing higher-order terms (3.8%) not included in the TSM.

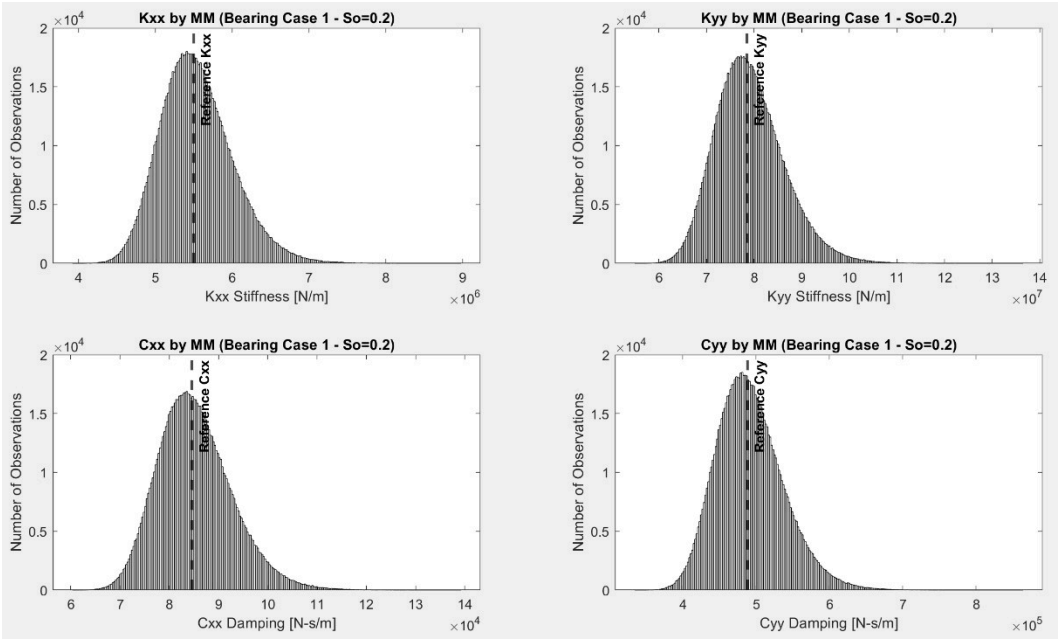

Figure 2.4: Histogram of main coefficients, for bearing case3, by the MCM

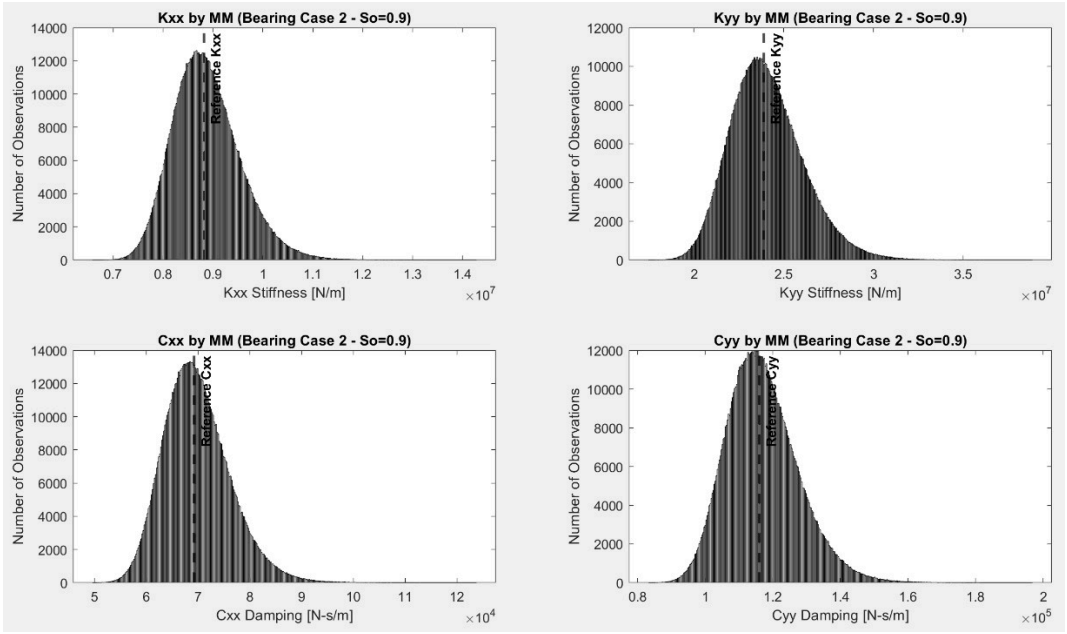

Figure 2.5: Histogram of main coefficients, for bearing case 2, by the MCM

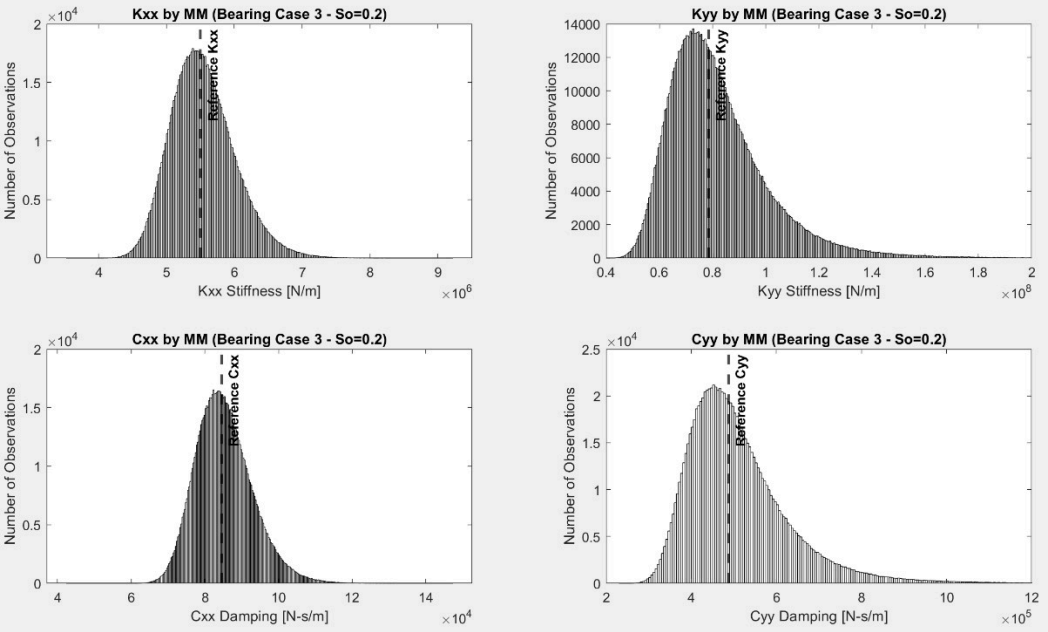

Figure 2.6: Histogram of main coefficients, for bearing case3, by the MCM

2.2.3 Random uncertainty of instruments in the frequency domain.

Previous uncertainty estimations of single-sample single-frequency dynamic coefficients [3, 11, 18, 19] have applied the resolution of the sensors as the random uncertainty to be propagated. However, the magnitudes of resolution provided by the sensors' manufacturers are in the time domain, and no consideration has been given to the fact that random uncertainty of the instruments (in the time domain) is propagated over data in the frequency domain. This section presents an analysis in which the random uncertainty of the instruments is first propagated in the time domain, and later transformed to the frequency domain, which is more realistic. Results will also show this analysis has the feature of producing significantly smaller uncertainty estimations for the dynamic coefficients.

The data from dynamic displacements and forces is collected in the time domain at equal intervals of time, and this is known as the sampling rate or frequency, for example 1,000 samples/sec. Once data is collected, it will be processed in order to facilitate the analysis, and

one of these processes is the Digital Fourier Transform (DFT), which converts the time domain (amplitude vs time) data into a frequency domain (amplitude vs frequency) spectrum.

The data of an ideal harmonic displacement, with a frequency of 15 hertz and an amplitude 12.5 μm, captured by an ideal displacement sensor, with no electrical noise, at a sampling rate of 1,000 samples/sec, would look, in the time domain, as shown in figure 2.7a. Nonetheless, the real situation is that the random uncertainty of the sensor produces uncertain measurements within the area indicated by the bars in figure 2.7b, despite the physical signal could be perfectly harmonic. The final result is that the obtained measurements could display innumerable random variations of the signal, within the area by the bars, given by the random error of the instrument at each reading. Now, if the set of data from figure 2.7a and a set of data from figure 2.7b are processed by a DFT, they look, in the frequency domain, as shown in figure 2.8. It can be seen that the DFT, for the ideal set of data (on the left side), is identifying that at 15 Hz the amplitude is exactly 12.5 μm (100% reliability); and surprisingly, the DFT is identifying, for the real set of data (on the right side), an amplitude of 12.49 μm (99.9 % reliability), despite the fact that each data point was corrupted in the time domain with a random gaussian error of ±2.5 μm (±20% or more of the true displacement!).

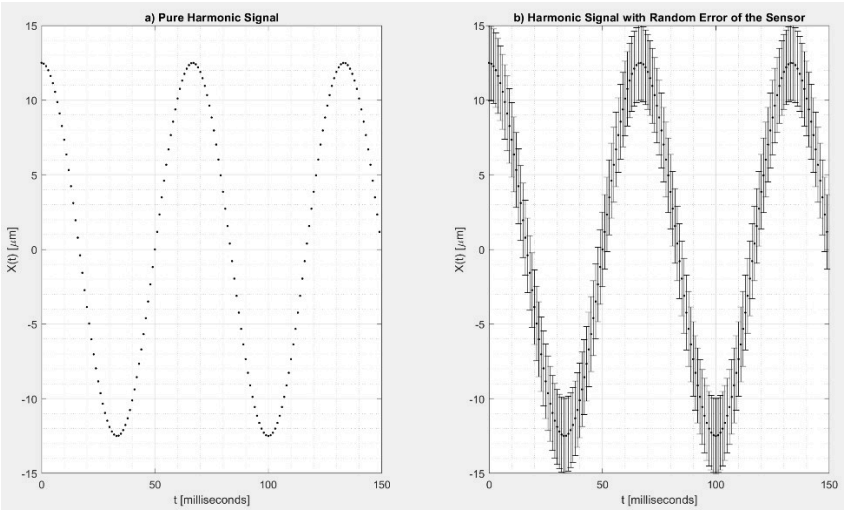

Figure 2.7: Harmonic signal measured by an ideal sensor vs a real sensor

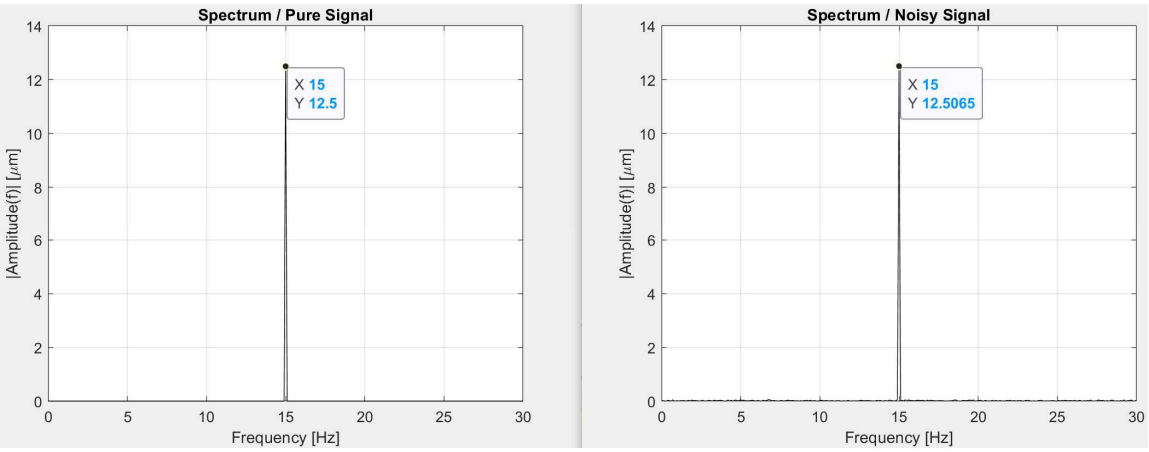

Figure 2.8: Spectrum for a noise-free and a noisy harmonic signal

Transforming an uncertainty of 20% of the reference signal into 0.1%, by converting data from the time to the frequency domain, is a promising result. Random processes can usually be characterized by their average and associated statistical uncertainties, and then the focus of this analysis will be to find the uncertainty of amplitude in the frequency domain, of all random signal to be measured, within the random error bars in figure 2.7b.

Before entering into the proposed method some particular details of the DFT will be briefly explained. The DFT is a discrete process, as its name says, and it performs the calculations with a limited amount of data points, corresponding to a limited amount of time *T* (time period), as selected. This *T* is important for the analysis in two ways:

- The general case is that *T* includes a non-integer number of cycles of the harmonic signal under analysis, and this requires an additional step of processing; however, by choosing *T*'s that contain exactly an integer number of the cycles the only processing required is the DFT; for example, a T of 0.2 secs contains exactly 3 cycles of 15 Hz. This analysis has selected only *T*'s that accommodate an integer number of the cycles in study, in order to have the DFT as the only process affecting the domain transformation of the uncertainty.

- The DFT is a discrete process and will not provide information about the continuous spectrum of frequencies, instead of that, it provides the amplitude at discrete frequencies, given by n*(1/*T*). Therefore, the selection of *T* is also a tool to influence how accurately the DFT calculates the amplitude for a single frequency; for example, the same *T* of 0.2 secs means the amplitudes will be calculated at discrete steps of 5 Hz (1/0.2), which is adequate when the signal is oscillating at 10 or 15 Hz. In order to avoid further processes, this analysis will also select *T*'s that provide the discrete frequencies in study, that is, 15 and 37.5 Hz.

Now that conditions for *T* are determined, the steps of the method to perform the conversion to the frequency domain, of the random uncertainty of an instrument measuring a harmonic signal, are defined, as follows:

1. Determine, from the test measurement, the amplitude and frequency of the harmonic signal to analyze.
2. Define quantitively the frequency distribution of the uncertainty to be applied to the harmonic signal; for example, setting the value of the standard deviation is enough for a gaussian distribution.
3. Determine the sampling rate at which the harmonic signal is being captured, during the test.
4. Determine the time period *T* to be analyzed by the DFT.
5. Calculate the discrete points of the harmonic signal, determined at step 1, at each time interval given by the sampling rate, and for the total time period *T*. The assistance of a math software is useful for this and subsequent steps.
6. Generate individual random values, according to the features determined in step 2, and apply each individual value to each individual discrete point calculated in step 5.
7. Apply the DFT to the data points generated in step 6.

8. Collect the amplitude information at the frequency in analysis.
9. Repeat steps 6, 7, and 8 for as many times as required, until a convergence criterion is achieved on the spread of all data collected from step 8.

To exhibit the efficacy and utility of the proposed method, an example signal is analyzed, performing the proposed steps. The characteristics to be obtained from steps 1, 2, 3, and 4 are defined in table 2.5. Three time periods were chosen in step 4, to evaluate the impact of this variable on the uncertainty transformation.

Signal to Analyze			
Signal Amplitude (Step 1)	12.5 µm		
Frequency of Signal (Step 1)	15 Hz		
Uncertainty Distribution (Step2)	Gaussian		
Uncertainty Magnitude (Step2)	±2.5 µm		
Standard Deviation (Step2)	1.1160 µm		
Sampling Rate (Step 3)	1000 points/sec		
Time Period (Step 4)	0.2 sec	1 sec	3 sec

Table 2.5: Features of the simulation to convert data from time to frequency domain

Table 2.6 shows the random process was repeated 1,000 times, for each *T*, until the σ calculated for this population, in the frequency domain, met a convergence criterion of *σ*±3%. The ratio between this converged *σ* (frequency domain) and the defined *σ* (time domain) in step 2 of the analysis, also shown in table 2.6, indicates that the domain transformation reduced the random uncertainty even to 2.6% of the value in the time domain. Therefore, a relevant benefit of applying this proposed analysis is that the uncertainty estimations of the experimental dynamic coefficients will become smaller than traditionally estimated (applying uncertainty in the time domain).

Additionally, these results indicate that selecting a longer *T* had an increased benefit in the reduction of the uncertainty region in the frequency domain. Even if there is some averaging in

the time domain for longer *T*'s; the fact that a T=0.2 secs, with only 3 cycles of the analyzed signal and minimum possibility of averaging, reached an uncertainty ratio of 10% the value in the time domain, seems to confirm that most of the reduction is due to the domain transformation.

	Frequency Domain			Time Domain
Time Period	**0.2 sec**	**1 sec**	**3 sec**	
σ[µm]	0.1131	0.0498	0.0292	1.1160
Number of Simulations	1000	1000	1000	N.A.
Convergence Criteria	σ ± 3%	σ ± 3%	σ ± 3%	N.A.
$\sigma_{freq.\ domain} / \sigma_{time\ domain}$	0.10	0.04	0.026	1.0

Table 2.6: Results of converting uncertainty from time to frequency domain (DFT process)

Additional to the domain transformation, some techniques also perform averaging in the frequency domain, and it was reported by Burrows and Sahinkaya [29] an enhanced effect of signal averaging in the frequency domain, to reject noise. Then, this study also included an analysis with signal averaging in the frequency domain. The steps are as already proposed in this chapter, with the only difference that in step 7 a Power Spectral Density (PSD) with averaging blocks, as defined in [30], is applied, instead of the DFT.

	Frequency Domain			Time Domain
Time Period	**0.2 secs**	**1 sec**	**3 sec**	
Averaging Blocks	**20**	**20**	**20**	
σ [µm]	0.0230	0.0107	0.0067	1.1160
Number of Simulation	100	100	100	N.A.
Convergence Criteria	σ ± 3%	σ ± 3%	σ ± 3%	N.A.
$\sigma_{freq.\ domain} / \sigma_{time\ domain}$	0.02	0.01	0.006	1.0

Table 2.7: Results of converting uncertainty from time to frequency domain, using a PSD + 20 averaging blocks process

Table 2.7 shows the results when the signal in table 2.5 was analyzed with a PSD method, including 20 averaging blocks for the three different *T*. The ratio between the converged σ (frequency domain) and the defined σ (time domain) in step 2 of the analysis indicate that

PSD+averaging reduced the uncertainties to 2%, and even to less than 1% the values they had in the time domain. Averaging produced smaller uncertainty windows than the DFT, in the frequency domain, but in general, these results confirm the significant reduction of the uncertainty window by transforming this signal to the frequency domain. The improvement of averaging comes with the expense of gathering more data in a longer time, and the consequent additional processing. For example, for the simulations with the DFT the longest simulated time of data acquisition was 3 secs, and this reduced the uncertainty to 3%, meanwhile, the signal averaging analysis reduced the uncertainty to less than 1%, but it was required to simulate 60 seconds of data points (a time window 20 times larger).

2.3 RESULTS

This section will discuss the results of the uncertainty estimations under the different methods, and for all cases the range of uncertainty results reported in [3] and shown in table 2.8 should be considered as the reference for this study. Uncertainties will be expressed in percentages (relative to the reference value of the coefficient), and results only include the main dynamic coefficients. The "reference" cross-coupled dynamic coefficients calculated by Maxbrg were of such a small magnitude (less than 1% the value of the smallest main stiffness or damping coefficient), that the uncertainty estimation for them was extremely sensitive and out of useful ranges.

	Uncertainty in [9] [%]
K_{xx}	±8 -±82
K_{yy}	±5 – ±45
C_{xx}	±9 – ±92
C_{yy}	±7 – ±82

Table 2.8: Uncertainty estimations reported by Wygant et al

Figure 2.9 shows the results of uncertainty estimations using the TSM. Test and bearing conditions were replicated from [3], however, some assumptions were made due to unreported information, for example specific static and dynamic loads. Despite these assumptions the estimations of uncertainty are well within the range of uncertainty reported in [3], providing confidence the assumptions were adequate. Although uncertainty was applied in magnitude and phase to each dynamic force and displacement, the uncertainty in the magnitude of dynamic displacement is by far the most important contributor to the uncertainty of the coefficients.

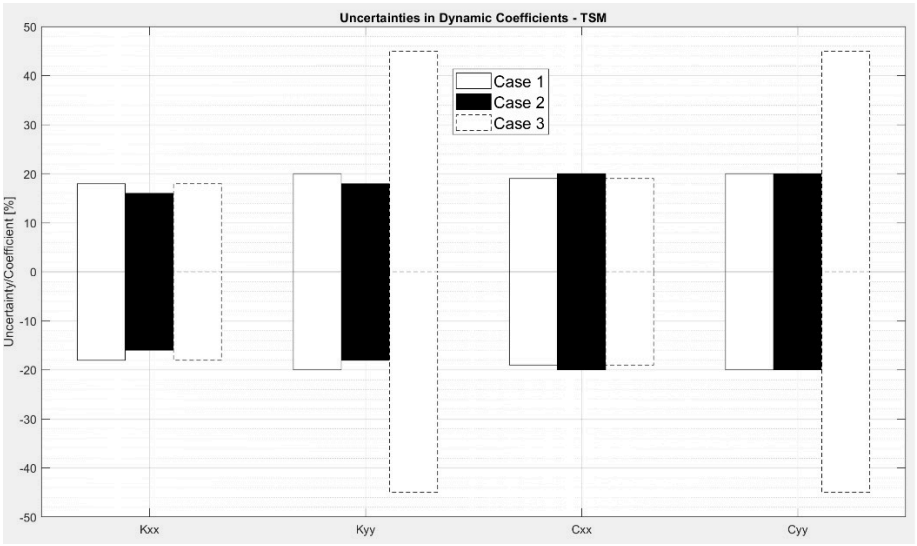

Figure 2.9: Uncertainties of dynamic coefficients by the TSM

Figure 2.10 shows the results of uncertainty using the MCM and the flowchart of figure 2.2. It was stressed in a previous section that one feature of the MCM is that it uses no assumptions to simplify the calculations, then it is a reliable method to replicate the real behavior of the system. Therefore, the results of the MCM are very useful to validate the findings on the non-linearity and asymmetry of the coefficients, and how they affect the accuracy of the estimations by the TSM.

For K_{xx}, the TSM predicted that the uncertainty was 16-18% for the three bearing cases, but the analysis showed that the weight of second order terms was around 3.0-3.4% (opposite sign).

Therefore, it is expected a more accurate uncertainty of K_{xx} to be around 13-15%, and that is precisely the range that the MCM is estimating for the three cases: 13.9-15.5%.

For K_{yy} and C_{yy}, the TSM predicted the uncertainty was around 45% for bearing case 3, and the analysis showed the weight of second-order terms is around 20.5% (opposite sign). Therefore, it is expected a more accurate estimation for these two coefficients to be close to 25%, and again, that is the estimation by the MCM: 30-31%.

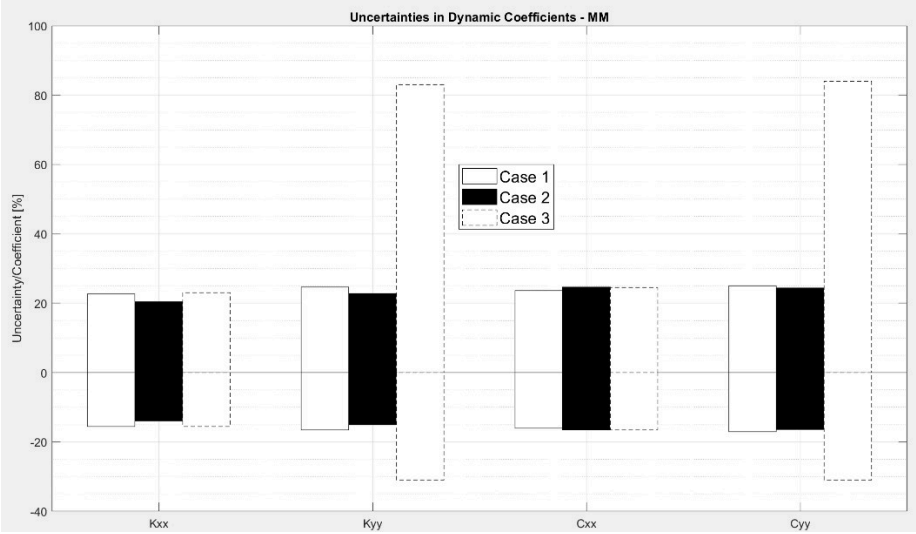

Figure 2.10: Uncertainties of dynamic coefficients by the MCM

Similar lines of reasoning can be followed for C_{xx} in all bearing cases, and K_{yy} and C_{yy} in cases 1 and 2, leading to the same finding: the MCM is providing more accurate uncertainty estimations for the coefficients and it is validating that the estimations by the TSM are inaccurate due to the existence of higher-order terms (non-linearity effect).

By comparing results between the MCM and the TSM, there is also another finding: the MCM is providing evidence the uncertainty range for the coefficients is asymmetric. For example, for K_{yy} in bearing case 3, the MCM predicted an asymmetric range of (-31) % to (+83) %. Meanwhile, the TSM is just predicting a single symmetric value of 45%, so on one side it is overpredicting the

estimation by 14% and on the other side is underpredicting the estimation by 38%, which is a significant underprediction. Similar findings can be made when comparing results for all coefficients and bearing cases. Therefore, the results of the MCM validate that another source of inaccuracy for the TSM is its inability to capture asymmetric uncertainty behavior when it exists.

Figure 2.11 shows results of uncertainty estimations of dynamic coefficients, when uncertainty in dynamic displacements is propagated from the frequency domain, by previously having used the conversion simulation (DFT process) explained in the analysis section. In general, figure 2.11 shows that in all cases the uncertainty estimations were reduced to values below 6%, which is a great benefit for the report of the dynamic coefficients. It is seen that the worse the estimations by propagating uncertainty in the time domain the greater the reduction by propagating it in the frequency domain; for example, K_{yy} was previously estimated to have uncertainties of 84 and 83% (figure 2.10), but now those values are 6 and 5%, by transforming displacement data with a DFT with a T that includes 3 cycles (figure 2.11a). If the T is increased to contain 45 cycles of the displacement signals (figure 2.11b), the uncertainty estimations of the coefficients decreased further to a range between 2 and 4%, for the main coefficients. These results indicate that increasing the time period T from 3 to 45 cycles reduced the uncertainty estimations, although not exactly in a linear relation to the increase in T; for example, r for K_{yy} and C_{xx} the reduction was clearly evident, while for K_{xx} and C_{yy} the reduction was less notorious. Overall, uncertainty estimations in figure 2.11 show reductions to a range between 5 and 15% of the values in figure 2.10, confirming the utility of considering the uncertainty windows of the dynamic signals in the frequency domain.

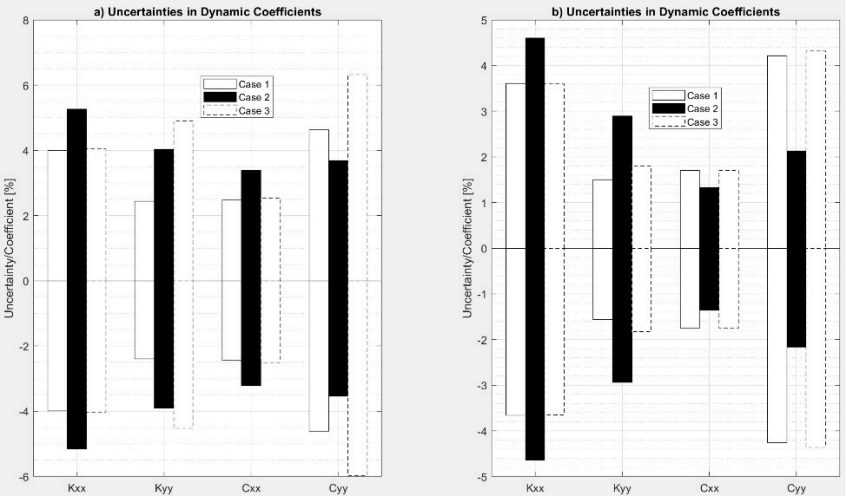

Figure 2.11: Uncertainties of dynamic coefficients when random uncertainty of the instrument is evaluated in the frequency domain by a DFT

Table 2.9 shows the uncertainty estimations for the dynamic coefficients when the transformation to the frequency domain is achieved using a PSD and 20 averaging blocks. These uncertainty estimations also showed a great reduction, compared to the estimations in figures 2.9 and 2.10, and in general all of them are below 5%, with the estimations for C_{xx} even between 1 and 2%. However, it is seen that the effect, on the uncertainty estimations, of increasing the time period from 0.2 to 3.0 seconds was only marginal. Moreover, when the uncertainty estimations for a T of 3.0 seconds in figure 11 (using a conventional DFT) are compared against the estimations in table 2.9 (using 20 averaging blocks), it can be seen that the differences are minor.

		Uncertainty by averaging 20 displacements blocks in the Frequency Domain using a PSD [%]			Uncertainty in [9] [%]
		Case 1	Case 2	Case 3	
T=3 cycles	K_{xx}	(-3.65) – (+3.58)	(-4.64) – (+4.59)	(-3.63) – (+3.58)	±8 -±82
	K_{yy}	(-1.45) – (+1.51)	(-2.92) – (+2.87)	(-1.62) – (+1.58)	±5 – ±45
	C_{xx}	(-1.72) – (+1.66)	(-1.32) – (+1.29)	(-1.71) – (+1.65)	±9 – ±92
	C_{yy}	(-4.24) – (+4.18)	(-2.13) – (+2.08)	(-4.28) – (+4.23)	±7 – ±82
T=45 cycles	K_{xx}	(-3.62) – (+3.56)	(-4.61) – (+4.54)	(-3.63) – (+3.57)	±8 -±82
	K_{yy}	(-1.48) – (+1.42)	(-2.85) – (+2.80)	(-1.49) – (+1.43)	±5 – ±45
	C_{xx}	(-1.68) – (+1.63)	(-1.11) – (+1.06)	(-1.69) – (+1.63)	±9 – ±92
	C_{yy}	(-4.24) – (+4.17)	(-2.03) – (+1.97)	(-4.22) – (+4.18)	±7 – ±82

Table 2.9: Uncertainty estimations using data converted to the frequency domain by a PSD + 20 averaging blocks process

2.4 CONCLUSIONS

This study presents an analysis on uncertainty estimation of experimental dynamic coefficients obtained by single-sample single-harmonic frequency tests.

- The Taylor Series Method has been examined for specific conditions, and it has been shown, for the first time, that the non-linearity of the dynamic coefficients with respect to the dynamic forces and displacements is producing detectable inaccuracies in the uncertainty estimations by this method.
- The analysis on the TSM also shows, for the first time, that the non-linearity is also expressed as an asymmetric behavior of the uncertainty that the TSM was not developed to capture, which adds more inaccuracies to the uncertainty estimations of dynamic coefficients.
- The amount of inaccuracy of the uncertainty estimations by the TSM will depend on the specific dynamic conditions of the test and the resolution of the used sensors, but for example for K_{yy}, in one of the simulated cases, the TSM predicted an uncertainty of 45%, while more accurate estimations provided by the MCM showed an asymmetric range of (-31)% to (+84)%. Although the non-linearity of the coefficients will always affect the uncertainty estimations by the TSM, the level of impact will be different depending on the specific hardware and test conditions of each particular test.
- In case the TSM is the selected method to estimate the uncertainty on the dynamic coefficients, it is advisable to quantify the effect of the non-linearities on the accuracy following a similar analysis, as in this study.
- The Monte Carlo Method is presented as an alternative method to estimate the uncertainties in experimental dynamic coefficients. It is analyzed that one superior feature of this method is that it makes no assumptions, then it faithfully replicates the real behavior of the model relating coefficients and dynamic forces and displacements. Uncertainty estimations by the MCM can be considered to be more accurate, as they faithfully represent the nonlinearities and

asymmetries of the dynamic coefficients, without any additional correction or inspection of accuracy.

- Previous uncertainty estimations for single-sample single frequency tests have applied the resolution of the displacement and force sensors as one source of uncertainty, and this is equivalent to apply the range of the resolution in the time domain. However, this study proposes one analysis to transform that value of resolution from the time to the frequency domain. The analysis works with different conversion methods, but in this study the Discrete Fourier Transform (DFT) and Power Spectrum Density (PSD) with averaging were the selected tools. Conversion to the frequency domain has shown to be useful in reducing the value of the uncertainty region in the output of sensors to even less than 1% the value in the time domain, for the specific conditions analyzed in this study.
- The method proposed in this study, to transform the uncertainty of sensors from the time to the frequency domain, has shown to be highly beneficial to reduce the uncertainty estimations of the dynamic coefficients. The uncertainty analysis in [3], applied the uncertainty of the sensors in the time domain, produced uncertainty estimation in a range from 5 to 82%. However, the analysis in this study indicates that by taking the uncertainty data to the frequency domain, using the novel method proposed here, the uncertainty estimations could actually be less than 6% for all the coefficients, and even less than 2% for K_{yy} and C_{xx}, which is certainly a remarkable improvement in the accuracy of the coefficients.
- The analyses showed that increasing the time periods and performing PSD and averaging in the frequency domain had an evident and increased benefit in reducing the region of uncertainty, when converting to the frequency domain. Nonetheless, this additional reduction of the uncertainty region was not always reflected in additional reductions on the uncertainty estimations of the dynamic coefficients, or at least not in significant reductions. Therefore, the longest time period or the longest averaging number will not always be the most efficient process, as to uncertainty estimations.

- Uncertainty analyses are also a valuable tool in selecting the adequate sensor technology for a test rig, during a stage of design or a refurbishment. However, one conclusion that could be extrapolated, from the analyses and results reported in this chapter, is that for experimental dynamic coefficients the analytical conversion of dynamic data to the frequency domain is a key aspect to consider and not only the resolution of the sensor in the time domain.

Chapter 3

Identification of Dynamic Coefficients of Fluid Film Journal Bearings Supporting a Flexible Rotor

The safe and reliable operation of rotating machinery depends on accurate rotordynamic analyses. Especially important for high-speed applications is a lateral rotordynamic analysis, which is dependent on the geometry and elastic properties of the rotor and strongly influenced by the dynamic characteristics of the fluid film journal bearings that support the rotor. Therefore, the use of accurate dynamic characteristics of the journal bearings is a key requirement to obtain accurate lateral rotordynamic predictions [1,6].

The dynamic characteristics of a fluid film journal bearing are usually represented by a set of four stiffness and four damping coefficients [7,9]. Most experimental techniques to obtain these eight coefficients relate measurements of dynamic displacements (vibration) and dynamic forces (excitation), under the ideal assumption that they act at the midplane of the bearing [10]. Some conditions suitable for this ideal assumption may be feasible at research facilities, such as low loads, short rotors and bearings, and rotating speeds far away from any critical speeds. These conditions reduce or eliminate the relevance of the axial location of the displacement sensors by producing a rigid or quasi-rigid rotor such that the lateral vibrations are nearly the same at the

bearing midplane as at the sensor location. However, in most real machines the displacement sensors are not located at the bearing(s) midplane and the rotor exhibits flexible behavior. The consequence of these real conditions is that the measured vibrations have different amplitude and phase than the vibration actually occurring at the bearings midplane, and this will be reflected as a significant error in the identified dynamic coefficients.

The purpose of this chapter is to propose a novel method for accurately identifying the dynamic coefficients of fluid film journal bearings in the presence of sensor miscollocation and rotor flexibility. The proposed method is conceptually applicable to almost any configuration of rotor and fluid film journal bearings, unlike previous methods that are applicable to the specific configuration for which they were developed. The wider applicability of the novel method proposed here is shown with three different rotor-bearing configurations. The method is numerically applied to a first case with a single test bearing floating around a test rotor, similar to many test rigs, and to a second and third case where the test rotor is supported by two identical or different test bearings (as is the case in most real machines).

Even though sensor miscollocation along with rotor flexibility can have a significant impact on the identification of accurate dynamic coefficients, the literature on this topic is very limited. Some methods that include miscollocation have been presented in the past, but with very limited scope of applicability. For example, Brockwell and Dmochowsky [4] asserted that the dynamic coefficients were not accurate, unless the identification model included the miscollocation and the rotor flexibility. Therefore, the identification model included these two features; however, the applicability was limited to a configuration with a floating bearing housing oscillating around a rotor and to journal bearings with non-existent cross-coupled stiffness and damping dynamic coefficients.

De Santiago and San Andres have presented two methods [5, 31] to identify the coefficients of two identical fluid film journal bearings supporting a flexible one-inch diameter rotor. This method is based on building a matrix model of the rotor flexibility and then applying a specific

reordering of the matrix system. This specific reordering leads to calculating the hydraulic bearing force acting on the specific nodes assigned at the midplane of the bearings. Finally, the dynamic coefficients are identified by relating these calculated forces with the displacements at the same nodes. The vibration measured by the sensors was applied to these nodes in [31] assuming the miscollocation was negligible. Meanwhile, an approximation was implemented in [5] to correct the miscollocation, although specific details were not provided. Unfortunately, the applicability of the method is limited to the rotor-bearing configuration considered in the analysis and to the condition that both bearings have identical dynamic behavior. Despite the miscollocation was included in [5], no details were provided to replicate the approximation.

A different approach has been presented by Tiwari et al [32] for the identification of stiffness and damping coefficients, including the rotor flexibility. This analysis was applied to a 12 mm diameter rotor supported directly by three rolling bearings, which rested on supports with some level of flexibility and damping. The flexible behavior of the rotor was represented by a finite element model, and using roller bearings allowed for a more straightforward measurement of the vibration at the bearing locations by using accelerometers on the bearing housings. However, this measurement setup is not directly applicable to identifying dynamic coefficients of fluid film bearings, as the bearing housing vibration is different than the rotor vibration, due to the relative displacement between the bearing housing and the rotor in fluid film bearings.

A configuration with a test rotor supported by two fluid film journal bearings with a bearingless motor located in the middle of the gap between the two bearings, was used by Chen et al [33] to find the dynamic coefficients of the fluid film bearings and the current-force and displacement-force coefficients of the motor. The rotor flexibility is represented by a finite element model, and the identification process is performed by changing the Proportional Integral Derivative (PID) control parameters of the bearingless motor to obtain and measure different rotor responses (vibration) and control currents. These responses are related to the unknown dynamic coefficients through a proposed regression equation that finally allows their calculation. However, it is not

completely clear how the miscollocation is considered in the regression, and the method is applicable only to the analyzed configuration, which includes a bearingless motor at a specific location.

The objective of this chapter is to contribute to the limited literature on this topic, by proposing a new method of increased accuracy to identify all eight dynamic coefficients for fluid film journal bearings. More specifically, this chapter contributes in the following aspects:

- To the author's knowledge, the proposed identification method is the first time in the open literature that sensor miscollocation is clearly included in a standard way to increase the accuracy of the eight identified dynamic coefficients of a fluid film journal bearing.
- The identification method presented in this chapter is the first that simultaneously includes the rotor flexibility and the miscollocation of displacement sensors to identify the eight dynamic coefficients of a single fixed-geometry fluid film journal bearing tested in a floating bearing housing. The floating housing is probably the most common configuration for research test rigs evaluating the dynamic characteristics of fluid film journal bearings [4, 11, 22, 34, 35]. The method in [4] did include the rotor flexibility and the miscollocation, but only identified the four main dynamic coefficients.
- The identification method in this chapter is also applicable to a configuration with a flexible rotor supported by two identical or different fluid film journal bearings, including any real location of the displacement sensors, unlike other methods. The method leads to the identification of either the eight (for identical bearings) or sixteen (for two different bearings) dynamic coefficients of fixed-geometry fluid film journal bearings. This capability is important, as this configuration has been used in research studies [36-38], and is a common configuration for rotating machines in operation.

The method in this chapter uses a mathematical matrix model to represent the flexible behavior of a rotor, based on Timoshenko's beam theory, similar to the standard approach implemented by other studies [5, 31, 32, 33]. However, the novelty of the approach here is to

consider that at any axial location of the rotor, the relative dynamic displacement (in the frequency domain) between the rotor and the bearing housing, produced as a response to a harmonic excitation applied to the rotor-bearing(s) system, is a function of the dynamic coefficients of the fluid film journal bearing(s). The advantage of this new approach is that it eliminates the need to perform the identification of the dynamic coefficients from displacement data at the midplane of the bearings and instead opens the possibility of using data from any axial location of the rotor. Therefore, this new approach appropriately includes data from any location where the sensors may be measuring the dynamic displacements and eliminates the error of identifying the coefficients with displacement sensors miscollocated with respect to the midplane of the bearings.

This novel approach uses a Newton-Raphson iterative process, due to the non-linearity of the dynamic coefficients [39], in which a converging process should lead to a successful identification of the values of the dynamic coefficients. The success of the iterative process is controlled by the convergence, within certain tolerance margins, to some experimentally obtained reference measured displacements, at the sensor's locations, as the dynamic coefficients are being iterated upon.

The remainder of this chapter has the following structure: the next section presents the geometry of the rotors and details of the rotor-bearing(s) system used for the numerical analyses, this is followed by a description of the steps of the proposed method to identify the dynamic coefficients of the fluid film journal bearing(s), a results section shows the identified dynamic coefficients when this method is applied to several chosen examples in order to confirm its validity and utility, and finally, a conclusion section discusses the significant findings.

3.1 DESCRIPTION OF THE ROTOR-BEARING SYSTEMS

This section provides a description of the rotor-bearing(s) configurations used to show the validity of the new method proposed in this chapter to accurately identify the dynamic coefficients of fluid film journal bearings. These configurations are all based on actual machines that have

been used in testing and described in the open literature. The description includes the geometry of the rotor for each configuration, the axial location of the displacement sensors and fluid film journal bearings, and the characteristics of these fixed-geometry journal bearings. This information is provided for description purposes and for the matrix model of the flexible behavior of the test rotor.

3.1.1 Configuration 1: one fluid film journal bearing floating around a fixed flexible rotor.

A prevalent configuration in test rigs for identifying the dynamic coefficients of fluid film journal bearings [4, 11, 22, 34, 35] during the last 50 years has been a housing enclosing a single test fluid film journal bearing that is floating around a test rotor, where the rotor is supported by a pair of ball or roller bearings. However, despite the prevalence and long use of this configuration, the identification model still assumes a rigid behavior of the rotor, as pointed out by Tiwari [10].

The identification method proposed by this chapter is applicable to this floating-housing configuration and aims to increase the accuracy in the identification of the dynamic coefficients, by including the rotor flexibility and the sensor miscollocation.

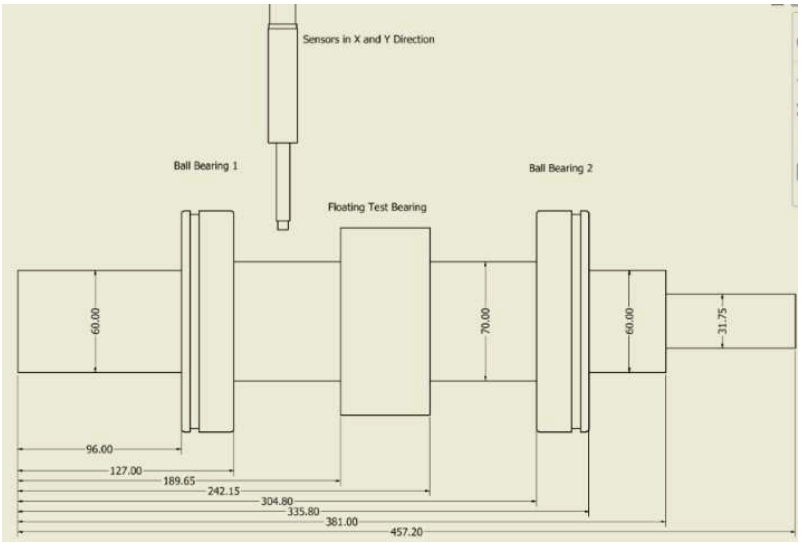

Figure 3.1: Rotor-Bearing System for Config. 1 (mm)

The analyzed rotor-bearing system for this configuration is shown in figure 3.1 and replicates the rotor dimensions of a real test rig [22] used in numerous studies to identify dynamic coefficients [3, 11, 40]. The test rotor was made of steel with a nominal diameter of 70 mm in the area of the floating test bearing. The dynamic excitation was applied to the floating bearing housing, by means of two independent actuators located at 90 degrees from each other such that the test bearing oscillated around the test rotor. Two displacement sensors, located axially at 45.7 mm from the midplane of the test bearing measured the relative displacement between the bearing and the rotor in two orthogonal directions *x* and *y*.

	Configuration 1
Journal Dia.	70 mm
L/D ratio	0.75
Offset	0.5
Cb	76 µm
Pad Thickness	10 mm
Speed	2,000 rpm
Static Load	5,427 N
Sommerfeld	0.1
Amplitude Oscillation	8 µm 0-Pk
Lubricant	ISO VG 32
Viscosity at 40° C	0.0256 N.s/m^2
Viscosity at 99° C	0.0043 N.s/m^2

Table 3.1: Specification for test bearing to identify in Configuration 1

	Configuration 1
Kxx [N/m]	1.0912e+08
Kxy [N/m]	-1.1865e+07
Kyx [N/m]	-2.6128e+08
Kyy [N/m]	3.6368e+08
Cxx [N-s/m]	4.2310e+05
Cxy [N-s/m]	-5.9399e+05
Cyx [N-s/m]	-5.9399e+05
Cyy [N-s/m]	2.3808e+06

Table 3.2: Reference Dynamic Coefficients for Configuration 1

The fluid film journal bearing to be analyzed with this Configuration 1 is a fixed geometry bearing with specifications as defined in table 3.1. The journal diameter is 70 mm and the axial

length of the bearing is 52.5 mm, for a 0.75 L/D (length/diameter) ratio. The specific load applied to this bearing is 1,489 kPa, which produces a noticeable flexible behavior of the test rotor. The dynamic coefficients to be used as a reference in this analysis are listed in table 3.2 and were numerically found using MAXBRG [23], an industry-standard finite element computer code for performing steady state thermo-elasto-hydrodynamic (TEHD) analysis of journal bearings.

3.1.2 Configuration 2: one flexible rotor supported by two identical fixed-geometry fluid film journal bearings.

This configuration has been used by several researchers to identify the dynamic coefficients of fluid film journal bearings [5, 31, 36, 37], but its use has been much less common than the floating bearing configuration. However, configuration 2 is of great practical interest as it represents a quite common configuration in industrial rotating machinery, where the rotor oscillates within the clearance of the two fluid film journal bearings that support it.

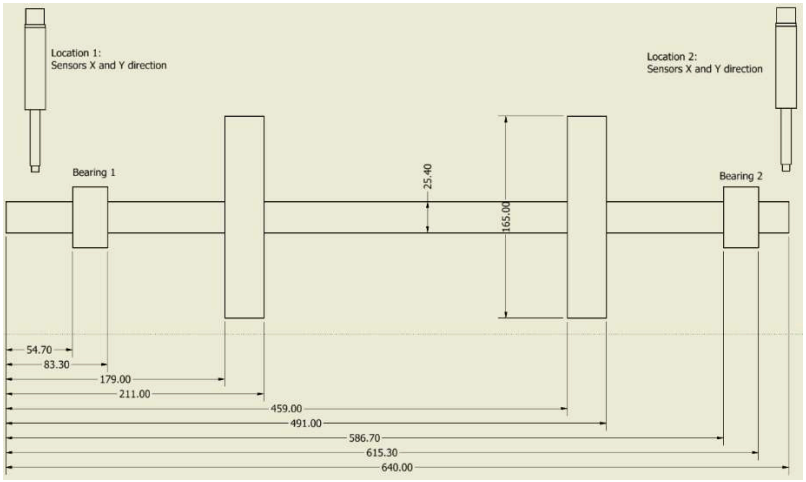

Figure 3.2: Rotor-Bearing System for Config. 2 (mm)

The analyzed rotor-bearing system for this configuration 2 is shown in figure 3.2 and replicates the dimensions of the slender rotor used by De Santiago and San Andres in [5, 31]. The rotor is made of steel with a nominal diameter of 25.4 mm throughout its length of 640 mm. The rotor also

includes two disks, 31.8 mm in length and 165 mm in diameter, mounted 280 mm from each other. The gap between the two bearings is 532 mm, for a ratio of this gap to rotor diameter of 20.9, which as pointed out in [31] is an extremely flexible rotor. The dynamic excitation is intended to be applied to the rotor at the locations of the two disks in the form of unbalance masses, impact forces with instrumented hammers, or magnetic bearings. Sets of two displacement sensors, located axially at 39.0 mm from the midplane of each of the fluid film journal bearings, measure the relative displacement between the bearings and the rotor, in two orthogonal directions *x* and *y*.

	Configuration 2
Journal Dia.	25 mm
Bearing Length	28.5 mm
Offset	0.5
Cb	38 µm
Pad Thickness	6.5 mm
Speed	2,000 rpm
Static Load	71 N
Sommerfeld	0.26
Amplitude Oscillation	6 µm 0-Pk
Lubricant	ISO VG 32
Viscosity at 40° C	0.0256 N.s/m^2
Viscosity at 99° C	0.0043 N.s/m^2

Table 3.3: Specification for test bearing to identify in Configuration 2

	Configuration 2
Kxx [N/m]	3.0338e+06
Kxy [N/m]	2.1950e+06
Kyx [N/m]	-6.9069e+06
Kyy [N/m]	3.1139e+06
Cxx [N-s/m]	2.5657e+04
Cxy [N-s/m]	-1.7452e+04
Cyx [N-s/m]	-1.7452e+04
Cyy [N-s/m]	6.8164e+04

Table 3.4: Reference Dynamic Coefficients for Configuration 2

The fluid film journal bearings to be analyzed with Configuration 2 are two identical fixed geometry bearings, with the specifications listed in table 3.3. The journal diameter is 25.4 mm and the axial length of each bearing is 28.5 mm, for a 1.12 L/D (length/diameter) ratio. The specific

load applied to each of these bearings is 88.2 kPa, which represents the pressure from half the weight of the rotor. The reference dynamic coefficients of these bearings are shown in table 3.4 and were numerically found using MAXBRG [23].

De Santiago and San Andres experimentally identified the free-free natural frequencies of this rotor, by hanging it from vertical ropes and impacting it along a horizontal plane to measure its response [5]. The first free-free natural frequency was experimentally identified at 196 Hz and the second natural frequency at 384 Hz. The numerical rotor model used in this chapter predicted the first and second natural frequencies at 192 and 370 Hz. Then, the predicted value is within 2.0% of the tested first natural frequencies and within 3.5% of the second one, verifying the accuracy of the rotor model used in this chapter.

3.1.3 Configuration 3: one flexible rotor supported by two different fixed-geometry fluid film journal bearings.

Configuration 3 has been rarely used by researchers to identify the dynamic coefficients of fluid film journal bearings [32, 38] due to the complexity of determining sixteen unknown coefficients while accounting for the flexibility of the test rotor. However, configuration 3 is of great practical interest as it is a common configuration in industrial rotating machinery, where the rotor oscillates within the clearances of the fluid film journal bearings that have different technical specifications.

The analyzed rotor-bearing system for this configuration is shown in figure 3.3 and exactly replicates the axial dimensions of the rotor used in configuration 2. The only difference with respect to the rotor in configuration 2 is that the rotor has a nominal diameter of 50.8 mm, instead of 25.4 mm. This rotor also includes two disks, 31.8 mm in length and 165 mm in diameter, mounted 280 mm from each other. The dynamic excitation is intended to be applied to the rotor at the location of these two disks, in the form of unbalance masses, impact forces with instrumented hammers, or magnetic bearings. Sets of two displacement sensors, located axially

at 39.0 mm from the midplane of each of the fluid film journal bearings, measure the relative displacement between the bearings and the rotor in two orthogonal directions *x* and *y*.

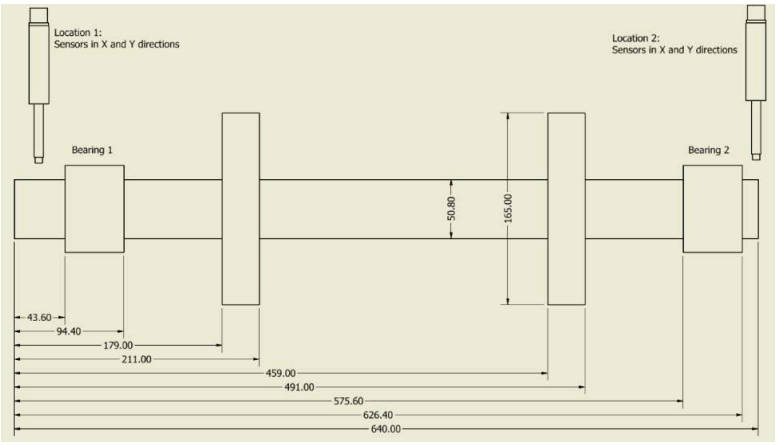

Figure 3.3: Rotor-Bearing System for Config. 3 (mm)

	Configuration 3 Bearing 1	Configuration 3 Bearing 2
Journal Dia.	50.8 mm	50.8 mm
Bearing Length	50.8 mm	50.8 mm
Offset	0.5	0.5
Cb	76 µm	91.5 µm
Pad Thickness	9 mm	9 mm
Speed	2,000 rpm	2,000 rpm
Static Load	2,670 N	2,670 N
Sommerfeld	0.075	0.05
Amplitude Oscillation	9 µm 0-Pk	7 µm 0-Pk
Lubricant	ISO VG 32	ISO VG 32
Viscosity at 40° C	0.0256 N.s/m^2	0.0256 N.s/m^2
Viscosity at 99° C	0.0043 N.s/m^2	0.0043 N.s/m^2

Table 3.5: Specifications for test bearings to identify in Configuration 3

	Configuration 3 Bearing 1	Configuration 3 Bearing 2
Kxx [N/m]	5.1068e+07	4.2091e+07
Kxy [N/m]	-2.4289e+06	-9.8166e+06
Kyx [N/m]	-1.1946e+08	-1.0626e+08
Kyy [N/m]	1.5512e+08	1.6557e+08
Cxx [N-s/m]	2.1125e+05	1.4732e+05
Cxy [N-s/m]	-2.8834e+05	-2.3144e+05
Cyx [N-s/m]	-2.8834e+05	-2.3144e+05
Cyy [N-s/m]	1.1530e+06	1.0109e+06

Table 3.6: Reference Dynamic Coefficients for Configuration 3

The fluid film journal bearings to be analyzed with Configuration 3 are two different fixed geometry bearings, with specifications listed in table 3.5. The journal diameter is 50.8 mm and the axial length of each bearing is 50.8 mm, for a 1.0 L/D (length/diameter) ratio. The specific load applied to each of these bearings is 1034 kPa, and the reference dynamic coefficients for these bearings are shown in table 3.6 and were numerically found using MAXBRG [23].

3.2 PROPOSED IDENTIFICATION METHOD

This section details the steps of the proposed novel method to identify the dynamic coefficients of fluid film journal bearings. The method has been divided into seven steps, with steps 1 and 2 detailing how to build the model of the rotor-bearing(s) system, step 3 sets the conditions of the experimental dynamic displacements to be used as the convergence reference for this method, and the remaining steps cover the application of the Newton-Raphson iteration.

3.2.1 Step 1: Modeling the flexibility of the rotor in two dimensions.

The flexibility of the rotor is modeled using the Timoshenko beam theory, while the disks in the rotor are considered rigid. The model includes gyroscopic effects and inertia of masses. The equations of motion for a generic flexible rotor are:

$$[\mathbf{M_R}]\ddot{\mathbf{Q}}_\mathbf{R} + [\mathbf{C_R}]\dot{\mathbf{Q}}_\mathbf{R} + \Omega[\mathbf{G_R}]\dot{\mathbf{Q}}_\mathbf{R} + [\mathbf{K_R}]\mathbf{Q_R} = \mathbf{F_R} \tag{3.1}$$

where $[M_R]$, $[C_R]$, $[G_R]$, and $[K_R]$ are the rotor matrices of inertia, damping, gyroscopic, and stiffness, respectively. F_R is a vector that includes all external dynamic forces applied to the rotor, and Q_R is the vector of displacements at the defined nodal locations of the model, and Ω is the rotational frequency of the rotor.

The vector F_R includes the excitation dynamic forces received directly by the rotor, the forces from the fluid film journal bearing(s), and any other dynamic force received directly by the rotor. Meanwhile, the vector Q_R provides the lateral displacements and the angular deflections for each node of the model, in two orthogonal directions *x* and *y*. Additionally, it is assumed that all dynamic

excitations are harmonic at a given frequency, and thus the dynamic response forces and displacements are also harmonic, with the same frequency as the excitation. Therefore, $\boldsymbol{F_R} = \boldsymbol{Fu_R}e^{i\omega t}$ and $\boldsymbol{Q_R} = \boldsymbol{Qu_R}e^{i\omega t}$, and by substituting these two expressions equation (3.1) is transformed to:

$$[\mathbf{K_R} - \omega^2\mathbf{M_R} + \mathrm{i}\omega\mathbf{C_R} + \mathrm{i}\omega\Omega\mathbf{G_R}]\mathbf{Qu_R} = [\mathbf{H_R}]\mathbf{Qu_R} = \mathbf{Fu_R} \tag{3.2}$$

where ω is the frequency of excitation, $\boldsymbol{Fu_R}$ is a vector with the complex amplitude of the harmonic excitations and $\boldsymbol{Qu_R}$ is a vector with the complex amplitude of the harmonic displacements at the nodal locations. For the cases analyzed in this chapter $\omega=\Omega$, that is the excitation forces are synchronous with the rotational frequency of the rotor.

One important consideration for an accurate rotor-bearing(s) model is that it should include nodes at the exact locations of: the fluid film journal bearings (preferably the midplane), the displacement sensors, and the points of application of dynamic forces to the rotor.

3.2.2 Step 2: Adding the bearing coefficients of the journal bearing(s) to the model.

For a fluid film journal bearing, the linearized oil-film bearing dynamic force in orthogonal directions *x* and *y* is represented by

$$\begin{bmatrix}\mathrm{F_X}\\ \mathrm{F_Y}\end{bmatrix} = \begin{bmatrix}\mathrm{K_{XX}} & \mathrm{K_{XY}}\\ \mathrm{K_{YX}} & \mathrm{K_{YY}}\end{bmatrix}\begin{pmatrix}\Delta\mathrm{X}\\ \Delta\mathrm{Y}\end{pmatrix} + \begin{bmatrix}\mathrm{C_{XX}} & \mathrm{C_{XY}}\\ \mathrm{C_{YX}} & \mathrm{C_{YY}}\end{bmatrix}\begin{pmatrix}\Delta\dot{\mathrm{X}}\\ \Delta\dot{\mathrm{Y}}\end{pmatrix} \tag{3.3}$$

where F_x and F_y are the dynamic hydrodynamic bearing forces, ΔX and ΔY are the dynamic displacements of the oil film at the midplane of the bearing, K_{xx} and K_{yy} are the direct stiffness coefficients in the *x* and *y* directions, K_{xy} and K_{yx} are the cross-coupled stiffness coefficients, C_{xx} and C_{yy} are the direct damping coefficients and C_{xy} and C_{yx} are the cross-coupled damping coefficients. Now, by using the same previous consideration that response forces and displacements are harmonic, then equation (3.3) is transformed to:

$$\begin{bmatrix}\mathrm{F_{Xb}}\\ \mathrm{F_{Yb}}\end{bmatrix} = \begin{bmatrix}\mathrm{K_{XX}} & \mathrm{K_{XY}}\\ \mathrm{K_{YX}} & \mathrm{K_{YY}}\end{bmatrix}\begin{pmatrix}\mathrm{X_b}\\ \mathrm{Y_b}\end{pmatrix} + \mathrm{i}\omega\begin{bmatrix}\mathrm{C_{XX}} & \mathrm{C_{XY}}\\ \mathrm{C_{YX}} & \mathrm{C_{YY}}\end{bmatrix}\begin{pmatrix}\mathrm{X_b}\\ \mathrm{Y_b}\end{pmatrix} = ([\mathbf{K_b}] + \mathrm{i}\omega[\mathbf{C_b}])\begin{pmatrix}\mathrm{X_b}\\ \mathrm{Y_b}\end{pmatrix} \tag{3.4}$$

where F_{xb} and F_{yb} are the complex amplitudes of the harmonic forces exerted by a fluid film journal bearing, and X_b, and Y_b are the complex amplitudes of the harmonic displacements of the oil film at the midplane of the bearing, in the x and y direction.

It is seen that the amplitude of the hydrodynamic force applied by each fluid film bearing is a function of the amplitude of the dynamic displacement in the area of the bearing.

The rotor-bearing(s) model should have nodes located, preferably, at the midplane of each bearing, as mentioned in step 1. Then, the displacements at the midplane of the bearings are contained in the vector $\boldsymbol{Qu_R}$. and the bearing forces can be represented as the multiplication of a diagonal matrix $\boldsymbol{H_B}$, the same size as the matrix $\boldsymbol{H_R}$, and the vector $\boldsymbol{Qu_R}$. The only non-zero entries in the diagonal matrix $\boldsymbol{H_B}$ will be the dynamic coefficients of each journal bearing interacting with the rotor at the location(s) corresponding to the position of the bearing node(s) in the vector $\boldsymbol{Qu_R}$. For example, if the displacements of the node located at the midplane of bearing 1 have the fifth position in the vector $\boldsymbol{Qu_R}$, then the dynamic coefficients of bearing 1 are located in the diagonal section corresponding to the fifth column or row of the matrix $\boldsymbol{H_B}$.

Then, the rotor-bearing(s) system can be mathematically represented by:

$$[\mathbf{H_R}]\mathbf{Qu_R} + [\mathbf{H_B}]\mathbf{Qu_R} = \mathbf{Fu_R} \tag{3.5}$$

$$[\mathbf{H_R} + \mathbf{H_B}]\mathbf{Qu_R} = \mathbf{Fu_R} \tag{3.6}$$

3.2.3 Step 3: Obtaining a set of reference measurement data with the displacement sensors.

The success of this proposed identification method is proven by the convergence of the Newton-Raphson iterations to a determined set of reference values. Then the harmonic displacement data collected in this step have the role of acting as that reference set.

Each individual displacement sensor provides two pieces of data for a harmonic displacement: an amplitude and a phase difference. Two orthogonal sensors at any axial location then provide four reference data points. The number of data points to be referenced depends on the number of dynamic coefficients to be identified: one data point is required for each coefficient. For

example, to identify the eight dynamic coefficients of the two identical fluid film journal bearings in configuration 2, eight data points must be measured and arranged as an 8x1 vector that will be called $\boldsymbol{R_{EF}}$, to have the information for eight independent equations. However, the method presented in this chapter requires the application of, at least, two independent harmonic excitations, due to the sensitivity of the method to high condition numbers as will be explained in step 6. Four data points could be obtained at a single axial location, provided there are two orthogonal sensors at that location, with the application of the first harmonic excitation. The other four data points could be measured at the same or at a different location with the application of the second independent harmonic excitation.

It is also important to have exact values for the rotor rotating speed, as well as the location, amplitude, and frequency of the applied harmonic excitations for which the reference data were collected, because these values are applied to the rotor-bearing(s) model in equation (3.6) when iterating for the dynamic coefficients in subsequent steps.

3.2.4 Step 4: Selecting a first estimation for the dynamic coefficients.

The Newton-Raphson iteration method is applied by using equation (3.6) and the data points measured in step 3, arranged as vector $\boldsymbol{R_{EF}}$. The iteration starts by assuming a good first estimate for the unknown dynamic coefficients. For example, this first estimation could be obtained by assuming a rigid rotor, or by using an estimate from a numerical bearing code. These estimated values are substituted in equation (3.6), together with the conditions of the two independent harmonic excitations selected in step 3. This substitution allows a numerical calculation of two vectors $\boldsymbol{Qu_{R1}}$.and $\boldsymbol{Qu_{R2}}$, in which each vector holds the data of the harmonic displacements generated as a response to each one of the applied harmonic excitations. $\boldsymbol{Qu_{R1}}$.and $\boldsymbol{Qu_{R2}}$ contain the amplitude and phase for each node of the rotor model; however, the method only requires the amplitude and phase at the location(s) selected during step 3, and by extracting this data a new vector, called $\boldsymbol{Q_1}$, is arranged. The size of $\boldsymbol{Q_1}$ is 8x1 if eight dynamic coefficients are being

identified (following the same example in step 3), or 16x1 if the dynamic coefficients of two different bearings are being identified.

3.2.5 Step 5: Calculating the change in Q_1 for a new set of dynamic coefficients.

It will usually be the case that the values of $\boldsymbol{Q_1}$ are different than the values of $\boldsymbol{R_{EF}}$, which means that the first estimate of the dynamic coefficients is not correct. Then, each dynamic coefficient should be individually incremented or decremented in a given amount, over the value used in step 4, and applied with the conditions of the two harmonic excitations to equation (3.6), and this leads to the numerical calculation of two new vectors $\boldsymbol{Qu_R}$. For example, if only the coefficient K_{xx} is incremented (keeping constant the values of all the other coefficients), two vectors $\boldsymbol{Qu_{R1A}}$.and $\boldsymbol{Qu_{R2A}}$ are obtained, and by extracting from them only the eight data points of interest, a new vector $\boldsymbol{Q_A}$ is formed. As the process is repeated for the other coefficients, seven new vectors are obtained (one per each incremented coefficient): $\boldsymbol{Q_B, Q_C, Q_D, Q_E, Q_F, Q_G, Q_H}$. These vectors can be arranged in such a way to obtain a matrix $\boldsymbol{[\Delta]}$ that contains the increment in each data point per the applied increment in each coefficient.

$$[\Delta]_{8x8} = [\mathbf{Q_A Q_B Q_C Q_D Q_E Q_F Q_G Q_H}]_{8X8} - [\mathbf{Q_1 Q_1 Q_1 Q_1 Q_1 Q_1 Q_1 Q_1}]_{8X8} \qquad (3.7)$$

3.2.6 Step 6: Performing a preconditioning in the matrix [Δ] and obtaining the condition number.

The steps presented in this chapter have been implemented in Matlab, allowing the use of a standard Matlab algorithm called “Equilibrate” [41], which preconditions the original square matrix $\boldsymbol{[\Delta]_{nxn}}$ to produce a new matrix $\boldsymbol{[B]_{nxn}}$. The objective of preconditioning a matrix is to improve the condition number and the stability of the linear system. The condition number of a matrix $\boldsymbol{A}$ is defined as the ratio of the largest singular value to the smallest singular value of that matrix, or it is also defined as the product of the norm of $\boldsymbol{A}$ and the norm of $\boldsymbol{A^{-1}}$. If A is part of a linear system of equations $\boldsymbol{Ax=b}$, then the condition number of $\boldsymbol{A}$ is a measure of how much error in the output $\boldsymbol{b}$ of the linear system is amplified when some error is contained in the input, $\boldsymbol{x}$. In the cases

analyzed here, the sources of error in the input are the uncertainty in the measurements and/or errors in the installation of the sensors, and they are reflected as deviations in the experimental measurements.

The specific preconditioning used here calculates three matrices ***R***, ***P***, and ***C***, such that ***B=R*P*[Δ]*C*** has values in its diagonal equal to 1, and values smaller than 1 in the other locations of the matrix. Different characteristics of the rotor and the journal bearings lead to a large range in the original condition numbers of ***[Δ]*** making it difficult to use this number to predict the suitability of the linear system. Therefore, a significant advantage of applying this preconditioning to ***[Δ]*** is to obtain a more standard condition number, despite the unique features of each rotor-bearing system.

The condition number of the preconditioned matrix, ***B,*** will be a better predictor of the linear system to provide a successful result. Condition numbers of ***B*** smaller than 150 are recommended, as this indicates that ***B*** or its original matrix ***Δ*** constitute a linear system that is an excellent candidate for the required convergence of the method. On the other hand, condition numbers larger than 150 may present difficulties in achieving the required convergence of the Newton-Raphson method, and/or difficulties in dealing with the usual noise or disturbances encountered during experimental measurements.

3.2.7 Step 7: Applying the Newton-Raphson method.

As mentioned earlier, the first estimation of the dynamic coefficients (step 4) will not lead to a perfect match with the vector ***Q1***, so an adjustment of the value of the coefficients is found with equation (3.8).

$$[\mathbf{R}] * [\mathbf{P}] * (\mathbf{R_{EF}} - \mathbf{Q_1}) = [\mathbf{B}] * \mathbf{Y_m} \qquad (3.8)$$

where matrices ***R***, ***P***, and ***B*** were defined in step 6, and vectors $\boldsymbol{R_{EF}}$ and $\boldsymbol{Q_1}$ were defined in step 4. $\boldsymbol{Y_m}$ is the unknown vector in the equation and contains the information of the adjustment

$\boldsymbol{\Delta_{COEF}}$ to apply to the first estimates of the dynamic coefficients and can be extracted with equation (3.9).

$$\Delta_{\mathbf{COEF}} = \mathbf{C} * \mathbf{Y_m} \quad (3.9)$$

Here, $\boldsymbol{\Delta_{COEF}}$ is a vector that contains the values by which each dynamic coefficient needs to be incremented or decremented, and it delivers the values in the same order in which vectors $\boldsymbol{Q_A}$ – $\boldsymbol{Q_H}$ are ordered in equation (3.7). For example, if $\boldsymbol{Q_A}$ is the first column and relates to the increment in K_{xx}, then the first location in $\boldsymbol{\Delta_{COEF}}$ is the increment to be applied to the estimation of K_{xx}; if $\boldsymbol{Q_B}$ is the second column and relates to the increment in K_{xy}, then the second location in $\boldsymbol{\Delta_{COEF}}$ is the increment to be applied to K_{xy}; and if $\boldsymbol{Q_E}$ is the fifth column and relates to the increment in C_{xx}, then the fifth location in $\boldsymbol{\Delta_{COEF}}$ is the increment to be applied to C_{xx}, and so on for the other columns and dynamic coefficients.

One important observation is that $\boldsymbol{\Delta_{COEF}}$ does not provide the increment of the dynamic coefficients in absolute value. Instead, it provides the increment in units of the increment applied in step 5. For example, if the increment applied to K_{xx} in step 5 was 500, and $\boldsymbol{\Delta_{COEF}}$ provided a value of 98.8 for K_{xx}, then the absolute increment to apply to K_{xx} is 500*98.8=49,400.

Successive applications of steps 5, 6, and 7 are required with a termination criterion for the convergence of the eight or sixteen dynamic coefficients involved. Successful convergence is given by obtaining a defined and small amount of error when comparing the output coefficients of two successive iterations. The convergence can be defined as an absolute (equation 3.10) or as a percentage comparison (equation 3.11).

$$|\mathbf{Defined\ Error}| \leq |\mathbf{Coef_{n+1}} - \mathbf{Coef_n}| \quad (3.10)$$

$$|\mathbf{Defined\ Error}\ (\%)| \leq \left|\frac{\mathbf{Coef_{n+1}} - \mathbf{Coef_n}}{\mathbf{Coef_{n+1}}}\right| \quad (3.11)$$

Alternatively, the progress of the convergence could be done by comparing vectors $\boldsymbol{Q_1}$ and $\boldsymbol{R_{ef}}$ at the end of each iteration.

3.3 RESULTS

This section presents the results of applying the method proposed here to identify the dynamic coefficients of fluid film journal bearings for the configurations detailed in the second section. As explained in step 3, the standard procedure for the method is to obtain the reference data points of the vector $\boldsymbol{R_{EF}}$ by experimental measurements. However, the results presented in this chapter come from numerically generating vectors $\boldsymbol{R_{EF}}$ using the same rotor-bearing(s) models developed in steps 1 and 2, which has the advantage of knowing exactly the reference dynamic coefficients that a successful identification method should estimate.

The results of applying the proposed method are presented highlighting two main aspects: the first is the convergence behavior of the Newton-Raphson iterations for the identification of the dynamic coefficients, and the second is the impact of random errors in the displacement measurements, that will be expressed as a range of random uncertainty in the identified dynamic coefficients.

The convergence behavior is presented in figures 3.4 to 3.11. In each figure the *y*-axis represents the value of the dynamic coefficient and the *x*-axis represents the number of the iteration. A dashed horizontal line shows the reference value of the dynamic coefficient to which a successful iteration process should converge. The initial guess for each coefficient, chosen in step 4 above, is reflected as the value assigned to iteration 1. Specific properties of convergence for each test case are discussed below.

Tables 3.7, 3.8 and 3.9 present the calculated uncertainty for the identified dynamic coefficients in each of the test configurations. The calculated ranges are the result of propagating a random uncertainty of ±0.18 μm in the amplitude and ±0.25 degrees in the phase of the displacement measurements, with a confidence interval of 95%. The uncertainty analyses were performed with Monte Carlo simulations leading to the identification of 10,000 different sets of dynamic coefficients [42]. The resolution value of 0.18 μm was taken from commercial catalogs

for an average Eddy-Current sensor (probe diameter= 5 mm) coupled with an average-resolution data-acquisition driver. The values of uncertainty reported in the tables can be used as a reference, but it is important to note that uncertainty analyses are specific to the actual case, and even for the same case uncertainty values could be smaller with the use of finer resolution sensors of the same technology (Eddy-Current), or with finer-resolution sensors of different technology, that are available in the market.

3.3.1 Results for configuration 1: one fluid film journal bearing floating around a fixed flexible rotor.

The results presented for this configuration were obtained with the numerical application of two independent synchronous harmonic dynamic excitations at the mid-plane of the bearing housing: one of 600 N in the *x*-direction, and one of 2,800 N in the *y* direction. In this configuration, the purpose is to identify the eight dynamic coefficients of a single fluid film journal bearing, and figures 3.4 and 3.5 show the progress of this identification.

Figure 3.4 shows the progress of the identification for the direct stiffness and damping coefficients, while figure 3.5 shows the identification for the cross-coupled stiffness and damping coefficients. Both figures show that by the fourth iteration all eight dynamic coefficients have converged, within an error of less than 0.001% to the reference values, and thus the proposed method has performed an accurate identification of the eight dynamic coefficients (direct and cross-coupled).

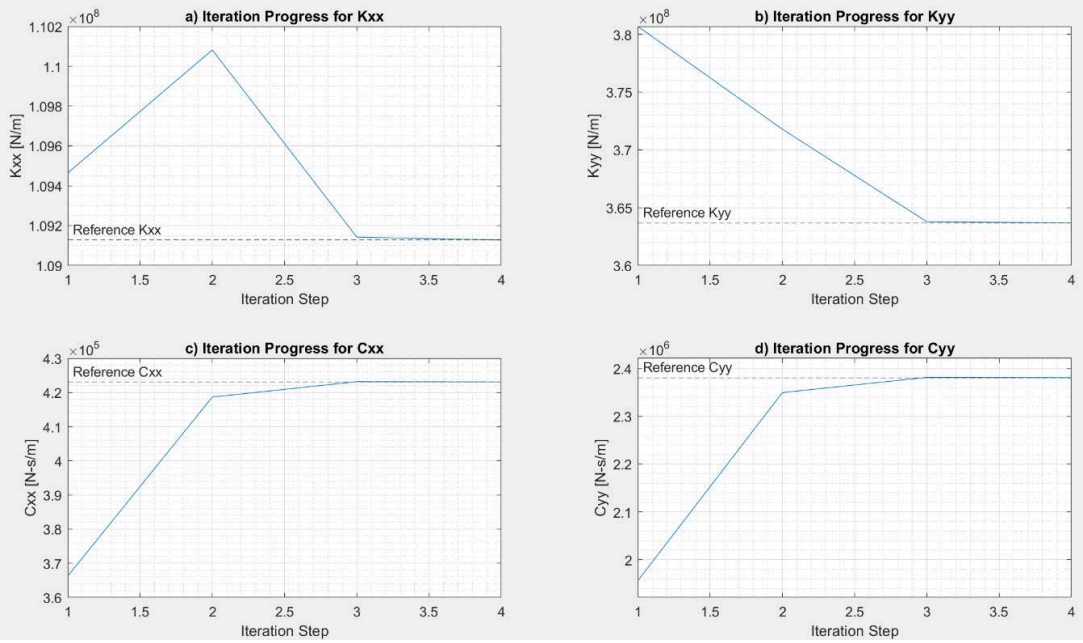

Figure 3.4: Evolution of iteration for the main dynamic coefficients (Config. 1)

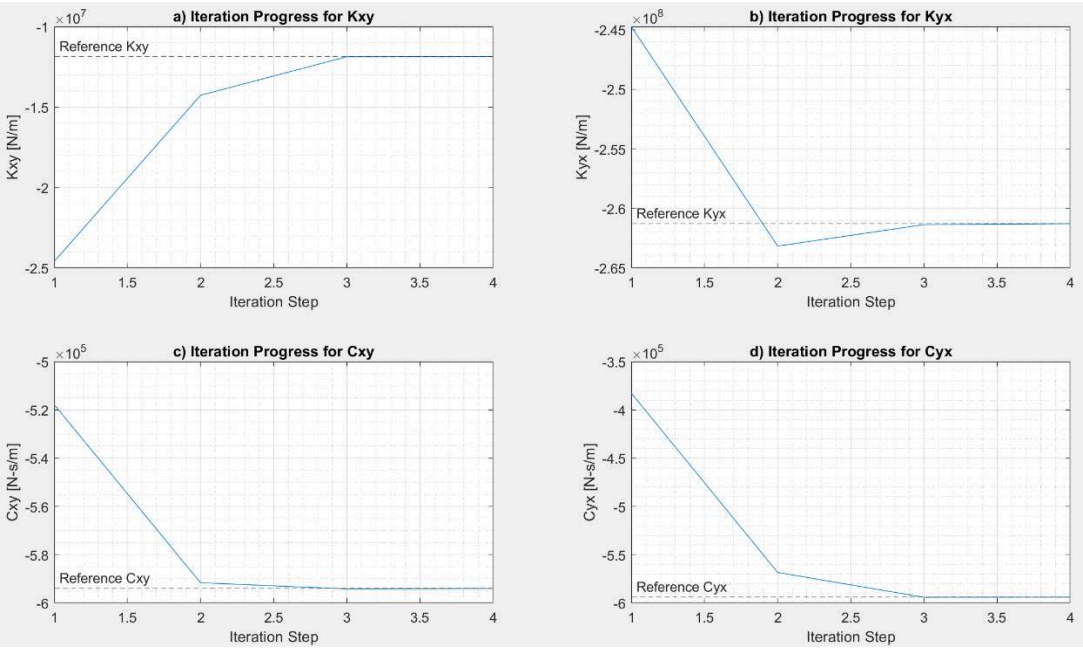

Figure 3.5: Evolution of iteration for the cross-coupled dynamic coefficients (Config. 1)

Table 3.7 shows the calculated range of uncertainty for the dynamic coefficients, including a resolution of 0.18 μm for the displacement sensors during the uncertainty analysis. This table shows that the largest calculated uncertainty is for K_{xy} with a range of around ±14%; however, for

the other 7 dynamic coefficients the uncertainty is smaller than ±2.6% of the respective reference coefficient. These small values of uncertainty show the ability of the method handle levels of noise, particularly since the identification includes the cross-coupled dynamic coefficients, which are much more sensitive to errors in measurements than the direct coefficients.

	Uncertainty Range
Kxx [N/m]	± 1.02 %
Kxy [N/m]	± 14 %
Kyx [N/m]	± 1.13 %
Kyy [N/m]	± 1.6 %
Cxx [N-s/m]	± 1.0 %
Cxy [N-s/m]	± 0.6 %
Cyx [N-s/m]	± 2.6 %
Cyy [N-s/m]	± 0.6 %

Table 3.7: Estimated Uncertainty range for coefficients – Configuration 1

3.3.2 Results for configuration 2: one flexible rotor supported by two identical fixed-geometry fluid film journal bearings.

Configuration 2 uses two fluid film journal bearings. In this case; however, it is assumed that the manufacturing and assembly characteristics as well as the static loading conditions are so similar that both bearings may be assumed to have identical dynamic coefficients, which reduces the identification requirement from sixteen to only eight dynamic coefficients.

The results presented for this configuration were obtained with the numerical application of two independent synchronous harmonic dynamic excitations. The first excitation is 25 N in the *x*-direction, at the location of disk 1; and the second excitation is one unbalance of 0.0004140 kg-m, at the location of disk 2. The purpose of this configuration is the identification of the eight dynamic coefficients of the two identical fluid film journal bearings supporting a flexible 1-inch diameter rotor. Figures 3.6 and 3.7 show the progress of this identification.

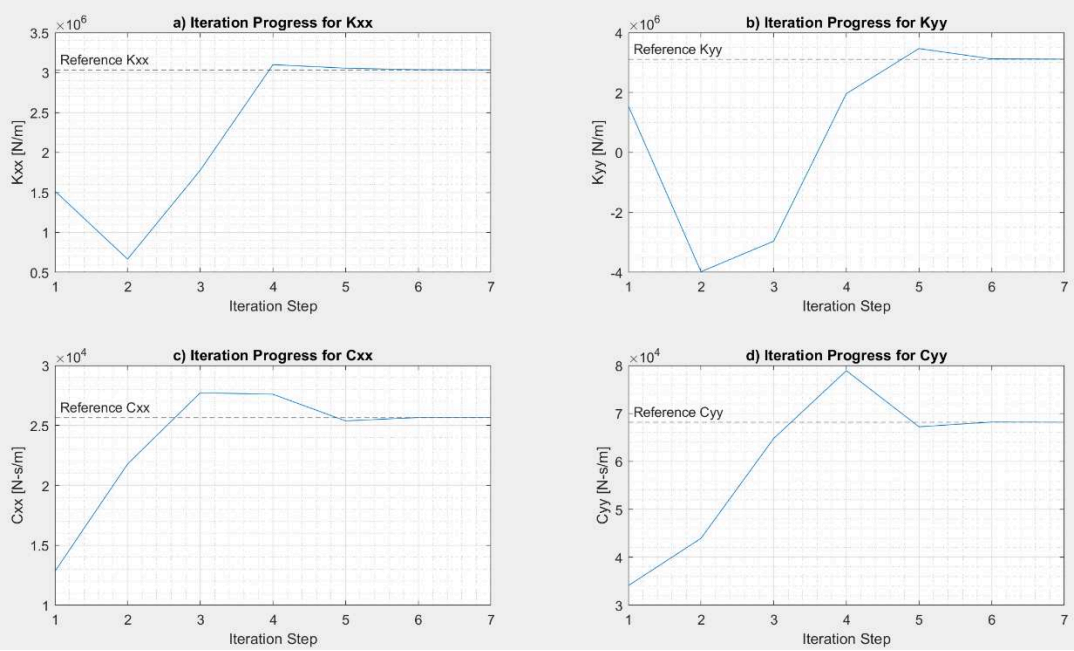

Figure 3.6: Evolution of iteration for the main dynamic coefficients (Config. 2)

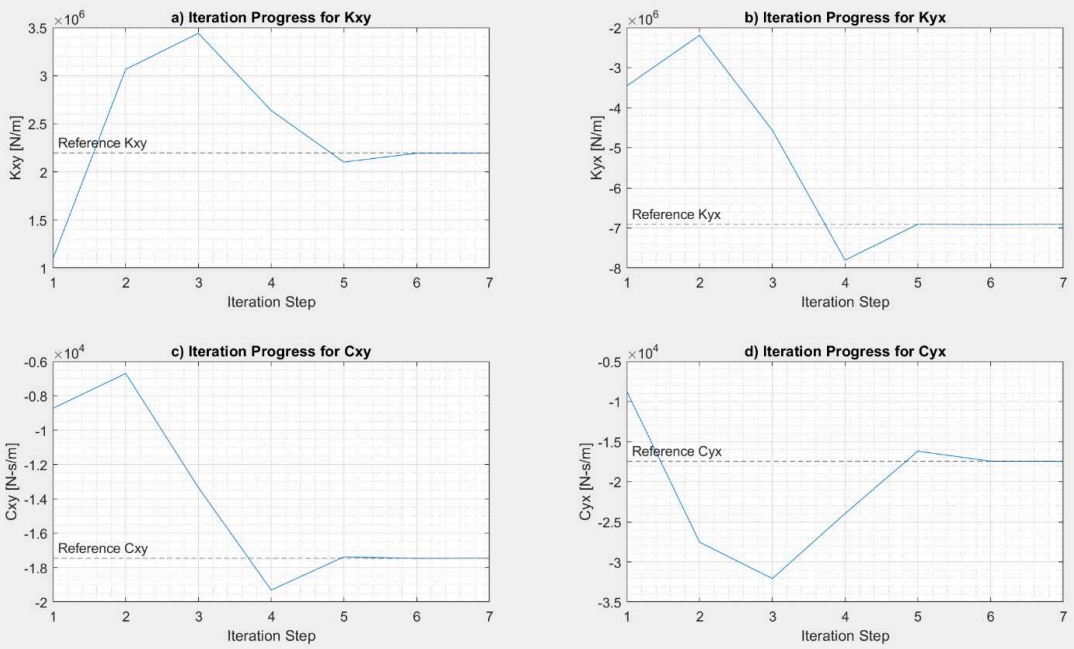

Figure 3.7: Evolution of iteration for the cross-coupled dynamic coefficients (Config. 2)

Figure 3.6 shows the progress of the identification for the direct stiffness and damping coefficients, while figure 3.7 shows the identification for the cross-coupled stiffness and damping

coefficients. Both figures show that at the seventh iteration all eight dynamic coefficients have achieved convergence, within an error of less than 0.001%, to the reference values for the coefficients.

Table 3.8 shows the calculated range of uncertainty for the identified dynamic coefficients in configuration 2, when a resolution of 0.18 μm is considered for the displacement sensors. For K_{xx}, K_{yx}, C_{xx}, and C_{yy}, the uncertainty range is less than ±5.2%, while for K_{xy}, C_{xy}, and C_{yx} the uncertainty is between ±7% to ±12%. K_{yy} has the largest uncertainty with a value of ±19.8%. Again, the method has shown its ability to keep within acceptable limits (less than 20%) the uncertainty in the identification of all eight dynamic coefficients.

	Uncertainty Range
Kxx [N/m]	± 5.1 %
Kxy [N/m]	± 11.8 %
Kyx [N/m]	± 4.5 %
Kyy [N/m]	± 19.6 %
Cxx [N-s/m]	± 2.6 %
Cxy [N-s/m]	± 7.3 %
Cyx [N-s/m]	± 8.4 %
Cyy [N-s/m]	± 3.4 %

Table 3.8: Estimated Uncertainty range for coefficients – Configuration 2

3.3.3 Results for Configuration 3: one flexible rotor supported by two different fixed-geometry fluid film journal bearings.

Configuration 3 uses two fluid film journal bearings with different specifications, such that the eight dynamic coefficients of bearing 1 are different than the coefficients of bearing 2, and the method must identify all sixteen dynamic coefficients.

The results presented for this configuration were obtained with the numerical application of two independent synchronous harmonic dynamic excitations. The first excitation is 500 N in the *x*-direction, at the location of disk 1; and the second excitation is one unbalance of 0.008782 kg-m, at the location of disk 2. The purpose of this configuration is the identification of the sixteen dynamic coefficients of the two fluid film journal bearings supporting a flexible 2-inch diameter

rotor. Figures 3.8 and 3.9 show the progress of the identification for the coefficients of bearing 1, while figures 3.10 and 3.11 show the progress for the coefficients of bearing 2.

Figures 3.8 and 3.10 show the progress of the identification for the direct stiffness and damping coefficients of the two bearings, while figures 3.9 and 3.11 show the identification for the cross-coupled stiffness and damping coefficients. The four figures show that at the sixth iteration the identification process for the sixteen dynamic coefficients has achieved convergence, within an error of less than 0.001%, to the reference values for the respective coefficients, and therefore the proposed method has performed a successful identification of all sixteen dynamic coefficients involved in this configuration.

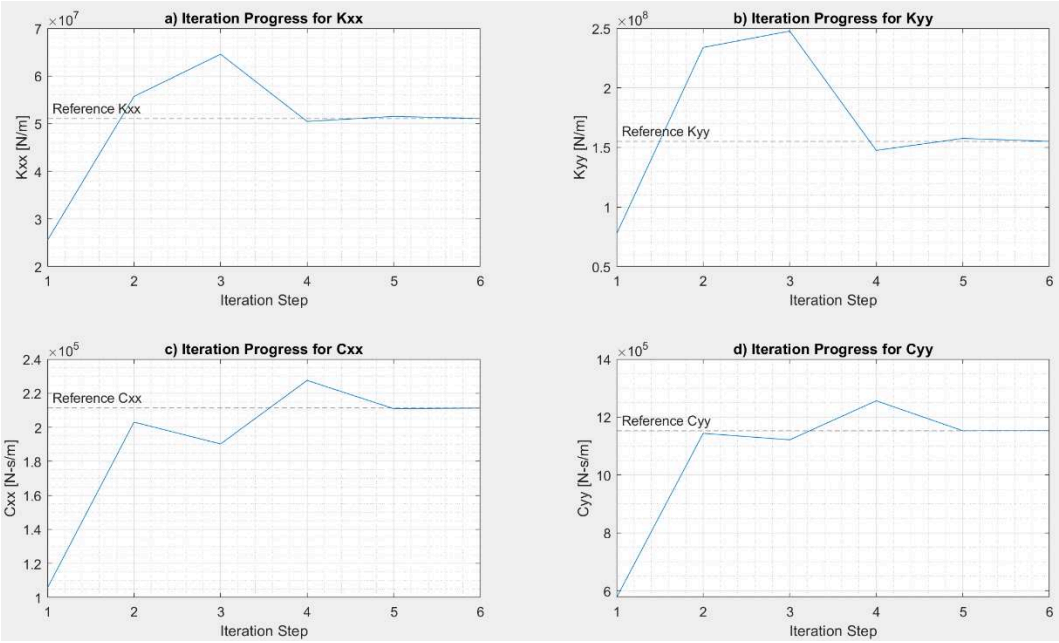

Figure 3.8: Evolution of iteration for the main dynamic coefficients (Config. 3 – Bearing 1)

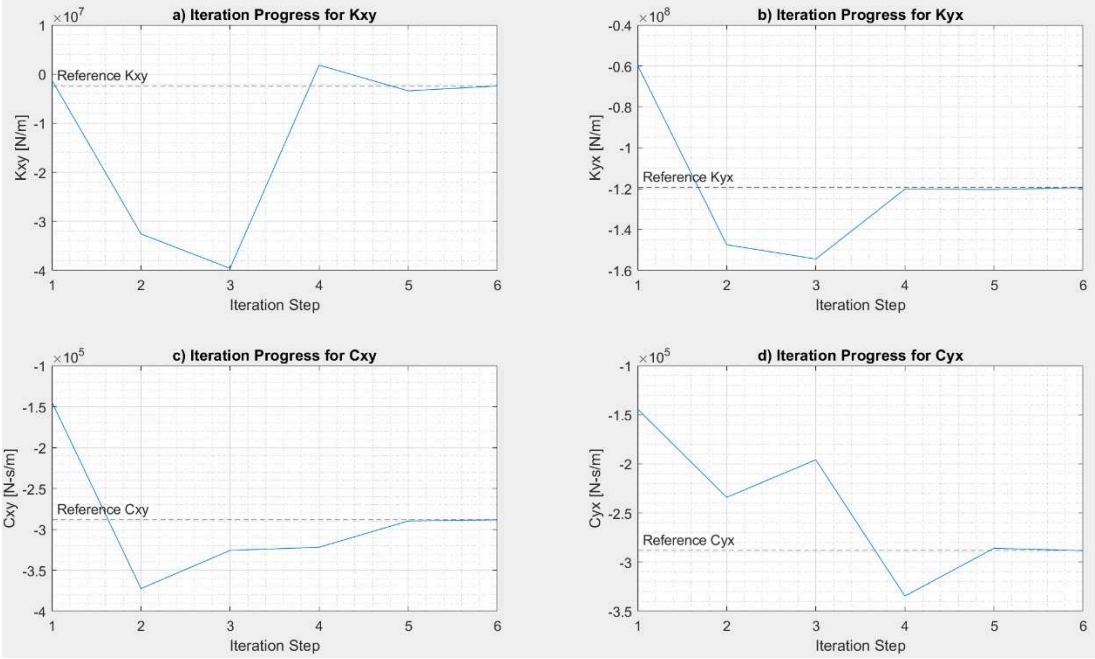

Figure 3.9: Evolution of iteration for the cross-coupled dynamic coefficients (Config. 3 – Bearing 1)

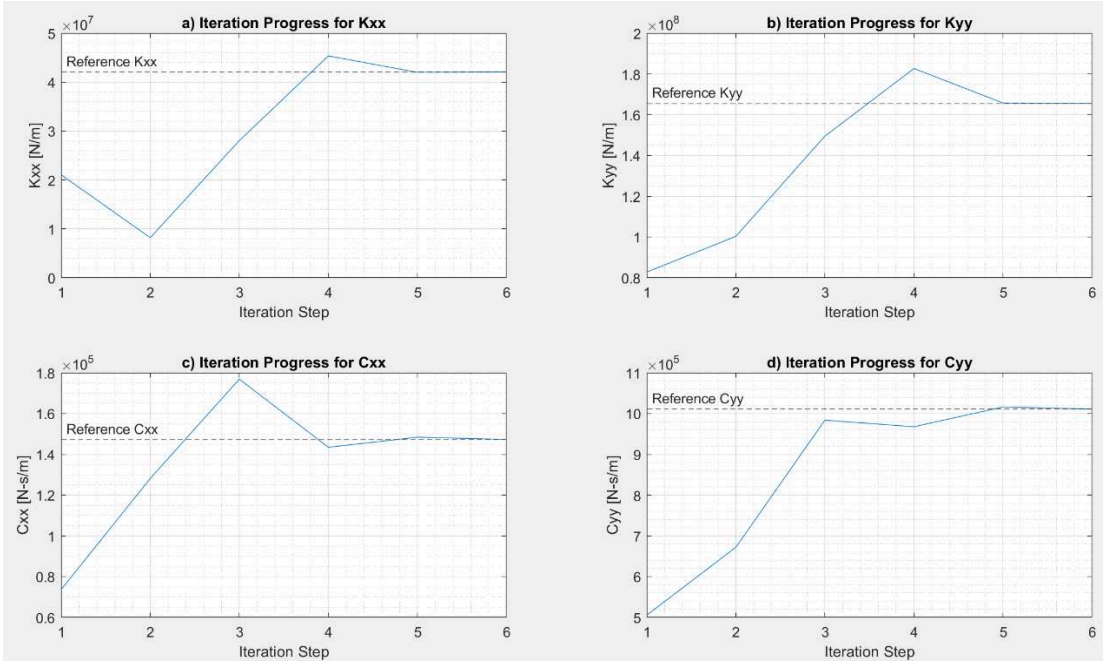

Figure 3.10: Evolution of iteration for the main dynamic coefficients (Config. 3 – Bearing 2)

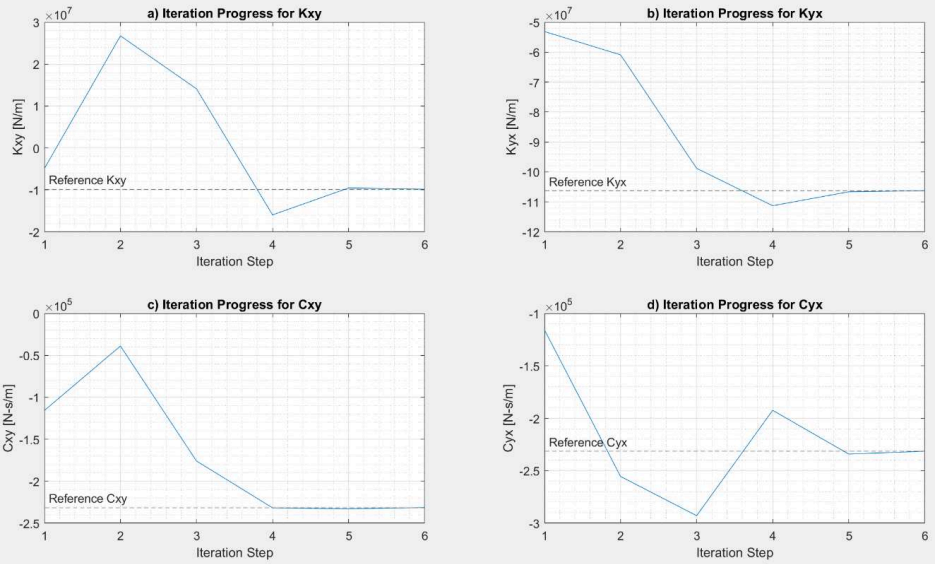

Figure 3.11: Evolution of iteration for the cross-coupled dynamic coefficients (Config. 3 – Bearing 2)

Table 3.9 shows the range of uncertainty for the identified dynamic coefficients of the two bearings in configuration 3, when a resolution of 0.18 μm is considered for the displacement sensors during the uncertainty analysis. This table shows that for 12 of the 16 identified coefficients the uncertainty range is less than ±8.0%, for C_{yx} in both bearings the uncertainty is around ±12%, and K_{xy} has the largest uncertainty with a value of ±22% for bearing 2 and ±146% for bearing 1. The proposed method has shown its ability to keep within acceptable boundaries (less than 15%) the uncertainty of 14 out of the 16 coefficients, including 6 out of the 8 cross-coupled dynamic coefficients in this configuration. The uncertainty values for K_{xy} could be reduced by applying more excitation rounds and simultaneously processing that data.

	Uncertainty Range Bearing 1	Uncertainty Range Bearing 2
Kxx [N/m]	± 3.5 %	± 2.5 %
Kxy [N/m]	± 146 %	±22%
Kyx [N/m]	± 4.1 %	± 3.0 %
Kyy [N/m]	± 6.6 %	± 4.7 %
Cxx [N-s/m]	± 3.6 %	± 2.8 %
Cxy [N-s/m]	± 6.6 %	± 4.3 %
Cyx [N-s/m]	(-12%) - (+10.8%)	± 8.2 %
Cyy [N-s/m]	± 5.7 %	± 3.6 %

Table 3.9: Estimated Uncertainty range for coefficients – Configuration 3

3.4 CONCLUSIONS

This chapter presents a new method for the identification of dynamic coefficients of fluid film journal bearings. The method includes rotor flexibility and miscollocation of displacement sensors with respect to the midplane of the bearings, which are often neglected in traditional identification methods. This method assumes that the dynamic displacement of the rotor at any axial location is a function of the dynamic coefficients, which provides a higher accuracy of the identified dynamic coefficients by eliminating the errors due to the miscollocation of the sensors and the rotor flexibility.

The method has been numerically applied to three different configurations of rotor-bearing systems, to show the efficacy of the method in identifying the eight dynamic coefficients of fixed-geometry fluid film journal bearings. The first configuration is a single floating test bearing around a flexible test rotor, which is a very common configuration in test rigs, and requires the identification of four direct and four cross-coupled dynamic coefficients. The second configuration is two identical test bearings supporting a flexible test rotor, which again requires the identification of four direct and four cross-coupled dynamic coefficients. The third configuration is two different test bearings supporting a flexible rotor, which requires the identification of eight direct and eight cross-coupled coefficients. The second and third configurations are common designs in practical rotating machinery. In all three configurations, the proposed method is able to identify all direct and cross-coupled dynamic coefficients, with an error of less than 0.001%.

The proposed identification method requires the application of two independent harmonic excitations, in the form of unbalance masses, impact forces with instrumented hammers, or magnetic bearings. Additionally, the method is sensitive to the condition number of the matrix $\boldsymbol{[\Delta]}$ or the preconditioned matrix $\boldsymbol{[B]}$, and different conditions of the excitation, combinations of excitations, and locations of the sensors may lead to different condition numbers. Large condition

numbers of ***[B]*** may produce difficulties for the method to converge and identify the right dynamic coefficients or lead to an excessive amplification of the inevitable errors inherent to experimental measurements.

The ability of the method to keep the uncertainty of the identified coefficients within acceptable levels was tested by performing uncertainty analyses that propagated values of random error in the displacement sensors. 30 out of the 32 identified dynamic coefficients had values of uncertainty smaller than 20%, which gives confidence in the ability of the method to reliably identify bearing coefficients, including the cross-coupled ones, which are highly sensitive to errors in the inputs to the method.

Chapter 4

Design Methodology for a Test Rig to Estimate Experimental Dynamic Coefficients of Fluid Film Journal Bearings

Modern rotating machinery is required to handle large loads and operate at high speeds, leading to potential rotordynamic challenges, such as: operation through critical speeds, instability, and excessive vibration. Fortunately, fluid film bearings are well suited to support rotors under large loads and high operating speeds while providing significant damping to the lateral response. Damping is especially useful for suppressing instabilities, facilitating transit through critical speeds, and reducing vibration levels [6]. Due to these features, fluid film bearings are a preferred component for most rotating machinery, and knowing their dynamic properties is crucial in making rotordynamic predictions for a machine [7, 9].

The dynamic force of a fluid film bearing around a static point of equilibrium can be expressed as a linear function of eight dynamic coefficients: four of them represent the stiffness properties and the other four the damping properties of the bearing [43]. These fluid film dynamic coefficients (FFDC) may be found by experimental tests or by numerical bearing codes [44]. However, a 2007 survey of results from several industry-standard bearing codes showed ranges of up to 1000% in some coefficients [17]. Experimental validation of the codes was recommended; however, that

validation is still missing from the public record. New demands for fluid film bearings are driving a need for rigs able to operate under ever more challenging conditions and experimental testing must provide reliable measurements for validation of computational bearing codes.

The dynamic characterization of fluid film bearings is a field in progress requiring the design and construction of new test rigs, updated to meet the demands of industry and research. However, this effort is a complex task involving: the design and selection of several major expensive components, the harmonious integration of the technical and operational characteristics of these components, and the integration of mechanical, electrical, and instrumentation systems. In addition, current demands point to rigs spinning faster than 15,000 rpm with journal diameters larger than 100 mm, which increases the investment to hundreds of thousands of dollars and puts more pressure in the integration of the components and the dynamic behavior of the rig as a unit, but without relaxing the requirement to produce and reliably measure small radial vibrations of less than 12.5 μm.

Several researchers have described test rigs they have designed or operated. However, no attempt has been made in the literature to provide guidelines or key aspects for the researcher involved in such design work to consider. Therefore, the purpose of this chapter is to cover this gap of information, by providing useful guidelines for a test rig design, so the designer can proceed quickly and with more technical confidence. Some recommendations are specific, but considering the inherent flexibility of a design work, key aspects are also mentioned to provide the general background required to make appropriate design decisions.

Hagg and Sankey [45] were some of the first researchers to experimentally measure FFDC. Their test rig was in a vertical orientation and driven directly by an electric motor up to 2,000 rpm. A lever applied static loads to the bearing housing while the dynamic excitation was produced by unbalance masses at defined locations on the rotor. The published description of the rig is only of limited assistance in a design process due to a lack of discussion of design decisions, limitations, and considerations.

A test rig in a horizontal orientation, with a 63.5 mm test rotor driven by a variable speed 3 hp electric motor, was used by Mitchell et al [46]. The bearing housing floated around the rotor and was statically loaded with weights. Once static equilibrium was achieved, the loads incremented in the x and y directions to modify the equilibrium position and estimate the four stiffness coefficients. The focus of the paper was measuring the coefficients, with little detail and/or discussion of the rig design.

Glienicke [47] obtained the eight FFDC for bearings up to 100 mm in diameter using a horizontal test rig. The bearing housing floated around a rotor fixed by ball bearings while statically loaded with three orthogonal pneumatic devices. An ingenious mechanism using an additional rotor (0-10,000 rpm) applied dynamic excitations. The description of the rig is informative including several cross-sectional drawings. However, there is little discussion of the design process.

A test rig at the University of Virginia was used to test 70 mm diameter bearings, at speeds up to 2,500 rpm [22]. A floating housing was loaded statically and dynamically using electric actuators, and the eight FFDC were estimated by correlating the measurements of strain gauges (force) and eddy-current probes (vibration). The published description of the rig is detailed as to graphics, but there was little discussion of design considerations or dimensions.

A rig for testing large-scale fluid film bearings within a floating housing, was developed at Toshiba to be driven by a 2,400 kW steam turbine at a maximum speed of 4,000 rpm. The housing was instrumented with load cells, accelerometers and proximity probes and could receive a maximum static load (pneumatic) of 980 kN, and a dynamic load (hydraulic) of 90 kN. Ikeda et al [18] used this rig to obtain the eight FFDC for a 580 mm diameter bearing. Again, only an informative description of the rig was provided.

Nordman and Schollhorn [36, 48] implemented two different excitation techniques, each in a different test rig. The first was to apply an excitation using the impact of a 1.2 kgs hammer to a rotor supported by two test fluid film bearings (50 mm diameter) [36]. The second method was to use a fixed bearing housing combined with two magnetic bearings, which provided both support,

and dynamic excitation to the rotor [48]. In both cases, the eight FFDC were estimated. Unfortunately, the focus of the rig description was conceptual.

A recent test rig, capable of testing fluid film bearings up to 300 mm in diameter with maximum speed of 20,000 rpm, has been reported in [35]. The rig is driven by a variable speed 670 kW electric motor coupled to a 6:1 increasing gearbox. Static and dynamic loads are applied by hydraulic actuators to a floating housing instrumented with sensors. The published article provides a good description of some components of the rig, but the focus was again more on the description than on the design details and decisions.

The general technique for estimating the FFDC is based on the correlation between an applied force and the resulting displacement of the rotor or the housing. Despite this simple relation, it is clear from the above descriptions that forces can be applied in many ways (static, dynamic, mechanical, impact, hydraulic, etc), producing a variety of rig configurations. Furthermore, even two rigs using the same excitation technique can use significantly different technologies in the main components [18, 22]. Designing a new test rig requires a consideration of several and diverse possibilities, and this demands a broad knowledge and understanding of the experimental technique, the quantification of the design requirements, and the available technical choices. It is the purpose of this study to provide the designer with the knowledge to quantify the design requirements, and understand the different technical choices that may be considered.

Currently, there is lack of experimental data for fluid film bearings with diameters larger than 100 mm operating at speeds higher than 15,000 rpm. Likewise, there is a shortage of test rigs with the capacity to exceed these two parameters. New rigs should address this deficiency as well as provide insight to the existing discrepancy between FFDC obtained from experimental tests and analytical predictions [49]. Even in recent comparisons discrepancies around 50% are not uncommon [50]. An additional issue is the variation of up to 1000% in FFDC produced by bearing codes [17]. The need for new test rigs to keep up with the needs of industry is clear, but

there is also a demand for producing experimental data that can be analyzed towards resolving the still-present differences between experimental and analytical predictions.

Thus, the purpose of this chapter is to present a guideline on how to design a test rig to accurately determine the eight dynamic coefficients of a radial tilting-pad bearing. Most of the recommendations are valid for rigs with other purposes such as studying static parameters, or instabilities. This design guideline covers the following sections:

1. The first section describes the needs a new rig should address. Ideally, these needs should exist as the input to the process, but if that is not the case some background is provided so the designer can assign values to produce a design of ample applicability.
2. The second section discusses how these needs may be translated into technical design requirements for the rig and recommends procedures to obtain the most critical requirements.
3. The third section explains the main components of a rig and recommends steps and considerations for their selection or design.
4. Finally, a fourth section presents some verification for a design once it has been assembled in order, to validate whether or not results are acceptable or if modifications should be made to the individual components.

4.1 CUSTOMER NEEDS FOR A TEST RIG

The starting point for the design of a test rig is the existence of some customer (industry/research) needs to obtain experimental data for fluid film journal bearings. These needs are later translated into design requirements, which are the technical benchmarks for the design. Therefore, the designer needs to understand the connection between needs and requirements. This section covers some of the important needs to be satisfied by the rig and provides background on how their variation can affect the design requirements. The analytical predictions of tilting-pad fluid film bearings in this chapter, were performed using MAXBRG, which is an

industry-standard finite-element based computer code that performs steady state thermo-elasto-hydrodynamic (TEHD) analysis [23].

4.1.1 Test bearing parameters

Often, a customer has the need to obtain experimental data for some specific bearings. Then, a list of these bearings, including their geometrical parameters, is an ideal input for the designer of the test rig. On the other hand, while a single critical test bearing will define most of the design requirements, it may not supply the complete picture that the designer needs. In lieu of this list, the following paragraphs present how certain features of the bearing to be tested could affect the design requirements of the rig.

4.1.1.1 Journal diameter

The journal diameter has a direct influence on the following design requirements:

- The peripheral surface speed.
- The power requirement for the test bearing.
- The oil flow rate to the test bearing.

Most rigs have tested bearings under 100 mm in diameter. Hence, there is a current interest to experimentally observe the behavior of bearings with larger diameters and achieve peripheral speeds (the product of journal diameter and rotating speed) higher than 115 m/s, that induce a turbulent flow regime in the oil film. The peripheral speed is directly related to the viscous shearing losses per length of a fluid film bearing and, therefore to the power required to test the bearing.

The journal diameter, also has a direct influence on the oil flow rate required by the test bearing, as can be seen in figure 4.1, where the flowrate (obtained from MAXBRG) is plotted as a function of journal diameter at several rotating speed for a set of similar geometrical bearing parameters.

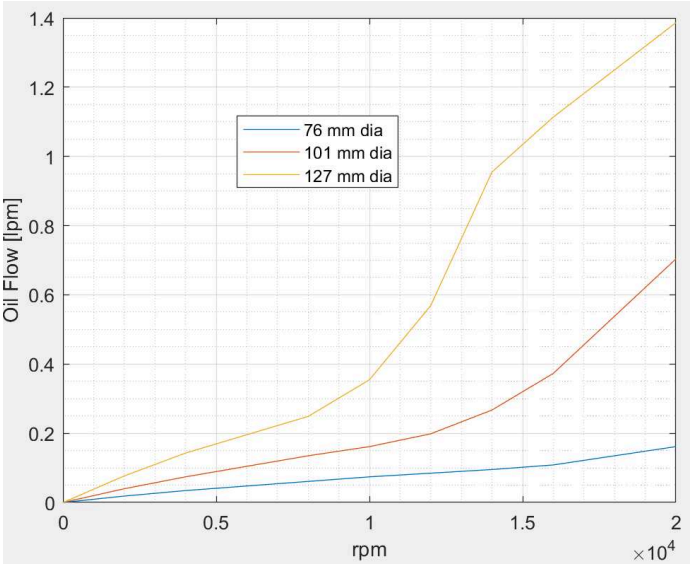

Figure 4.1: Flowrate vs Journal diameter (ISO VG 32)

4.1.1.2 Bearing length.

This dimension is usually expressed by the length to diameter ratio, or L/D of the bearing, and has a direct influence on the following design requirements:

- The oil flow rate.
- The power requirements.
- The value of the dynamic coefficients.

For instance, a 127 mm diameter bearing with an L/D ratio of 0.75 spinning at 20,000 rpm is predicted by MAXBRG to require 109.4 l/min (28.9 GPM) of lubricant, to dissipate 109.35 kW (146.6 HP) in viscous losses, and to have a K_{yy} of 45,585 N/m. An otherwise identical bearing with a L/D ratio of 0.5 is predicted to require 76.65 l/min (20.25 GPM), 72.7 kW (97.5 HP) in viscous losses, and has a K_{yy} of 21,083 N/m. In this case, the oil flow rate and power requirements scale approximately with L/D, but K_{yy} does not.

4.1.1.3 Bearing offset.

This feature has an impact on:

- The oil flow rate.
- The temperature of the pads.
- The value of the dynamic coefficients.

Bearings with central-pivot pads(offset=50%) usually exhibit higher pad temperature [51], require smaller oil flow rates, and have lower stiffness properties than bearings with offset-pivot (typical offset= 55 or 60. As an example, a 127 mm diameter central-pivot pad bearing operating at 20,000 rpm is expected to require 20.44 l/min (5.4 GPM) of oil, and have a maximum pad temperature of 126.4° C (259.5° F) with a K_{yy} of 31,400 N/m. The same bearing with an offset of 0.6 is expected to need 108.25 l/min (28.6 GPM) of oil, and have a maximum pad temperature of 115.5° C (240° F) with a K_{yy} of 50,251 N/m.

4.1.2 Rotational speed

The desired maximum rotational speed is of critical importance for the test rig designer and it should be obtained/derived from the needs of the end user. Nowadays, only a few test rigs have the capability to operate at 20,000 rpm or faster [35]. The operating speed has an influence on:

- The viscous losses, which are a quadratic function of speed (figure 4.2).
- The maximum temperature of the test bearing.
- The selection of the driver equipment.

It should be noted that electric motors or turbines with rotating speeds higher than 12,000 rpm are usually customized designs, due to the technical challenges involved. The minimum speed at which bearings are expected to be tested in a test rig must also be taken into consideration, due to limitations in the operational range of driver equipment.

4.1.3 Lubricants

ISO VG 32 is the generic denomination for the most common lubricant used in fluid film bearings for industrial applications, but it is not the only one. Therefore, it is recommended to

confirm needs of additional lubricants in the test bearings and to check the specifications of these lubricants. The following actions are suggested:

- Analyze the expected bearing cases using each desired lubricant to understand how the design requirements (power, temperature, and expected dynamic coefficients) will be affected.
- Consider the impact of independent lubrication systems for each lubricant, including area of installation, quantity of connections and provisions for satisfactorily cleaning traces of the previous lubricant in use, when a change of lubricants is performed.

Figure 4.2: Viscous Power vs Rotating speed

4.1.4 Utilities

The test rig should be installed in a facility with sufficient resources for its operation. A single test bearing of 127 mm in diameter and operating at 20,000 rpm is predicted to have viscous losses on the order of 100 kW. Assuming a margin to account for other power demands of the rig, an approximate demand of 150 kW is reasonable. Hence, it is important to confirm if the facility

and surrounding grid have the capacity to supply the required power, or the equivalent energy in steam or pressurized.

It is important to note a test rig operates with auxiliary equipment including: pump(s) and/or fans for the lubrication system(s), hydraulic system(s) for the exciters, a cooling system for the Variable Frequency Drive (VFD), as well as instrumentation and data acquisition systems. A complete power estimation is important to confirm the total required demand.

Another significant consideration is the removal of heat generated by the test rig. The 100 kW viscous loss of the test bearing mentioned in the previous paragraph increases the temperature of the lubricant, and the typical means to remove this heat is through water or air heat exchangers. A water heat exchanger of appropriate size would require approximately of 70 l/min of water, which should flow in a closed industrial circuit and be recycled for cooling treatment.

4.2 DESIGN REQUIREMENTS

The design requirements are the set points the design must meet and are derived from the customer needs. For example, a customer wants to dynamically test a given set of bearings with a desired speed range and a defined lubricant. It is the designer's job to ensure the rig has enough power, lubricant flowrate, and the capacity to operate, at the desired speed range with the defined lubricant. Therefore, this section will cover the calculation of the design requirements for a rig.

4.2.1 Maximum power required by the test section.

The power consumed at any instant during the rotation of the test rotor must be supplied by the drive train. Therefore, the maximum power requirement is a key quantity for selecting the drive train. This estimation should include viscous losses in the test bearing(s) along with any other bearings in the train and test section, and windage losses, if relevant.

The power requirement for the test bearing(s) is found at the maximum rotational speed, the maximum journal diameter, and the maximum bearing length. The properties of the lubricant and

geometrical features of the bearings to test, such as the clearances and the preload have a dominant effect on the power; however, their impact is predicted by coupled partial differential equations [23]. Hence, it is advisable to analyze all these conditions using a TEHD bearing code, such as MAXBRG, and to apply a suitable safety factor (SF) in the absence of code validation.

Other bearings to consider in this requirement include those that support the test rotor, and the bearings in any other equipment in the drive train, for example an increasing gearbox. As a reference point, a 76.2 mm diameter fluid film bearing could require approximately 7.45 kW at 20,000 rpm. Windage losses will generally be small compared to viscous losses in fluid film bearings; however, they should be calculated, as each design condition is different [52].

4.2.2 Oil flow rate

The estimated oil flow rate should include the test bearing(s) along with any other bearings and equipment to provide a total requirement for the test rig.

The maximum oil flow rate required by the test bearing(s) is estimated at the maximum rotational speed, the maximum journal diameter, and the maximum length of the bearing, for a condition with a 60% pad offset. However, iterations with increased flow rates may be required to obtain cooler bearings, or to meet an American Petroleum Institute (API) recommendation that the temperature increase of the lubricant should never exceed 28 K [53]. It is again recommended to use a TEHD bearing code and a suitable SF.

A similar process should be followed for other fluid film bearings in the rig to find their maximum lubricant flow rates. However, bearings within the scope of supply of purchased equipment (gearbox, electric motor, turbine, etc.) may have required oil flowrates defined by their manufacturers.

Along with these estimations, it is recommended that all bearings be designed for the same lubricant to have the benefit of sharing one single lubrication system for the rig. Using different lubricants will add more cost and technical complexity.

4.2.3 Maximum dynamic force

The designer needs to determine the magnitude of the maximum dynamic force the rig will have the capacity to apply during a test to find the dynamic coefficients of a bearing. This magnitude drives the selection of the dynamic exciters and impacts the selection of the load transducers.

From previous design requirements, the most critical bearing cases should have been analyzed using a TEHD bearing code, which should also provide expected values for the dynamic coefficients. Now, the designer should consider the largest magnitude of dynamic coefficients as they will provide the highest force magnitude. Equations (4.1) and (4.2) can be used to calculate the expected dynamic forces and displacements for a given set of dynamic coefficients:

$$\begin{bmatrix} (K_{xx} - M\omega^2) + i\omega C_{xx} \\ K_{yx} + i\omega C_{yx} \end{bmatrix} X = \begin{pmatrix} F_{x1} \\ F_{y1} \end{pmatrix} \qquad (4.1)$$

$$\begin{bmatrix} K_{xy} + i\omega C_{xy} \\ (K_{yy} - M\omega^2) + i\omega C_{yy} \end{bmatrix} Y = \begin{pmatrix} F_{x2} \\ F_{y2} \end{pmatrix} \qquad (4.2)$$

where X and Y are the maximum amplitudes of the planned dynamic oscillation, in those orthogonal directions; F_{x1} and F_{y1} are the forces in complex form, in orthogonal directions x and y, required to produce an oscillation of amplitude X; F_{x2} and F_{y2} are the forces in complex form to produce an oscillation of amplitude Y; M is the expected mass for the bearing housing or the test rotor, depending on whether the design is considering a floating or fixed bearing housing; and ω is the frequency of the excitation.

The amplitude of the dynamic forces is given by (4.3) and (4.4):

$$F_x = |F_{x1} + F_{x2}| \qquad (4.3)$$

$$F_y = |F_{y1} + F_{y2}| \qquad (4.4)$$

Usually, the amplitude of X and Y should be between 2.5 and 12.7 μm 0-Pk [4]. The exact value is determined by considering the resolution of the displacement sensors and the expected uncertainty for the dynamic coefficients. Additionally, the larger the oscillation and force, the more

restricted the selection of the exciter. For example, for a 5-inch diameter bearing with a specific load of 3.1 MPa, MAXBRG predicts the relatively stiff dynamic coefficients as shown in table 4.1 and equations (4.1) – (4.4) give the dynamic force for a 2.5 μm oscillation to be approximately 5,400 N. For a 12.7 μm oscillation the required force increased to 27,100 N.

	Values
Kxx [N/m]	1.55e+09
Kxy [N/m]	10.60e+06
Kyx [N/m]	19.25e+06
Kyy [N/m]	1.55e+09
Cxx [N-s/m]	0.65+06
Cxy [N-s/m]	2.90+03
Cyx [N-s/m]	0.87+03
Cyy [N-s/m]	0.65+06

Table 4.1: Values of dynamic coefficients

4.3 DESIGN/SELECTION OF COMPONENTS

A test rig to identify dynamic coefficients of a fluid film journal bearing will, in general, be an assembly of the following components: a drive train, a bearing housing, a system to apply dynamic forces, rotor couplings, a baseplate, a lubrication system, and a set of instrumentation. This section provides recommendations for the selection or design of these components (figure 4.3).

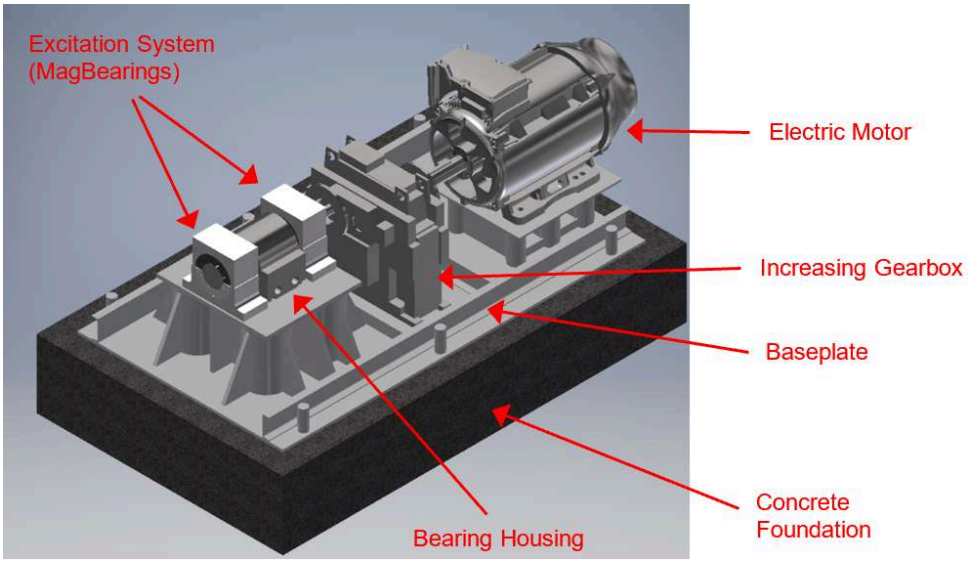

Figure 4.3: A test rig and main components

4.3.1 Drive train selection

The drive train includes all pieces of equipment to mechanically drive the spinning of the test rotor. A satisfactory selection must meet the following conditions:

- Provide the required power for the rig to operate at the most demanding conditions.
- Operate over the expected range of rotating speeds.
- Provide the required torque at all operating conditions.
- Operate with the available utilities.

Due to the current shortage of test rigs able to rotate at 20,000 rpm and higher, two common alternatives for achieving this specific purpose will be considered here. One alternative is to select a single piece of equipment, with its output rotor capable of spinning at the range of required speeds and providing the required power and torque. This equipment could be, for instance, a variable speed electric motor, or a steam/pneumatic turbine. A second alternative is a two-piece set, where the rotor of the first piece meets the power requirements, but with a reduced range of speed, and is then mechanically coupled to the second piece of equipment. The second piece of equipment then increases the rotating speed, so the test rotor can spin at the desired speeds but does not add any power. An example of this second arrangement is shown in figure 4.4 for a variable speed electric motor with a maximum speed of 4,400 rpm, connected to the low-speed shaft of an increasing gearbox with a speed ratio of 5.0, which means the high-speed shaft of the gearbox could spin up to 22,000 rpm. Table 4.2 summarizes some advantages and disadvantages of these two alternatives.

Figure 4.4: Drive train: electric motor & gearbox

	Advantages	Disadvantages
Single Equipment (Driver)	• The density of equipment for the rig will be lower than in other configurations • The modal behavior of the assembly will contain less resonant modes. • During operation, only one point of alignment (driver - test rotor) is required. • The thermal expansion of a single driver is simpler, and alignment adjustments will probably be only in the vertical direction	• The equipment will be custom designed and manufactured. • Only a few manufacturers are specialized to supply high-speed drivers. • If the driver is an electric motor, liquid cooling could be required for the coils and the bearings (utilities should be confirmed) • A turbine could decrease even more the density of equipment in the rig, but it is quite unusual to have a supply of steam or compressed air
Equipment+Gearbox	• More manufacturers can be found to supply a low-speed driver. • The driver could not be exactly a standard product, but manufacturers are much more familiar with providing solutions at low speeds. • The lubrication system for a low-speed driver is usually simpler. Bearings could even be grease lubricated.	• The addition of the gearbox increases the density of equipment for the test rig: additional lubrication demands, additional instruments, and more electrical connections. • The gearbox will probably introduce three additional resonant frequencies (lateral, twisting, and axial mode) to the modal behavior of the assembly • During operation, two points of alignment will be required. • The thermal expansion of a gearbox is more complex, and alignment will include horizontal and vertical adjustments.

Table 4.2: Pros / Cons Single equipment vs Equipment + Gearbox

It is important to keep in mind that rotating drivers have limitations as to the minimum speed they can achieve and in their range of operation. Furthermore, the efficiency is affected by significant changes in speed and load; for instance, the efficiency of a National Electrical Manufacturers Association (NEMA) motor may drop below 50% of its maximum value if the load (a quadratic function of speed for radial bearings) is decreased to approximately 10% of the full-load [54]. Therefore, the designer needs to analyze the alternatives for meeting this minimum speed requirement and the consequences in terms of energy.

4.3.2 Bearing housing

Bearing housings are not usually available to select and purchase. Therefore, it is likely they will have to be designed and manufactured for the specific installation. It is recommended the following points be clearly defined:

- External physical dimensions of the test bearing(s) to be installed in the bearing housing.
- Definition of whether the bearing housing is floating or fixed. In the floating bearing housing configuration, the housing is not rigidly attached to the rig and oscillates around the test rotor in response to excitations received by the housing. In a fixed housing configuration, the housing is attached to the rig. The test rotor receives the dynamic excitations and oscillates with respect to the housing in response to those excitations.
- The maximum oil flow rate required by the test bearing(s).

The details and dimensions of the test bearing serve two purposes: to define the dimensions of the interface between housing and bearing as well as the size and location of the connections between the lubricant inlet/outlet ports of the bearing and the housing. Usually, the cartridge of tilting pad bearings contains an anulus, so the lubricant directly feeds each pad. The housing

should then have an equivalent cavity for the lubricant passage. Unfortunately, there are no published standards or industrial recommendation as to the size of this cavity. However, a recommendation in [55], points to flow velocities from 1 to 5 m/s, for single-phase liquid lines; and velocities from 3 to 5 m/s are indicated in [56], being careful not to reduce the static pressure of the lubricant.

The interface between the outlet ports of the bearing and the housing is a work of dimensional detail, and probably the main challenge is to size an adequate drainage in the bearing housing due to the lack of standards. For the 127 mm diameter bearing considered in previous sections, the maximum oil flow rate to drain is around 148 l/min, which is a rate that can flood a housing in less than 3 seconds. Fortunately, for sizing the drainage there is an industrial recommendation in [57] that suggests a pipe diameter of 150 mm for a flowrate of around 170 l/min, with a lubricant velocity of less than 0.38 m/s, and no more than half the cross-sectional area of the pipe wetted by the lubricant. The difficulty with this recommendation is to accommodate this large drainage area in the housing.

The housing design also needs to consider the drain method in the bearing. Some bearings have axial end seals to restrict axial drainage and direct the lubricant through outlet ports in the bearing cartridge. Adequate inner channels should be included in the design of the bearing housing, for these bearings.

For a floating housing configuration, it will be simpler to assign the area for the drain, because all surfaces are free of any attachment to the rig. The lubricant drains by gravity and the best area for locating the drain is the bottom surface of the housing. For a housing in a fixed configuration, the bottom surface may be attached to the rig forcing the drain to be through the lateral surfaces. A disadvantage of a lateral drain is that one single drain will increase the housing dimensions and weight. However, an alternative is a split drain, as shown in figure 4.5, which is a design for a housing fixed to a baseplate, draining a maximum oil flow rate of 148 l/min trough two lateral drains.

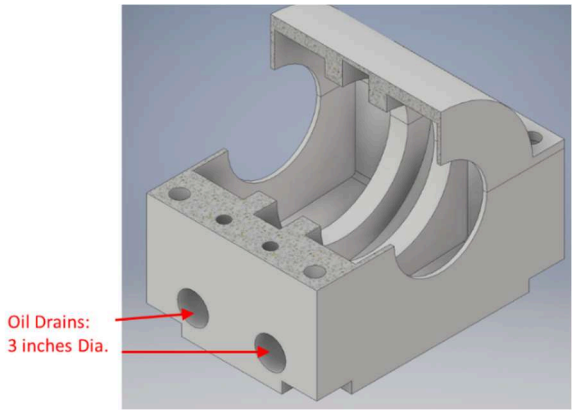

Figure 4.5: A bearing housing for a fixed configuration (lateral drain)

An additional detail to be considered for floating housings is their tendency for axial misalignment with respect to the bearing journal, due to the lack of a rigid support. This misalignment will be reflected as a conical vibration of the housing when excited. A solution to this situation in many housings is to include tensioning wires connecting the housing to fixed parts of the rig. Usually, the connection points on the housing are distributed at 120 degrees, over the circumference [22]. By individually tensioning these wires, the axial alignment of the housing can be kept within adequate levels.

On the other hand, for a fixed housing configuration the dynamic excitation will be applied to the rotor, often by use magnetic actuators. Therefore, the test rig will have a test section holding the housings for two magnetic actuators as well as the test bearing. These additional masses introduce an effect on the dynamic behavior of the test rig, similar to an inverted pendulum. In this case, it is recommended to perform a modal analysis of the test rig structure, to confirm resonances in the expected range of operating frequencies for the rig. Reducing the mass of the bearing housing will increase the associated resonant frequencies and probably eliminate any potential operating interferences. The use of lighter material for the housings is also a possibility if dynamic interferences are a concern.

4.3.3 Dynamic excitation system

Most techniques to estimate the dynamic coefficients rely on the application of dynamic excitations, either to the rotor or the bearing housing. For floating housings, the excitation is usually applied by means of two hydraulic linear actuators [18, 22], located orthogonally, while for fixed housings the excitation can be applied to the rotor by using magnetic radial actuators [48]. The mentioned actuators have the capacity to apply single or multi-frequency excitations, at a wide range of frequencies. Unbalance masses are not considered here due to their lack of flexibility in the excitation frequency to apply.

An adequate excitation system should meet the following requirements:

- Maximum dynamic force.
- Expected range of excitation frequencies.

Hydraulic linear actuators can be selected from various suppliers, and the complete system will require a hydraulic cylinder, a controller, and a hydraulic console. Standard available systems can provide sinusoidal forces up to 10,000 N at frequencies between 5 and 1,200 Hz, which should meet the requirements of most dynamic tests.

Magnetic radial actuators are systems comprising a magnetic stator piece with an electric coil to generate the required magnetic fields, a magnetic journal that is typically shrunk fit onto the rotor, an amplifier, a controller, and sensors [58]. Such a system may be difficult to buy off-the shelf, but may be developed in collaboration with a few specialized companies or designed in-house. An in-house design should combine a design effort with selection of some components. The design effort for a magnetic actuator should initially focus on the geometrical design of the stator, which in conjunction with the parameters of the coil will determine the maximum levels of magnetic force that the actuator can apply to the rotor. Variations in the electrical currents circulating through the coils, which are commanded by the controller/amplifier, generate the desired oscillating shape of the dynamic force. Standard amplifiers may offer loop times of 50 μs,

which means that 2,000 discrete points will be available to represent one cycle of a 500 Hz sinusoidal wave, offering an adequate representation.

The design of the magnetic stator is a bit of an art with a number of potential geometrical configurations and magnetic materials available. A full finite-element package such as ANSYS may be used to increase the speed and accuracy of the estimations. There are also free available tools such as Finite Element Methods Magnetic (FEMM), which performs 2-D magnetic calculations. Figure 4.6 shows the final design iteration of a stator and its coil arrangement, performed with the assistance of FEMM, for a magnetic radial actuator. The designer needs to define the materials and the geometry in a trial-and-error process, while FEMM calculates the magnetic field and force. The design requirement was that the actuator was able to provide 21,500 N of maximum force, including the static and dynamic loading.

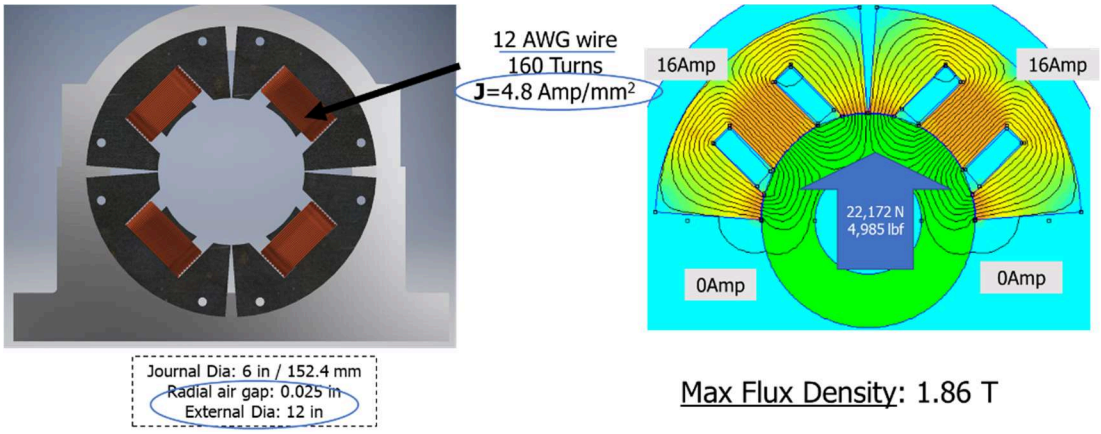

Figure 4.6: Magnetic bearing actuator

4.3.4 Baseplate

The baseplate is a common steel structure where some pieces of equipment, as defined by the customer, are installed and assembled for their operation. It is the interface between the civil foundation and the machine components and should be designed to provide stiffness and structural stability for the installation and operation of the assembly as a unit. The focus of this

section is the design of a baseplate to install the driver train and the test section of the rig (figure 4.7).

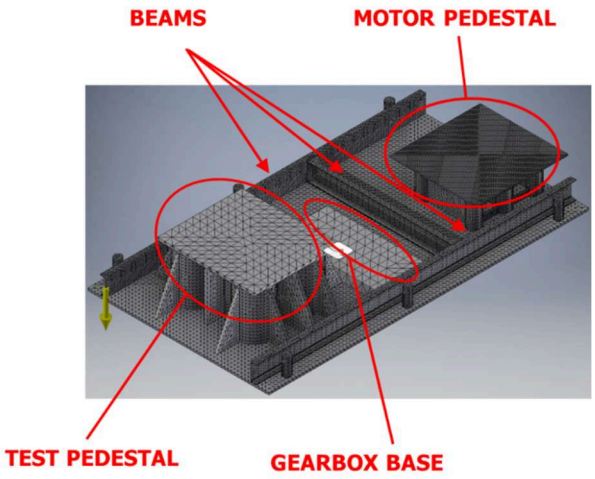

Figure 4.7: A baseplate for a test rig

A preliminary selection of the equipment to install on the baseplate should have been performed before starting the design of the baseplate. It is paramount to be based on the physical dimensions of the driver (electric motor, turbine, etc.), gearbox (if applicable), and the test section, which includes the bearing housing and supporting bearings. It is especially important to have, for each piece of equipment, the details and dimensions of the base, which defines the attachment to the baseplate, the vertical distance to the rotor axis such that the baseplate can align all axes should lie in the same horizontal plane, and the total mass.

All Original Equipment Manufacturers (OEM) of rotating machinery have experience in design and manufacturing of baseplates, and working with one of these OEM's is an efficient method to develop a baseplate. The design of a baseplate is basically a structural analysis; hence, an in-house design of the baseplate is possible with the assistance of a finite element-based engineering software. Additional considerations for the baseplate are given in [53]. Two recommendations important to consider are the following:

- The height of the axes with respect to the bottom of the baseplate should be minimized; however, adequate clearance should be provided for the drain piping and connections. The pedestals on the baseplate act as an inverted pendulum and the shorter they are the higher the resonant frequencies will be and thus less likely to interfere with the operating frequencies of the rig.
- The baseplate should be designed to contain any lubricant leakage and the bottom surface of the baseplate should be sloped toward the test section, where a tapped drain opening should be located to drain the leakage.

For an in-house design, some consideration should also be given to the manufacturing process. The baseplate requires significant welding of structural members and successive machining must provide flat surfaces on the pedestals, within tight tolerances.

One final note here is that although a baseplate is good practice and can facilitate installation and alignment, it is not strictly a requirement for a test rig. The designer has the freedom to choose other means that may be more appropriate to a specific facility or technical requirements.

4.3.5 Couplings

The couplings mechanically connect two rotors and transmit torque and power from one to the other. In the case of a test rig, one or two couplings may be required depending on whether the drive train includes a gearbox or not. One coupling would connect the driver to the test rotor or the gearbox, and a second coupling would connect the gearbox to the test rotor.

Couplings are selected from manufacturers based on the following information:

- The maximum torque to be transmitted by the coupling.
- The maximum speed at which the coupling will rotate.

- Tolerance of angular and parallel misalignment.
- The distance between shaft ends (DBSE), and the type of connection on the end of the rotors.
- The safety features of the coupling.

Usually, the maximum torque is experienced during the acceleration from rest to operating speed and it is not unusual to have values of 200 or 300% the maximum torque in normal operation (full-load torque). The actual value of this torque depends on the driver equipment, but this information may not be available during the design phase. An alternative method is the application of a safety factor, as found in design books [59] or from coupling manufacturers, to the torque obtained from the maximum rated power of the driver.

Note that a coupling tolerance to misalignment is not intended to avoid alignment adjustments. Rather, the alignment between rotors should always be corrected during the startup; however, some small residual misalignment may remain or develop during operation, which may be accommodated by a coupling with tolerance to misalignment. This will both increase the coupling life and reduce vibration in the test rig related to misalignment. Two additional characteristics to examine during the coupling selection are the DBSE and the available connections on the end of the rotors. A preliminary layout of the equipment on the baseplate or the foundation should help determine the DBSE, and once the coupling is selected minor adjustments could take place in the baseplate or the foundation. Most standard couplings are manufactured to connect cylindrical or tapered rotors; however, gearbox rotors are usually flanged, which must be considered in the coupling selection.

An all-metal flexible element, spacer-type coupling, is recommended in [53]. For this type of coupling, different spacers of different lengths could be provided for the same model, and this provides greater flexibility to accommodate the DBSE. Additionally, the flexible elements of this type of coupling can absorb angular and parallel misalignment, and some axial stress. This

coupling can also be selected with the safety feature that the spacer is retained and not expelled during rotation, in case the flexible elements fail due to excessive misalignment, controlling the most dangerous safety concern of the coupling.

Figure 4.8 shows the selected coupling for a low-speed connection up to 4,400 rpm, with a nominal torque to transmit of 1,220 N-m (10,800 lb-in). This coupling includes a metallic spacer of variable length and flexible metallic elements on both sides to accommodate misalignment. The specifications from the coupling manufacturer are on the left bottom part of the figure.

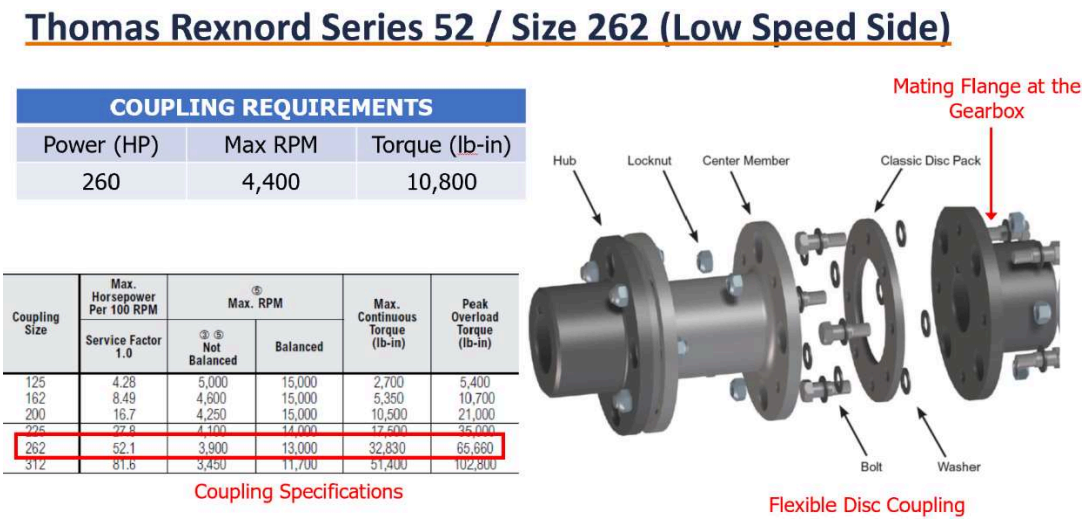

Figure 4.8: Selected coupling for a specific application

The universe of types, models, and manufacturers of couplings is substantial, and the designer should investigate the available catalogs. Usually, there will be more than one suitable standard coupling, and even in difficult selections a customized coupling could be ordered, to be designed and manufactured.

4.3.6 Instrumentation

Any test rig requires the use of instrumentation to monitor the operation of the rig and to collect data during the tests. At a minimum, the designer should consider the following data for monitoring purposes:

- Temperature of the internal wiring of the main electrical motor (driver).
- Temperature of the motor, turbine and/or gearbox bearings (radial and thrust).
- Relative rotor-bearing displacement (vibration) for fluid film bearings (radial and thrust) in the motor, turbine and/or gearbox.
- Housing vibration of the motor, turbine, and/or gearbox.

Moreover, the tests data also needs to be collected, including:

- Temperature of the bearing pads at different locations, as determined by the analyses to be performed.
- Dynamic displacement of the test rotor. Two orthogonal measurements for at least one axial location are required for the identification of dynamic coefficients.
- Acceleration of the bearing housing. Some identification techniques rely on orthogonal measurements of acceleration, instead of using derivations of the dynamic displacements.
- Dynamic force applied for the identification of bearing coefficients.
- Magnitude of the static force applied to the test bearing.
- If specific tests are planned to measure thickness and/or pressure of the oil film, then at least provisions for the wiring need to be considered.

Due to the diversity of sensors, some paragraphs are not enough to cover a particular selection process. Details about the types of sensors available for each one of the measurements

mentioned here, with descriptions of their main technical features are found in [60]. However, some important points to consider when selecting sensors for a test rig are:

- The voltage and current required by the sensors. Two alternatives may be considered: to include some transformer(s) in the design scope, or to include the power supply items within the scope of the purchased sensor(s).
- Characteristics of the sensor output. Most sensors typically provide their output as a 4-20 mA dc signal or as a 0-10 vdc signal, though some may use a different scale. Determining these outputs is important to specify the required acquisition system (DAQ).
- The range of measurement of the sensors should meet the specified range of measurements. For example, if displacements of 25.5 μm are specified, then the displacement sensor should be able to reliably capture displacements in that range.
- The expected level of accuracy in the measurement. Selected sensors should meet this expected accuracy, without magnification, as increased accuracy is typically more expensive.
- The dynamic response of the sensor. A test rig will experience excitations in a frequency range from 0 -500 H, and the related sensors should reliably capture those signals.

Finally, details of installation and location are also a consideration. Capacitive sensors are one available technology for measuring dynamic displacements in clean environments, with enhanced resolutions (1.0 nm) but small measurement ranges (200 μm). On the other hand, eddy current sensors operate reliably in oily environments with a range approximately 1,000 times larger, but a resolution 50 times larger. It is important that the selected axial location of the sensor is not at or close to a nodal location of the mode shape, otherwise the displacement measurements will not be significant with respect to the excitation. Ideally, sensors should be located close to the midplane of the bearing to avoid issues with the rotor flexibility; however, this

is not always achievable, but this situation can be controlled with a suitable identification method that includes the rotor flexibility and this miscollocation. Two orthogonal sensors, at one axial location, are enough for identifying eight dynamic coefficients with two rounds of excitation; however, additional sensors at different locations provide flexibility and the opportunity to confirm the repeatability of the identified coefficients. These examples show that a simple selection is not always possible; however, additional tools such as the new identification method in chapter 3 and the uncertainty analysis in [42] will certainly provide further guidance for comparing cases with different locations and technology for the sensors.

4.3.7 Lubrication system(s)

This system supplies the lubricant(s) to all equipment and components of the rig. It is ideal to have a single system with a unified lubricant, otherwise the cost increases. Detailed recommendations for lubrication systems in [61] should be a starting point for the development of particular specifications for the required system(s). These specifications determine the scope of the supply and assembly by specialized manufacturers. It is recommended to include in the supply the following components:

- A stainless-steel reservoir with at least one breather.
- A lubricant pump. The required flowrate will be variable depending on the bearing and test conditions and solutions should be considered for this situation; for example, a variable speed pump or less efficient valve regulation.
- A check valve and an outlet valve at the pump discharge.
- A pressure relief / safety valve system.
- A lubricant heat exchanger.
- An exchanger fan (in case the exchanger is not water-lubricant type).
- An adequate lubricant filter.

- A heater to supply oil at 120 F.
- A Temperature Control Valve (TCV) at the inlet to the cooler.
- Flow control valves to regulate flowrate to the required final points.

Furthermore, the following instrumentation is also recommended for the system(s):

- A level gauge and a temperature indicator in the reservoir.
- A pressure indicator at the discharge of the pump(s).
- A temperature transmitter downstream of the exchanger, which will also control the operation of the cooler fan.
- A pressure differential indicator for the filter.
- Flow meters to confirm the flowrate delivered to each final point.
- A pressure indicator at the input port to the test bearing.

4.4 ASSEMBLY OF THE COMPONENTS OF THE RIG

Once the individual components of the rig have been designed/selected, the designer should consider their assembly and confirm their harmonious integration by running the analyses described in this section.

4.4.1 Modal analysis

The test rig will be subjected to harmonic loads and a modal analysis assisted by an engineering software such as Ansys or Autodesk Inventor provides resonant frequencies and mode shapes. The objective of the analysis is to find possible interferences in the expected range of dynamic frequencies to be applied. The input for this analysis is a geometric model of the assembly of the rig. This model should include the designed components and representations of

the selected equipment, with the location on the baseplate or the foundation. The more detailed the model is, the more meaningful the output it provides for design or selection modifications.

Figure 4.6, for example, shows a lateral resonant mode of the test section, with respect to the rotor. The design in figure 4.6 was expected to be excited with frequencies from 0-500 Hz. The following observations can be made:

- Different software and modeling approaches may provide different predictions for the same mode, so resonant frequencies should be considered as a range, rather than an exact value. Critical modes in the operating range of the machine should be examined carefully and safety factors may be necessary to ensure adequate separation from the resonance.
- Some sections of the geometrical model may seem to be prone to certain independent resonant modes. However, it is recommended not to make that assumption and always analyze with a model as complete and detailed as possible. For the example in figure 4.9, the lateral mode at 452 Hz seemed to be affected only by the pieces in the figure; however, when the concrete foundation was included in the analysis, the prediction was unexpectedly reduced to 403 Hz, indicating a strong influence of the foundation on that mode.
- In case of doubts or noticeable non-repeatability in the results, apply mesh refinement to critical sections of the model and evaluate the convergence of results.

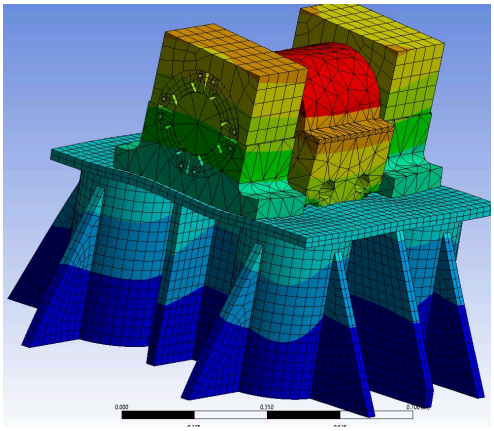

Figure 4.9: Lateral resonant mode for a test pedestal

The recommended time to perform the modal analysis is before any manufacturing process has begun to have the possibility for design modifications that eliminate or reduce unwanted issues.

4.4.2 Torsional rotordynamic analysis

A torsional analysis should be performed once all rotating pieces of equipment have been defined during the design stage. Dimensional and torsional information is required, so data from manufacturers is needed (motor, gearbox, coupling).

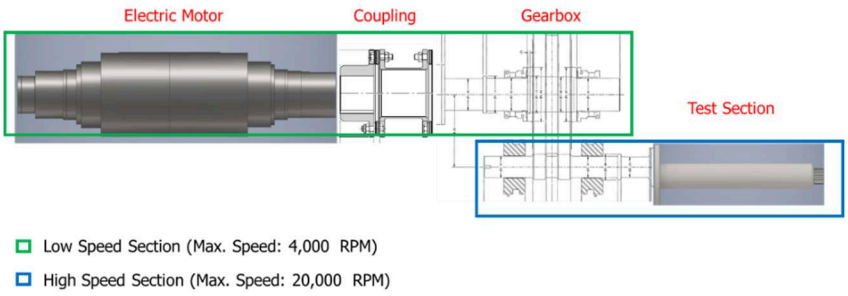

Figure 4.10: A rotating train for a torsional rotordynamic analysis

Once the information of these pieces is available, a lumped torsional model can be generated [1], and the critical torsional speeds can be calculated. Figure 4.10 shows an example of a rotating

train subject to a torsional analysis. Results are shown as a Campbell diagram, as seen in figure 4.11. These results indicate a first mode at around 4,000 rpm, which happens coincides with the maximum speed of the low-speed section; hence, some action, such as stiffening the softest component (coupling), is required to move this mode out of the operating range of the machine.

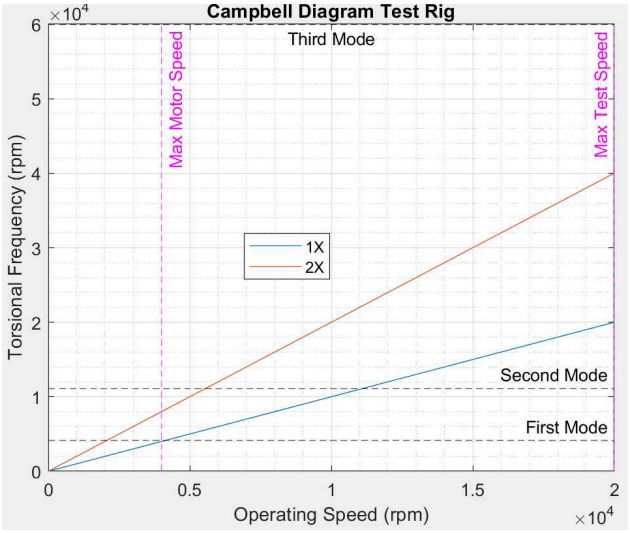

Figure 4.11: Campbell diagram from a rotordynamic analysis

4.4.3 Uncertainty analysis

The excitation frequency, the sensors resolution, the rotor flexibility, and the location of the sensors affect the accuracy of the obtained dynamic coefficients by producing a window of uncertainty. An uncertainty analysis [42] will show if the estimated uncertainties for the designed assembly are within the expectations of the customer or modifications should be implemented. An uncertainty analysis integrates the lateral rotordynamic model of the test rotor, the expected dynamic characteristics of the test bearing, the characteristics (resolution, calibration) of the sensors to measure the applied dynamic forces and the subsequent vibration, and the sensor location. Changing the model or technology of the sensors and/or their location is typically a direct way to reduce uncertainty.

4.5 CONCLUSIONS

This chapter has developed a methodology to design a rig by proceeding in four stages: from defining customer needs for a test rig, to defining design requirements, then to design and selection of components for the rig, to finally performing several design verifications of the rig as a unit (with components assembled) to ensure that the design will meet the requirements.

This chapter provides technical recommendations for the designer in each of the four stages, while also providing independent background information and references, so the designer understands key considerations and keeps the autonomy to deviate with confidence from the recommendations, whenever a different choice is more suitable for the design.

Performing a detailed design of the components of a rig, that will cost hundreds of thousands of dollars, without benchmarks from industry or previous experience could become quite expensive in terms of effort, time, and money, due to the lack of certainty. Therefore, this chapter provides as many benchmarks as possible, based on industrial recommendations and the experience of the authors. References are also given, for the designer interested in getting more illustration. It is the purpose of this article to guide the detailed design with reference points so that the designer has more technical confidence and can proceed more efficiently.

Some important points for the design of a test rig for obtaining dynamic coefficients can be summarized as:

- The decision of having a floating or fixed bearing housing is usually left to the designer, and it will impact the type of the exciter system, the selection of important sensors, and the design of the baseplate and the foundation. Therefore, it is a critical decision and the designer should reflect on the advantages and disadvantages, including cost and technical impact, of each alternative.

- As the rotating speed is higher and the journal diameter is larger, the rig will demand more power, and it is more important to confirm the available utilities and support infrastructure that can be supplied.
- Modern TEHD bearing codes are a useful tool to estimate the behavior of bearings and define design requirements. However, results should be considered with an uncertainty window, due to the lack of validation, and for design purposes the use of a reasonable safety factor is recommended.
- The drive train must provide the power required by the test bearing, but their rated power should not be excessive or the life of the driver could be reduced and the equipment will always operate at less than optimal efficiency.
- The baseplate may seem to be a structure to provide support. However, the modal analysis shows the significant influence of the baseplate and the foundation on the dynamic characteristic of the rig. It is recommended to do the modal analysis during the design stages, when modifications can still be performed, and before any manufacturing begins.
- The rotordynamic analysis is a critical validation of the design, because torsional vibration is not typically monitored. Fortunately, couplings are normally the softest torsional element and the designer may modify their stiffness to displace the resonant frequencies away from operating speeds.

CHAPTER 5

CONCLUSIONS

This dissertation has developed three objectives that have led to analyses and methods to increase the accuracy of experimentally identified dynamic coefficients of fluid film journal bearings. Chapter 2 presented analyses on uncertainty estimations applicable to experimental dynamic coefficients obtained by single-sample single-frequency dynamic tests. Chapter 3 considered how the experimental identification of the dynamic coefficients of a fluid film journal bearing is affected by test rotor flexibility and the location of the displacement sensors, which are usually not located at the midplane of the bearings. Finally, Chapter 4 developed a set of guidelines for researchers involved in the design of a test rig for the dynamic characterization of radial fluid film bearings.

The conclusions of this dissertation are presented in this chapter, divided in three groups according to the chapters and objectives to which they refer. Recommendations for possible research lines that extend these objectives are presented at the end.

5.1 RESEARCH CONCLUSIONS

This section presents the conclusions applicable to the analyses and the method proposed in Chapter 2, related to the uncertainty estimation of experimental dynamic coefficients obtained by single-sample single-harmonic frequency tests.

1. The non-linear nature of the dynamic coefficients produces detectable inaccuracies in uncertainty estimations generated by the Taylor Series Method (TSM), despite the TSM being the most prevalent method to estimate uncertainties for dynamic coefficients obtained by single-sample single-frequency dynamic tests.
2. The non-linearity of the dynamic coefficients produces asymmetric uncertainty bounds, whereas the uncertainty estimations by the TSM assume symmetric bounds.
3. Neglecting higher order terms in the uncertainty analysis, as is typically done with the TSM can lead to significant errors in the uncertainty estimates for the dynamic bearing coefficients. For the examples evaluated in this work, 2^{nd} order terms were found to range from 18% to 45% of the most significant 1^{st} order term for each coefficient.
4. The Monte Carlo Method (MCM) is presented as an alternative method to estimate the uncertainties in experimentally derived dynamic coefficients. Uncertainty estimations by the MCM more accuratetly represent the nonlinearities and asymmetries of the dynamic coefficients, without any additional correction or inspection of accuracy.
5. Transforming the random uncertainty of sensors from the time domain to the frequency domain significantly reduces the uncertainty estimations of the dynamic coefficients. Traditional uncertainty analyses apply the random uncertainty of the sensors in the time domain. For the examples in this dissertation, this produced uncertainty estimations from 5 to 82%. However, from the same input data and conditions, the use of the novel method proposed here produces uncertainty estimations of less than 6% for the coefficients, and less

than 2% for K_{yy} and C_{xx}, which is certainly a remarkable improvement in the accuracy of the coefficients.

This section now covers the conclusions related to the new method proposed in Chapter 3 to allow a more accurate identification of the eight dynamic coefficients of a fluid film journal bearing.

1. The novel method in this dissertation assumes that the dynamic displacement of the rotor at any axial location is a function of the dynamic bearing coefficients. Therefore, this method improves the accuracy of the identified dynamic coefficients by accounting for the location of the displacement sensors and eliminates errors due to the sensors not being located at the bearing midplane.
2. This proposed method also has the advantageous of not being restricted to only one rotor-bearing(s) configuration and has been applied by numerical simulation to three different rotor-bearing configurations. The first is a single floating test bearing around a flexible test rotor, which is a very common configuration in test rigs, and requires the identification of four direct and four cross-coupled dynamic coefficients. The second configuration is two identical test bearings supporting a flexible test rotor, which again requires the identification of four direct and four cross-coupled dynamic coefficients. The third configuration is two different test bearings supporting a flexible rotor, which requires the identification of eight direct and eight cross-coupled coefficients. The second and third configurations are common arrangements for rotating machinery. In numerical simulations of all three cases, the proposed method was used to identify all direct and cross-coupled dynamic coefficients with an error of less than 0.001%.
3. The identification method, as proposed, requires the application of two independent harmonic excitations as may be applied by magnetic bearings or shakers, or in the form of unbalance masses or impact forces with instrumented hammers. Additionally, different testing conditions,

as given by the combination of excitation methods and sensor location lead to different condition numbers for the matrix [Δ]. The identification method is sensitive to this condition number and large condition numbers may produce difficulties with convergence and identification of the right dynamic coefficients or to an excessive amplification of signal noise in experimental measurements that will finally lead to a non-convergence of the method.

4. The ability of the method to keep the uncertainty of the identified coefficients within acceptable bounds was tested by performing uncertainty analyses that propagated values of random error in the displacement sensors. 30 out of the 32 identified dynamic coefficients, during the numerical validation had values of uncertainty smaller than 20%. This included the cross-coupled coefficients, which are highly sensitive to signal noise and measurement errors.

Finally, this section presents the conclusions of the work developed in Chapter 4.

1. This dissertation has developed a methodology for designing a test rig by proceeding in four stages: from the customer needs, to defining design requirements, to design and selection of the rig components, to finally performing design verifications of the rig as a unit (with components assembled) and validating that the design meets the requirements.
2. Technical recommendations are provided for the designer for each of the four stages, but it is also intended to provide independent background, so the designer understands key considerations and maintains the autonomy to deviate with confidence from the recommendations where a different choice is more suitable for the design.
3. Detailed design of the components of a rig that meets current industrial needs will likely cost on the order of hundreds of thousands of dollars. Without benchmarks from industry or previous experience, this effort could become quite expensive in terms of effort, time, and money, due to the lack of certainty. Therefore, this dissertation provides as many benchmarks as possible, based on industrial recommendations and the experience of the authors. It is an

intent of this guideline to provide reference points so that the designer has more technical confidence and can proceed more efficiently.

4. Specific technical points for the design of a test rig for obtaining dynamic coefficients can be summarized as:

   - The decision to have a floating or fixed bearing housing is usually left to the designer, and will impact the type of exciter system, selection of important sensors, and design of the baseplate and foundation. Therefore, it is a major decision and the designer should reflect on the advantages and disadvantages, including cost and technical impact, of each alternative.
   - As the rotating speed is higher and the journal diameter is larger, the rig will demand more power, and it is important to confirm the available utilities and support infrastructure.
   - Modern TEHD bearing codes are a useful tool for estimating the behavior of bearings and defining design requirements. However, results should be considered with an uncertainty window, due to the lack of validation, and for design purposes the use of a reasonable safety factor is recommended.
   - The drive train must provide the power required by the test bearing, but it should not be excessively oversized, or the life of the driver could be reduced and the equipment will always operate at far lower than optimal efficiency.
   - The baseplate is, at first sight, a structure to provide support. However, the modal analysis reveals the significant influence of the baseplate and the foundation on the dynamic characteristic of the rig. It is recommended to perform a modal analysis during the design stages, when modifications can still be made, and before any manufacturing begins.
   - The rotordynamic analysis is a critical validation of the design, because torsional vibration is not typically monitored. Fortunately, the couplings are normally the softest torsional

element and the designer may modify their stiffness to displace the resonant frequencies away from the operating speeds.

5.2 RECOMMENDATIONS / FUTURE WORK

Based on the major findings of this dissertation, the following recommendations for future work are presented:

1. The analyses of uncertainty estimations, as developed in Chapter 2, have been proven here for dynamic coefficients obtained by single-sample single-frequency dynamic tests. However, an extension of these analyses should confirm if these results are also applicable to other techniques of dynamic testing; for example, multi-sample multi-frequency.
2. The new method, proposed in Chapter 2, to find the uncertainty estimations of dynamic coefficients was presented for specific sampling rates, and for time periods that are exactly an integer multiple of the period of the analyzed harmonic signal. However, more general conditions, including different sampling rates and different time periods are also possible. Analyzing these results under more general test conditions could provide additional insight into the behavior of this new method.
3. The new method, proposed in Chapter 3, to identify the dynamic coefficients of fluid film journal bearings is sensitive to the condition number of the matrix [Δ]. Therefore, more exhaustive research on preconditioning methods, that do not modify the behavior of [Δ] but improve its condition number, could expand the applicability of the method to more general test conditions and possibly make it simpler, for example, by reducing the required number of harmonic excitations to apply.
4. The new method, proposed in Chapter 3, to identify the dynamic coefficients of fluid film journal bearings has been validated numerically. However, additional comparisons to

experimental data would provide valuable data on the experimental behavior of the method before using it as a primary method.

5. The guideline for the design of a test rig, presented in Chapter 4, covers the main components and the most relevant background required by a designer. However, this guideline could be expanded with more details by including future stages of construction, installation and start up.

BIBLIOGRAPHY

[1] ANSI / API Recommended Practice 684, 2010, API Standard Paragraphs Rotordynamic Tutorial: Lateral Critical Speeds, Unbalance Response, Stability, Train Torsionals, and Rotor Balancing. American Petroleum Institute.

[2] He, M., Byrne, J., Cloud, H, and Vazquez, J., 2016. “Fundamentals of Fluid Film Journal Bearing Operation and Modeling”, Asia Turbomachinery & Pump Symposium.

[3] Wygant, K., Barrett, L., and Flack, R., 1999. “Influence of pad pivot friction on tilting-pad journal bearing measurements part ii: Dynamic coefficients”. Tribology Transactions, **42**(1), pp. 250–256.

[4] Brockwell, K. and Dmochowski, W., 1989, “Experimental Determination of the Journal Bearing Oil Film Coefficients by the Method of Selective Vibration Orbits,” Proc. 12th Biennial ASME Conference on Mechanics Vibration and Noise, **18**(1), pp. 251–259.

[5] De Santiago, O. and San Andres, L.,2007, “Experimental Identification of Bearing Dynamic Force Coefficients in A Flexible Rotor—Further Developments”, Tribology Transactions, **50**(1), pp. 114-126.

[6] Jia, C., Pang, H., Ma, W., and Qiu, M., 2017, “Dynamic Stability Prediction of Spherical Spiral Groove Hybrid Gas Bearings Rotor System”, ASME J. Tribol., **139**(2), 021701.

[7] Bhattacharya, A., Dutt, J., and Pandey, R., 2017, “Influence of Hydrodynamic Journal Bearings with Multiple Slip Zones on Rotordynamic Behavior”, ASME J. Tribol., **139**(6), 061701.

[8] Lund, J.W., 1974, “Stability and Damped Critical Speeds of a Flexible Rotor in Fluid-Film Bearings,” ASME J. Eng. Ind., **96**(2), pp. 509 – 517.

[9] Chen, C., Jing, J., Cong, J., Dai, Z, and Cheng, 2020, “Influence of Fluid Film Boundary Migration on Dynamic Coefficients of Journal Bearings and Behavior of Rotor System”, ASME J. Tribol., **142**(10), 101801.

[10] Tiwari, R., Lees, A., Friswell, M., 2004, “Identification of Dynamic Bearing Parameters: A Review”, The Shock and Vibration Digest, **36**(2), pp. 99 -124.

[11] Kostrzewsky, G.J., and Flack, R.D., 1990, “Accuracy Evaluation of Experimental Derived Dynamic Coefficients of Fluid-Film Bearings, Part I: Development of the Method,” Tribology Transactions, **33**(1), pp. 105–114.

[12] Kline. S. J., McClintock. F. A., 1953, "Describing Uncertainties in Single-Sample Experiments," Mech. Eng., pp 3-8.

[13] Rouvas, C., Murphy, B.T., and Hale, R.K., 1992, “Bearing Parameter Identification Using Power Spectral Density Methods,” Proceedings of the 5th International Conference on Vibration in Rotating Machinery, IMechE, Bath, UK, Paper C432/151, pp. 297–303.

[14] San Andres, L., and Delgado, A., 2007, “Identification of Force Coefficients in a Squeeze Film Damper with a Mechanical End Seal—Centered Circular Orbit Tests”, ASME J. Tribol., **129**(03), pp. 660-668.

[15] Pereira, H. and Nicoletti, R., 2019, “Design of Tilting-Pad Journal Bearings Considering Bearing Clearance Uncertainty and Reliability Analysis”, ASME J. Tribol., **141**(01), 021702.

[16] Barsanti, M., Ciulli, E., and Forte, P., 2019, “Random error propagation and uncertainty analysis in the dynamic characterization of Tilting Pad Journal Bearings” J. Phys.: Conf. Ser. **1264**, 012035.

[17] Kocur, J., Nicholas, J. and Chester, L., 2007. “Surveying Tilting Pad Journal Bearings and Gas Labyrinth Seal Coefficients and Their Effect on Rotor Stability”, Proceedings of the 36th Turbomachinery Symposium

[18] Ikeda, K., Hirano, T., Yamashita, T., Mikami, M., and Sakakida, H., 2006, “An Experimental Study of Static and Dynamic Characteristics of a 580 mm (22.8 in) Diameter Direct Lubrication Tilting Pad Journal Bearing”, ASME J. Tribol., **128**(1), pp. 146–154.

[19] Yamada, H., Taura, H., and Kaneko, S., 2018, “Numerical and Experimental Analyses of the Dynamic Characteristics of Journal Bearings with Square Dimples”, ASME J. Tribol., **140**(1),011703.

[20] ASME PTC 19.1, 2013, “Test Uncertainty”, The American Society of Mechanical Engineers.

[21] JCGM 100:2008 Evaluation of Measurement Data - Guide to the Expression of Uncertainty in Measurement (ISO-IEC Guide 98-3), 2008, Joint Committee for Guides in Metrology.

[22] Kostrzewsky, G., Taylor, D., and Flack, R., 1993, “A Hydrodynamic Journal Bearing Test Rig with Dynamic Measuring Capabilities”, Tribology Transactions, **36**(4), pp. 497–512.

[23] He. M., 2003, “Thermoelastohydrodynamic Analysis of Fluid Film Journal Bearings”, PhD Thesis, University of Virginia, Charlottesville.

[24] Robinson, L., Arauz, G., and San Andres, L., 1995, “A Test Rig for the Identification of Rotordynamic Coefficients of Fluid Film Bearing Elements”, ASME 1995 International Gas Turbine and Aeroengine Congress and Exposition, 95-GT-431.

[25] Delgado. A, 2010, “Identification of Force Coefficients in a Squeeze Film Damper with a Mechanical Seal”, Master Thesis, Texas A&M University.

[26] Sawicki, J., and Rao, T, 2004, “Nonlinear Prediction of Rotordynamic Coefficients for a Hydrodynamic Journal Bearing,” Int. J. Rotating Mach.,**10**(6), pp. 507-513.

[27] Metropolis, N. and Ulam, S., 1949, “The Monte Carlo Method”, Journal of the American Statistical Association, **44**(247), pp. 335 – 341.

[28] Saidi, P., 2019, “Theory, Application, and Implementation of Monte Carlo Method in Science and Technology”, IntechOpen, ISBN:978-1-78985-545-6

[29] Burrows, C., and Sahinkaya, M., 1982. “Frequency-Domain Estimations of Linearized Oil Film Coefficients”, ASME J. of Lubrication Tech, **104**(2), pp. 210-215.

[30] Sinha, J., 2021, Industrial Approaches in Vibration-Based Condition Monitoring, CRC Press, Chap. 5. ISBN:9781032241784

[31] San Andres, L. and De Santiago, O., 2004, “Identification of Bearing Force Coefficients from Measurements of Imbalance Response of a Flexible Rotor,” ASME Turbo Expo 2004: Power for Land, Sea and Air, GT2004-54160.

[32] Tiwari, R., Lees, A. and Friswell M., 2002, “Identification of Speed-Dependent Bearing Parameters”, Journal of Sound and Vibration, **254**(5), pp. 967-986.

[33] Chen, Y., Yang, R., Sugita, N., Mao, J. and Shinshi, T., 2021, “Identification of Bearing Dynamic Parameters and Unbalanced Forces in a Flexible Rotor System Supported by Oil-Film Bearings and Active Magnetic Devices”, Actuators 2021, **10**(9), 216.

[34] Rodriguez, L., Childs, D., 2006, “Frequency Dependency of Measured and Predicted Rotordynamic Coefficients for a Load-on-Pad Flexible-Pivot Tilting-Pad Bearing”, ASME J. Tribol., 128(2), pp. 388-395.

[35] Forte, P., Ciulli, E., Maestralle, F., Nuti, M., Librashi, M., 2018, “Commissioning of a Novel Test Apparatus for the Identification of the Dynamic Coefficients of Large Tilting Pad Journal Bearings”. Procedia Structural Integrity, **8**, pp. 462 – 473.

[36] Knopf, E. and Nordmann, R., 1980, “Identification of Stiffness and Damping Coefficients of Journal Bearings by Means of The Impact Method”. In 2nd International Conference on Vibrations in Rotating Machinery, pp. 231-238

[37] Chen, J. and Chen, A., 1995, “Estimation of Linearized Dynamic Characteristics of Bearings Using Synchronous Response”, International Journal of Mechanical Sciences, **37**(2), pp. 197-219.

[38] Yang, T. and Chaung, W., 2000, “Identification of Bearing Coefficients of Flexible Rotor-Bearing Systems”, ASME Turbo Expo 2000: Power for Land, Sea and Air, 2000-GT-0400.

[39] Müller-Karger, C. and Granados, A, 1997, “Derivation of Hydrodynamic Bearing Coefficients Using the Minimum Square Method,” ASME J. Tribol., **119**(4), pp. 802 –807.

[40] Pettinato, B., 1992, "Setup and Test Procedure for a Ruid Film Bearing Test Rig with Results for a Three Lobe Bearing", M.S. Thesis, University of Virginia, Charlottesville, VA.

[41] Duff, I. and Koster, J., 2001, “On Algorithms For Permuting Large Entries to the Diagonal of a Sparse Matrix”, SIAM Journal on Matrix Analysis and Applications, **22**(4), pp. 973–96.

[42] Herrera, P., Goyne, C., and Rockwell R., 2024, “Propagation of Uncertainty in Experimental Dynamic Coefficients of Fluid Film Journal Bearings”*,* ASME J. Tribol.*,*.

[43] Lund, J., 1987, “Review of the Concept of Dynamic Coefficients for Fluid Film Journal Bearings”, ASME J. Tribol., **109**(1), pp. 37-41.

[44] Goodwin, M., Ogrodnik, P., Roach, M., Fang, Y., 1997, “Calculation and Measurement of the Stiffness and Damping Coefficients for a Low-Impedance Hydrodynamic Bearing”, ASME J. Tribol., **119**(1), pp. 57-63.

[45] Hagg, A., and Sankey, G., 1958, "Elastic and Damping Properties of Oil- Film Journal Bearings for Application to Unbalance Vibration Calculations”, ASME Journal of Applied Mechanics, **25**, pp. 141-143.

[46] Mitchell, J.R., Holmes, R., and Ballegooyen, H.V., 1966, “Experimental Determination of a Bearing Oil Film Stiffness,” Proceedings of the 4th Lubrication and Wear Convention, IMechE, **180**(3K), pp. 90–96.

[47] Glienicke, J., 1966, "Experimental Investigation of the Stiffness and Damping Coefficients of Turbine Bearings and Their Application to Instability Predictions", Proceedings of the Institution of Mechanical Engineers, **181**(3B), pp. 116-129.

[48] Knopf, E. and Nordmann, R., 2000, “Identification of the dynamic characteristics of turbulent journal bearings using active magnetic bearings”. In 7th International Conference on Vibrations in Rotating Machinery, pp. 381 – 390.

[49] Lund, J., 1964, "Spring and Damping Coefficients for the Tilting Pad Journal Bearing," Trans. ASLE, **7**, pp. 342-352.

[50] Delgado, A., Vanini, G., Ertas, B., Drexel, M., Naldi, L., 2010, “Identification and Prediction of Force in a Five-Pad and Four-Pad Tilting Pad Bearing for Load-on-Pad and Load-Between-Pad Configurations”, Journal of Engineering for Gas Turbines and Power, **133**(9), 092503.

[51] Simmons, J. and Lawrence, C., 1996, “Performance Experiments with 200 mm, Offset Pivot Journal Pad Bearing”, Tribology Transactions, **39**, pp. 969-973.

[52] Vrancik, J., 1968, “Prediction of Windage Power Loss in Alternators”, TN-D4849, NASA.

[53] ANSI / API Standard 610, 2011, Centrifugal Pumps for Petroleum, Chemical, and Gas Industry Services. American Petroleum Institute.

[54] ANSI/NEMA MG 1, 2004, “Motors and Generators”. National Electrical Manufacturers Association.

[55] ANSI / API Recommended Practice 14E, 1991, “Design and Installation of Offshore Production Platform Piping Systems”, American Petroleum Institute.

[56] Bloch, H., 2009, Practical Lubrication for Industrial Facilities, CRC Press, Chap. 10.

[57] ANSI / API Standard 613, 2007, Special Purpose Gear Units for Petroleum, Chemical, and Gas Industry Services. American Petroleum Institute.

[58] Schweitzer, G., and Maslen, E., 2009, Magnetic Bearings: Theory, Design and Application to Rotating Machinery, Springer.

[59] Shigle, J., and Mischke. C., 1996, Standard Handbook of Machine Design, McGraw-Hill, Chap. 29.

[60] Sheel, S., 2014, Instrumentation: Theory and Applications. Alpha Science International Ltd.

[61] ANSI / API Standard 614, 2008, Lubrication, Shaft-sealing and Oil-control Systems and Auxiliaries. American Petroleum Institute.